

# Airflow in the Hyperloop System

**BEng Group 8:** Kieran Russell, Meng Zhang, Yehia El Gendi, Yuzhe Zhou



## Abstract

The hyperloop is a proposal for a new transportation system between Los Angeles and San Francisco consisting of a low pressure tube with pods levitated on air cushions travelling through nearly at sonic speed. The pods are accelerated via a linear induction motor and can carry up to 28 passengers with an expected travel time of 35 minutes. The flow of air in the hyperloop system is of utmost importance to its operation and plays a significant role in the pod's air compression and air suspension bearing subsystems. The vacuum pump system throughout the length of the tube is crucial in maintaining the low pressure system required for these high speeds. These three systems were chosen for further study in order to come up with real solutions to the problems in the original proposal. Using Matlab scripts, CFD packages and Simulink models, conditions in the tube were simulated in order to obtain accurate results for our work. Based on our work alone however, it is difficult to determine the feasibility of the hyperloop proposal as the safety, economics and cost were not considered. The work done in this report serves as a basis for further research into all the hyperloop's aspects rather than an all rounded effort to analyse the feasibility of the hyperloop. The results obtained show that the pod's dimensions may be too small for the required axial compressor, the solution being either to increase the power input to the compressor or to increase the pod's cross sectional area. The intercoolers and fluid storage tanks necessary for the compression system's operation were designed with the pod's dimensions in mind. The entire compression system was found to occupy roughly 16 m of pod length. Further work needs to be carried out to determine whether this is a suitable length for the pod to traverse the entire tube at high speed with all the turns involved. The air bearing suspension system was found to provide sufficient lift force for the 15 ton pods. Tilting the air skis at an angle of  $0.05^\circ$  does very little to alleviate lift force from the skis however, future work can be carried out to vary the shape or size of the skis to make this a more attractive option. It was found that 772 'Pascal 2063' rotary vane vacuum pumps can evacuate the entire 563 km length of tubing in roughly 6 hours 30 minutes.

## Personal Statements

For the BEng group project, I first researched the background information for the hyperloop, on the other modes of transport and finding the relevant transport information. I presented my findings on these in the interim presentation. For the main report, I was responsible for the entire ‘Vacuum system’ section. I researched all the different vacuum sections and also decided on the final findings of the vacuum section. I believe I found the most appropriate vacuum pump available that was suitable for the hyperloop system. I was also responsible for appendix E.

Kieran Russell, \_\_\_\_\_, s1242154, Group 8, 3/12/2015

I, Meng Zhang, work as a member in the Hyperloop air flow analysis group. My assignment in this project is designing a primary model for the compressor in the Hyperloop, which can be used to analysis the feasibility of the Hyperloop Alpha design from the views of thermodynamics and fluid mechanics. To accurate analysis the problem, I chose to use the one dimensional mean stream line method, and used the MATLAB to build a simulating model of the compressor. The MATLAB model is referenced from the model of Niclas Falck from Lund University. After totally understand the theories in his model, I rewrite the code with some changes with the consideration of the Hyperloop use. The final design and the results in the compressor part is generated from my MATLAB model for the Hyperloop compressor. I also used this model to make an analysis about the influence of each changeable parameters on the compressor. The input parameters of the final design is also based on this analysis. In the end, the final result suggests that the problems in the Hyperloop Alpha, and proved it is not feasible to have a compressor design with required dimension and power input. The detail parameters of the designed compressor and the MATLAB code I wrote will be in the Appendix A and B.

Meng Zhang, \_\_\_\_\_, s1469518, Group 8, 3/12/2015

My task was to research heat exchange technology to design the intercoolers in the air compression system. I carried out all the calculations on Matlab and compared the results to a Simulink model of the air compression system which was made using a thermodynamics extension module. I wrote the heat exchange part of the air compression section as well as the introduction and abstract.

Yehia El Gendi, \_\_\_\_\_, s1228932, Group 8, 3/12/2015

For the BEng group project, I take charge in the air bearing suspension part for the Hyperloop. My section is to check the feasibility of the idea whether it is possible for Hyperloop to float on an air cushion and give a robust design of the air bearing suspension system. For the aerodynamic air bearing, the CFD is done to carry out the analysis to support the discussion, but before that, an optimized shape design was made to make sure that the result of CFD was convincing so a whole CAD assembly is generated in Solidworks. I have done the flow simulation of the whole model and find out the flow pattern passing by the skis, in which I get the solution to the drag force and pressure distribution. For external pressurized bearing, I analyse different types of air bearings and give my orifice type design. To find out the flow rate required, I have a research and find the solution, and then MATLAB is used to find out the relationship between flow rate and pressure. Based on the analysis, I could check the feasibility and have further discussion. I finish the air bearing suspension section in the report.

Yuzhe Zhou, \_\_\_\_\_, s1471339, Group 8, 3/12/2015

# Contents

1. Introduction .....	8
2. Air Compression System .....	9
3. Compressor Design and Analysis .....	10
3.1. Background .....	10
3.1.1. Hyperloop.....	10
3.1.2. Compressor Choices .....	10
3.1.3. Design Choices .....	11
3.2. Design Requirements .....	11
3.3. Compressor Properties .....	12
3.3.1. Blade Geometries.....	12
3.3.2. Velocity Triangles.....	13
3.3.3. Compressor Stage and Thermodynamics .....	15
3.3.4. Stage Load Coefficient .....	16
3.3.5. Stage Flow Coefficient .....	16
3.3.6. Stage Reaction.....	17
3.3.7. De Haller Number.....	17
3.3.8. Compressor Loss.....	18
3.3.9. Efficiency .....	18
3.3.9.1. Isentropic Efficiency .....	19
3.3.9.2. Polytropic Efficiency .....	19
3.3.10. Compressor Type .....	19
3.3.11. Mass Flow .....	19
3.3.12. Pressure Ratio .....	20
3.3.13. Number of Stages.....	20
3.3.14. Rotation Speed .....	20
3.4. Blade Geometries .....	20

3.4.1. Tip Clearance .....	20
3.4.2. Aspect Ratio .....	21
3.4.3. Thickness Chord Ratio.....	21
3.4.4. Axial Velocity Ratio .....	21
3.4.5. Blockage Factor .....	21
3.4.6. Diffusion Factor .....	21
3.5. MATLAB Coding & Calculation Methods .....	22
3.5.1. Main Calculation Loop .....	22
3.5.2. Input Summary.....	24
3.5.3. Compressor Inlet Calculation .....	24
3.5.4. Rotor Inlet .....	25
3.5.5. Rotor Loop .....	27
3.5.6. Stator Loop.....	29
3.5.7. OGV Entropy Loop.....	30
3.5.8. Stage Reaction Loop .....	30
3.5.9. Pressure Ratio Loop .....	31
3.5.10. Blade Angle Loop .....	31
3.6. Final Design and Final Result Analysis.....	32
3.6.1. Property Optimization.....	33
3.6.1.1. Number of Stages.....	33
3.6.1.2. Rotation Speed .....	35
3.6.1.3. Inlet Angle.....	37
3.6.1.4. Stage Reaction .....	38
3.6.1.5. Compressor Type .....	39
3.6.2. Final Design .....	39
3.6.2.1. Overall Input Parameters .....	39
3.6.2.2. Design Performance.....	40

3.6.2.3. Discussion .....	41
4. Heat Exchange System.....	42
4.1. Specification.....	43
4.2. Shell and Tube Heat Exchanger Design .....	44
4.3. Theory and Calculations .....	46
4.4. Analysis.....	50
4.5. Storage Tanks.....	52
4.6. Improvements & Future Work.....	53
5. Suspension .....	54
5.1. Why Air Suspension Systems .....	54
5.1.1. Wheels & Magnetic Levitation.....	54
5.1.2. Air Bearing Suspension .....	54
5.2. Lift Force & Air Cushion Pressure Required Calculation.....	55
5.3. Aerodynamic Air Bearing Investigation.....	56
5.3.1. Shape Design.....	56
5.3.2. Aerodynamic Air Bearing Simulation .....	59
5.3.5. Discussion .....	63
5.4. External Pressurized Air Bearing Investigation .....	64
5.4.1. Shape Design.....	64
5.4.2. External Pressurized Air Bearing Flow Calculation.....	65
5.4.3. Discussion .....	67
5.5. Suspension Safety .....	68
6. Vacuum System .....	68
6.1. Introduction to Vacuum Details.....	68
6.1.1. Vacuum Proposal .....	68
6.1.2. Vacuum Pump Terminology .....	69
6.2. Research on Vacuum Pumps .....	69

6.2.1. Different Vacuum Pump Types .....	69
6.2.2. Different Positive Displacement Vacuum Pump .....	71
6.2.3. Market Research of Rotary Vane Pumps.....	73
6.3. Calculations for Hyperloop Vacuum Pumps .....	74
6.3.1 Initial Design Calculations.....	74
6.3.2. Decision on Numbers of Vacuum Pumps.....	75
6.3.3. Power Calculations .....	76
6.4. Sustaining the Vacuum .....	76
6.4.1. Vacuum Seals.....	76
6.4.2. Maintenance of Pumps.....	77
6.4.3. Future Improvements .....	77
7. Conclusion .....	78
8. Reference.....	80
Appendix .....	82
Appendix a .....	82
Appendix b .....	93
Appendix c .....	108
Appendix d .....	112
Appendix e .....	113

# 1. Introduction

The Hyperloop, a newly proposed “fifth mode of transport”, is a concept idea for a transport system that should take passengers from Los Angeles to San Francisco in 35 minutes. In a nutshell, the Hyperloop is a 620 km tube with air constantly being evacuated, leaving the pressure inside at one thousandth that of sea level. Pods capable of carrying 28 passengers travel at a top speed of 1220 km/h along the inside of the tube on cushions of air much like a puck on an air hockey table. The pods are accelerated via linear induction motors which act like a track for the pod to travel along.

The idea was proposed as an alternative mode of transport to the initial plan for a high speed railway connecting the two cities. Elon Musk, CEO of Tesla Motors and SpaceX, published a Hyperloop Alpha whitepaper proposal in which the main aspects of this system were outlined. The document suggests that the hyperloop is suitable for cities which are less than 1500 km apart, citing supersonic air travel such as the Concorde as a better option for distances which exceed that limit.

The proposal was meant to inspire an academic debate in the engineering community in order to address and tackle the numerous problems faced by the design. In Musk’s own words: “The intent of this document has been to create a new open source form of transportation that could revolutionize travel” [1]. SpaceX have since launched a competition aimed at university students and independent engineering teams, where the competitors submit complete pod designs for scrutineering. Those who are accepted to the subsequent rounds can then build a scaled version to take part in the competition final where the miniature pods are tested on a purpose-built track.

Air, having a significant role in the operation of the pods, is a huge part of this system and the way it flows and interacts with the pod and its systems is crucial in understanding how the Hyperloop works. The designed system requires minimal air inside the tube to reduce as much as possible the effects of drag forces, but at the same time requires lots of air to levitate the pods to eliminate any contact with the ground, again to reduce friction. For this reason, as well as the fact that it is quite difficult to maintain, the tube cannot be in full vacuum. As such, considerations must be made with regard to the air still inside the tube.

One such consideration is the Kantrowitz limit on the speed of the pod given a specific pod:tube diameter ratio. The nature of this limit will be explained in the next section but a solution to the problem has been included in the proposal and involves mounting an axial air compressor to the front of the pod. This actively shifts air from the front of the pod to the rear.

The aim of this project is to analyse the air compression system, the air bearing suspension system as well as the vacuum pump system working to draw air out of the tube. The compression system will be split into two main sections; the axial air compressor and the intercoolers. Each section will be analysed separately by considering the theory behind the operation followed by a look at existing technologies/applications. The details in the hyperloop alpha proposal related to each section will then be discussed to understand the design specification. The final step will be designing a solution to fulfil the requirements of the specific aspect of the hyperloop and critically analysing this with respect to the original proposal. This should offer a basis for determining the feasibility of the proposal and pinpointing the areas where further work needs to be done to fully understand the situation.

## 2. AIR COMPRESSION SYSTEM

Moving a pod through an air tight tube at high speeds raises some problems that need to be dealt with. As the pod moves through the tube, the volume of air it displaces gets forced into the gap between the pod and the tube walls. From the equation of continuity below, it can be seen that a reduction in area results in an increase in flow speed.

$$U_1 A_1 = U_2 A_2 \quad (1)$$

Depending on the geometry of the tube and the pod, there will be a certain limiting pod speed which causes the resulting displaced air to reach sonic speed in the gap; this is known as the Kantrowitz limit. Once this limit is reached, the pod acts like a syringe, pushing air in front of it and sucking air behind it, effectively moving a column of air through the whole tube.

Tackling this problem can be done by increasing the tube area to lower the speed of the displaced air, however this is impractical as it would drive up material and construction costs significantly. Another solution would be to travel much faster allowing the pod itself to break the sound barrier, this would compress the air to a point where flow isn't choked. However this would place the passengers at risk of injury as the accelerations experienced by them would exceed the maximum levels endurable comfortably by humans.

The solution proposed by Elon Musk in the Hyperloop Alpha whitepaper is to mount a compressor on the front of the pod. This takes in air from the front of the pod, compresses it and shoots it out the back, acting as a bypass. This serves multiple purposes: bypassing air through the pod instead of around it, providing air to the air suspension bearings and finally providing thrust force to the pod as it exits the compression system. The proposed system is shown in figure 1 below.

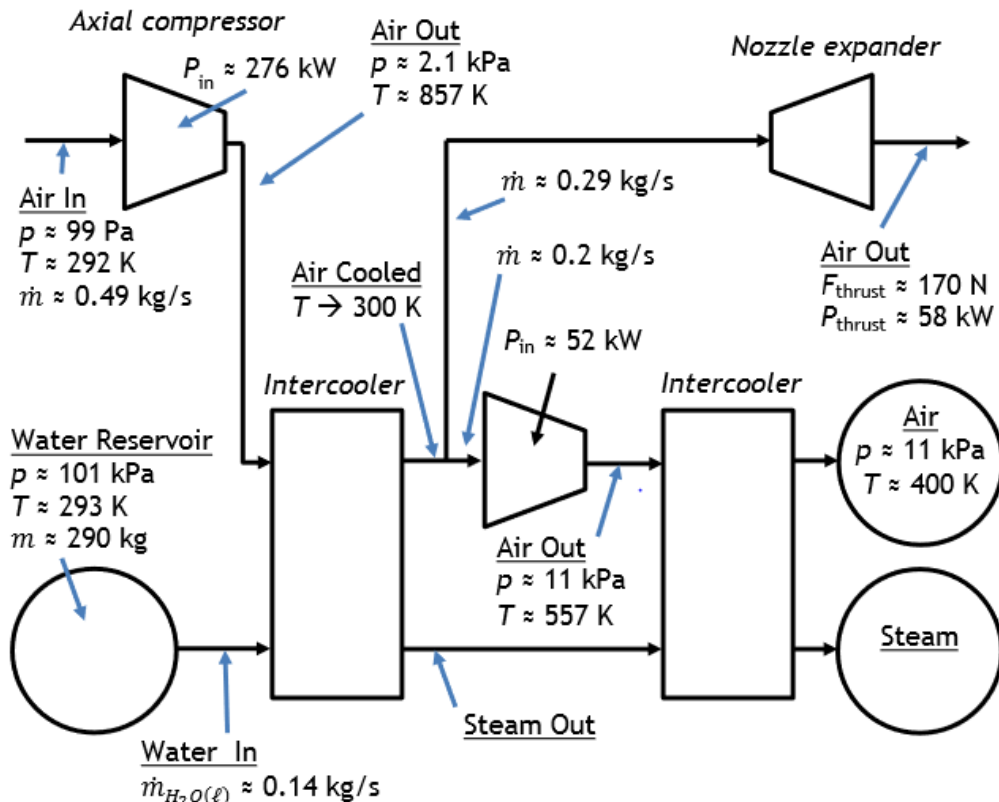


Figure 1: Hyperloop Alpha compressor system [1]

Without the air compression system, the pod would not be able to reach the high speeds it hopes to achieve, as such it is a crucial part of this design and must be studied in great detail. This section of the report will focus on the heat exchange subsystem as well as the spatial requirements with respect to the pod dimensions.

## 3. Compressor Design and Analysis

### 3.1 Background

#### 3.1.1 Hyperloop

In the Hyperloop Alpha design, a compressor is required to be mounted in front of the capsule, which is driven by the electricity from the on-board batteries. The first purpose of the compressor is to allow the capsule travelling through the relatively narrow tube without the existence of choked flow in a subsonic speed by compressing the air and make it pass through the inside capsule. Another purpose is to supply the air bearings with compressed air to support the weight of the capsule through the journey.

#### 3.1.2 Compressor Choices

In the industry, two different categories of compressors are widely used. One is the positive displacement, and another is dynamic. For the high speed vehicle use, like the Hyperloop and air jet, the dynamic compressor is the choice, which is suitable to be used under high flow rate and also in a small dimension.

The two types of dynamic compressors are axial-flow compressor and the radial compressor. Both of them have been used under the high flow rate, like the compressor of aircraft's engine.

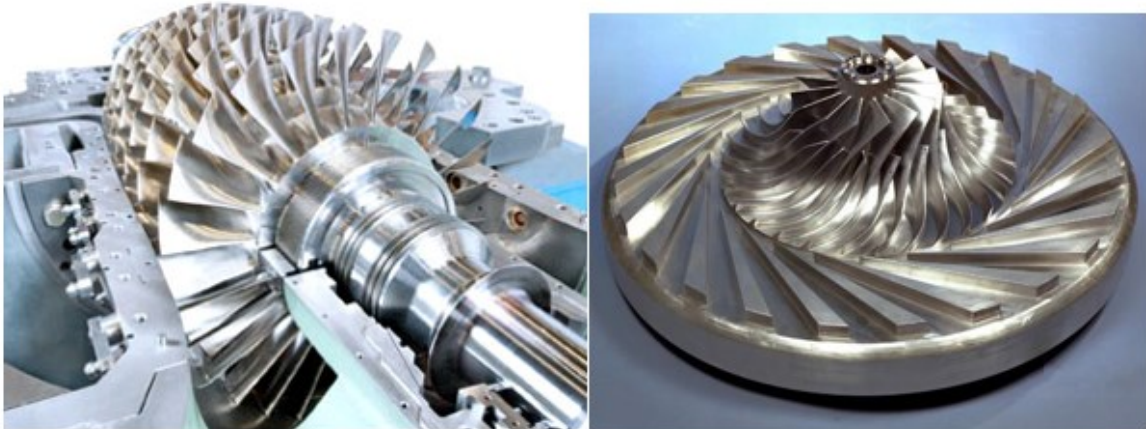


Figure 2: Axial flow Compressor (Left) and Radial Compressor (Right)

As shown in the Figure 2, an axial flow compressor consisted of several rows of rotors and stators, which can deal with a higher pressure ratio with bigger mass flow. To achieve the same pressure ratio, the axial flow compressor can divide the required ratio to each stage, which ensures a smaller diameter of the compressor compared with radial compressor. Except that, axial flow compressors are more efficient. Because the pressure ratio is divided, the air flow through the compressor experiences less changes of the flow directions, which means less perturbation through the blades.

The compressor of the Hyperloop works in the similar condition as the compressor of aircraft engine, which needs to provide a pressure ratio as 1:20, with a flow rate around 340 m/s. Meanwhile, the power supply of the compressor is the on-board batteries, which suggests less energy input. Considering from both dimensions and efficiencies, the axial-flow compressor is the better choice for the Hyperloop.

### 3.1.3 Design Choices

The most advanced fluid flow analysis method is the Computational Fluid Dynamics (CFD). The accurate analysis of air flow through a running axial-flow compressor is extremely complicated, which is suggested to be analysis in a high-speed supercomputer with a very detailed compressor design. However, this requires far more knowledges on sub-sonic fluid dynamics and proficient use of CFD software, which is very expensive and time-consuming. As mentioned before, the task of this report is to come up with an initial design of the inner fluid system of the Hyperloop and provide a feasibility analysis on the Hyperloop Alpha design of Elon Musk.

For these reasons, the mean stream line method is used here to modify the challenges, which can provide a basic design with relatively accurate result. This method simplified the complicated 3-dimension problems into stream line, which can create a basic compressor design that make up for 60-70% of the final design.

Based on that method, a MATLAB program is coded to calculate and generate the results. This method was published by Niclas Falck (2008) from Lund University [2]. The program in this report is based on idea and calculations in his paper. Meanwhile, some changes are made to fit the Hyperloop working conditions and requirements. The calculation methods, and modified program will be showed in later sections. This method simplified the complicated 3-dimension problems into stream line, which can create a basic compressor design that make up for 60-70% of the final design.

In the mean stream line, an important parameter is used to represent the air flow through the compressor, which is called root mean square radius. It is known as the quadratic mean of the radius in a cross-section of the compressor. In this case, it can be defined as

$$r_{rms} = \sqrt{\frac{1}{2}(r_{tip}^2 + r_{hub}^2)} \quad (2)$$

The detailed application of this parameter will be shown in the later calculation section.

## 3.2 Design Requirements

There are many geometries and properties need to be considered when design a compressor. In the Hyperloop design, the biggest challenge and problem is to design a small dimension compressor to provide 20 compress ratio. Pressure ratio and dimension are two primary parameters which are necessary to be satisfied.

In the Hyperloop Alpha design that released by Elon Musk, the pressure ratio is given as 20. The dimension of the compressor is unknown. However, the minimum width of the cross section is 1.1 m in the Hyperloop Alpha, which means the diameter of the compressor should be smaller than that. Considering the size of the casing. The diameter of the blade must be smaller than 1m.

Meanwhile, in the compressor schematic of Hyperloop Alpha, the power supply is designed to be around 276 kW. The temperature and mass flow also mentioned in the schematic. However, some figures are not correct and feasible, which will be discussed later.

Table 1: Design expectation

Air Inlet Pressure	99 [Pa]
Air Inlet Temperature	292 [K]
Outlet Pressure	2.1 [kPa]
Outlet Temperature	857 [K]
Mass Flow	0.57 [kg/s]
Maximum Diameter	1.1 [m]
Input Power	276

### 3.3 Compressor Properties

#### 3.3.1 Blade Geometries

Axial flow compressors are made up by several stages. One single stage consists of a rotor and a stator. The general blade shapes of the rotor and stator are similar as shown in the Figure 3. The convex side of the blade is the suction side, and the concave side is the pressure side. Other parameters are shown as following. The symmetry line between the suction side and pressure side is called camber line.

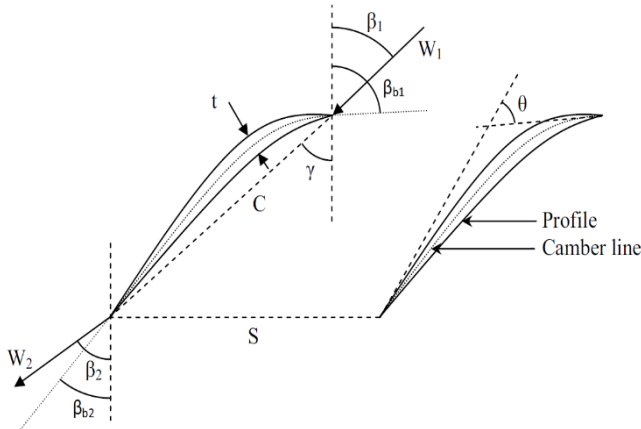


Figure 3: Compressor blade's dimensions

- $t$ , the maximum thickness of the blade
- $C$ , Chord length
- $S$ , Staggered spacing (Pitch between two blades)
- $\sigma$ , Solidicity,  $C/S$
- $\gamma$ , Stagger angle (angle between the axial direction and the chordline)
- $\theta$ , Camber angle (turning angle of the camberline)
- $\beta_1$ , Relative outlet flow angle

- $\beta_{b1}$ , *Inlet blade angle*  
 $\beta_2$ , *Relative outlet flow angle*  
 $\beta_{b2}$ , *Outlet blade angle*  
*i*, *Incidence angle,  $\beta_1 - \beta_{b1}$  (angle between the relative inlet flow and blade)*  
 $\delta$ , *Deviation angle,  $\beta_2 - \beta_{b2}$  (angle between the relative inlet flow and blade)*  
 $W_1$ , *Relative inlet flow rate to blades*  
 $W_2$ , *Relative outlet flow rate to blades*

In the calculation section, the chose blade type is Double Circular Arc (DCA), which is one kind of fundamental blade shape for the axial compressor under the transonic high pressure environment. As the relative speed of air flow to the Hyperloop capsule is subsonic (around 340 m/s), the compressor inlet will accelerate the flow to transonic speed, which can be proved in the result of the calculations later. The performance of this airfoil family is well understand after several years cascade tests (Aungier, 2003), which can be used to generate more accurate results [3].

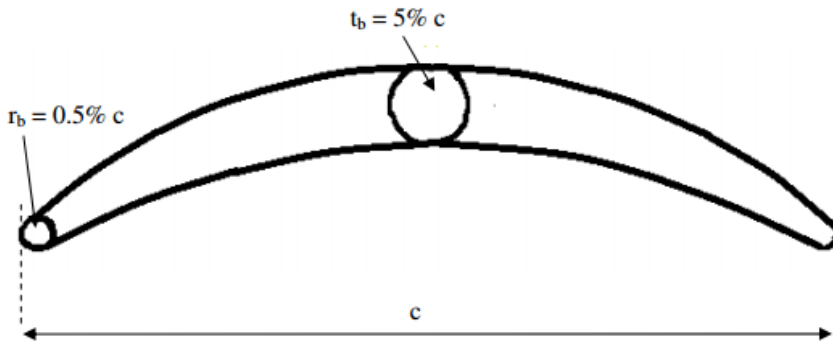


Figure 4: Double Circular Arc (DCA) Airfoil Profile

As shown in the Figure 4, both suction and pressure side of the DCA are formed by circular arcs. The thickness, leading and trailing edges are all related to the chord length.

### 3.3.2 Velocity Triangles

Flow properties changed at every stage through the whole compressor, as well as the blade geometries. All these changes follows the laws of simple thermodynamic and aerodynamics, which can be used to analysis the flow rate through the compressor.

The velocity triangle is a fundamental and widely used process to describe the flow properties and the blade parameters. The velocities of the flow can be divided into absolute and relative velocities. The detailed parameters are shown as following.

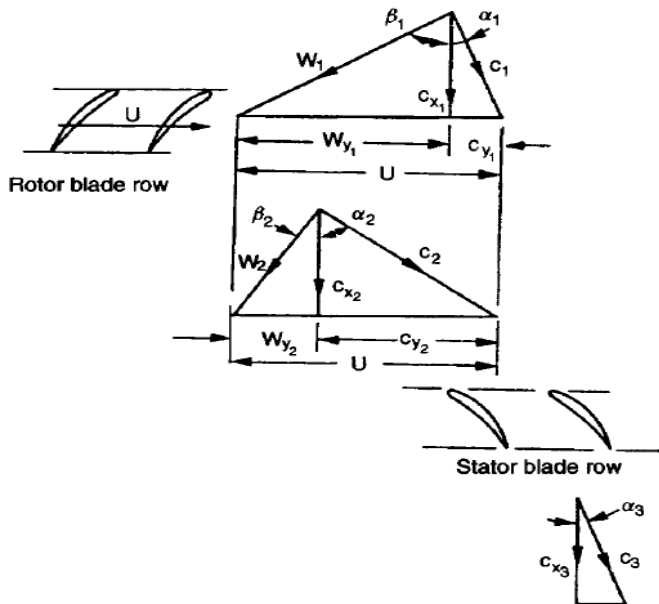


Figure 5: Velocity triangles of rotor and stator

- $C_1$ , *absolute velocity of the rotor's inlet flow*
- $C_{1m}(C_{x1})$ , *axial velocity at the rotor's inlet*
- $C_{1\theta} (C_{y1})$ , *absolute swirl flow velocity of the rotor's inlet*
- $W_{1\theta}(W_{y1})$ , *relative swirl velocity at the rotor's inlet*
- $U$ , *blade velocity*
- $C_2$ , *absolute velocity of the rotor's outlet (stator's inlet) flow*
- $C_{2m} (C_{x2})$ , *axial velocity at the rotor's outlet (stator's inlet)*
- $C_{2\theta} (C_{y2})$ , *absolute swirl flow velocity of the rotor's outlet (stator's inlet)*
- $W_{2\theta}(W_{y2})$ , *relative swirl velocity at the rotor's outlet*
- $C_3$ , *absolute velocity of the stator's outlet flow*
- $C_{\theta3} (C_{x3})$ , *axial velocity at the stator's outlet*

When the flow pass through the rotor, the kinetic energy with rotation speed  $U$  of the rotor blades will pass to the flow, which will increase the both the enthalpy and absolute velocity of the flow. After the flow enter the stator, a large part of the axial velocity of the flow will be eliminated, and instead transfer to the enthalpy of the flow with a higher pressure and temperature.

### 3.3.3 Compressor Stage and Thermodynamics

The fundamental law in turbomachinery is the steady flow energy equation, which can be written as:

$$Q - \dot{W} = \dot{m} \left[ (h_2 - h_1) + \frac{1}{2} (c_2^2 - c_1^2) + g(z_2 - z_1) \right] \quad (3)$$

In our case, the air flow through the whole compressor can be simply regarded as an adiabatic process, where the heat loss  $Q$  is regarded as 0. Meanwhile, the potential energy changes by the gravity can be ignored, because the compressor is working in a horizontal condition.

In the low speed analysis ( $M < 4$ ), the enthalpy can be used to represents the total energy of the flow, because the kinetic energy can be ignored. However, in the Hyperloop design, the highest speed is around 0.99 Mach, where the kinetic energy will be noticeable. To make the later calculation easier, the total energy can be represented by stagnation enthalpy, which is written as:

$$h_0 = h + \frac{1}{2} c^2 \quad (4)$$

Meanwhile, both of the temperature and pressure can be represented in the stagnation way.

$$T_0 = T + \frac{V^2}{2C_p} \quad (5)$$

$$\frac{P_0}{p} = \left( \frac{T_0}{T} \right)^{\gamma/(\gamma-1)} \quad (6)$$

The term  $V^2/C_p$  is regarded as the dynamic temperature in an adiabatic process, where  $C_p$  is the specific heat value of the flow. The term  $\gamma$  represented the specific heat ratio,  $C_p/C_v$ .

Back to the energy equation. The energy changes through the Hyperloop compressor can be written as:

$$\dot{W} = \dot{m}(h_{02} - h_{01}) \quad (7)$$

The work done by a compressor can be represented by the Euler work equation. The specific work being done is:

$$\Delta W = \frac{\dot{W}}{\dot{m}} = U_2 c_{\theta 2} - U_1 c_{\theta 1} \quad (8)$$

Combining this with the energy equation, we can achieve a constant value along a streamline through the whole compressor, which is called rothalpy  $I$ .

$$I = h_1 + \frac{1}{2} c_1^2 - U_1 c_{\theta 1} = h_2 + \frac{1}{2} c_2^2 - U_2 c_{\theta 2} \quad (9)$$

The velocities can be represented by the rotation speed of rotor and also the relative velocities. Then the rothalpy can be written as:

$$I = h + \frac{1}{2} (w^2 + U^2 + 2Uw_{\theta}) - U(w_{\theta} + U) = h_{0rel} - \frac{1}{2} U^2 \quad (10)$$

The term  $h_{0rel}$  is defined as the relative stagnation enthalpy, which is also supposed to be constant through any axial turbomachine's rotor, considering that the rothalpy and rotation speed are constant.

$$h_{0rel} = h + \frac{1}{2} w^2 \quad (11)$$

The thermodynamic stages of the compressor can be shown in both T-S (temperature - entropy) diagram and H-S (enthalpy - entropy) diagram. The stagnation values of temperature can be represented by the static temperatures and the dynamic ones. The stagnation enthalpies can be achieved from the static enthalpies and the velocities.

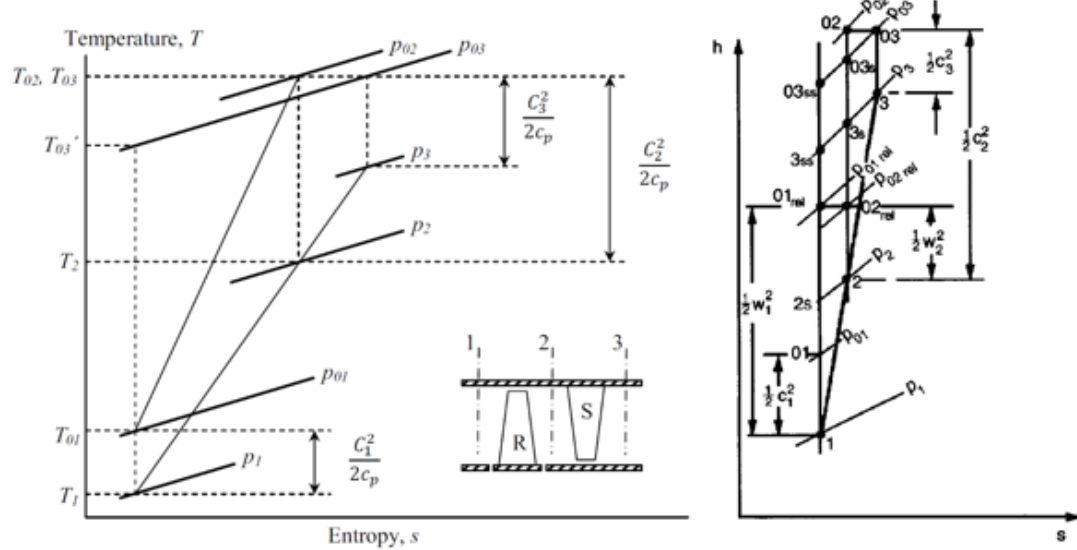


Figure 6: Thermodynamic stage of the compressor in one stage

### 3.3.4 Stage load coefficient

The stage load coefficient is used to describe the work capability of one stage in compressor, which strongly affects the off-design performance characteristics of the compressor. It is defined as the ratio of the energy rise through a stage and the kinetic energy exited by the circumference, which can be defined as:

$$\Psi = \frac{\Delta H}{U^2} = \frac{(C_{y2} - C_{y1})}{U} \quad (12)$$

This parameter helps to relate the compressor blade speed to the enthalpy increase. For the axial flow compressor used for the Hyperloop, there will be no change in U through the inlet and outlet of a rotor. The stage load coefficient can be defined by the change of the swirl flow velocity, as shown above [4].

### 3.3.5 Stage flow coefficient

Another useful and strongly influential parameter of the compressible flow machine. In the axial flow compressor, the stage flow coefficient is defined as the ratio of the meridional velocity of the inlet flow and the rotor speed.

$$\Phi = \frac{C_m}{U} \quad (13)$$

Stage flow coefficient also closely relates with the load coefficient. Using some simplifying assumptions, it can be written as:

$$\Psi = \Phi[\tan(\beta_1) - \tan(\beta_2)] \quad (14)$$

Which also relates both of them with the velocity triangle. Meanwhile, the increase of the stage flow coefficient is also means the increase of stage load coefficient. Higher flow coefficient is useful to generate a compressor with smaller dimensions. However, a high flow coefficient means the high rotation speed, which may causes shocks on the air flow. As a result, a typical value for stage flow coefficient is between 0.4 – 0.8 (Dixon 2010) [5].

In the calculation process later, the stage flow coefficient of the first stage is required to be settled. In the design program, flow coefficient 0.65 is chose, which help reduce the engine size, but also avoid the shocks.

### 3.3.6 Stage reaction (Degree of reaction)

Stage reaction, also known as the stage degree of reaction, is the ratio of the static enthalpy rise through a rotor divided by the stagnation enthalpy rise through the whole stage.

$$R = \frac{h_2 - h_1}{h_{03} - h_{01}} \quad (15)$$

The stage reaction has a great influence on the stage efficiency, which related to the stage diffusion. The widely suggested value of the stage reaction is around 0.5. If the ratio is 0, all of the diffusion and static enthalpy rise is from the stator. If the ratio is around 1, all of the diffusion and enthalpy rise is on rotor. The ideal condition is divided the diffusion by both the rotor and stator. As a result, the enthalpy rise can be divided equally by the stator and rotor with  $R = 0.5$ , which can minimize the blade boundary layer and thus reduce the stagnation pressure losses [5].

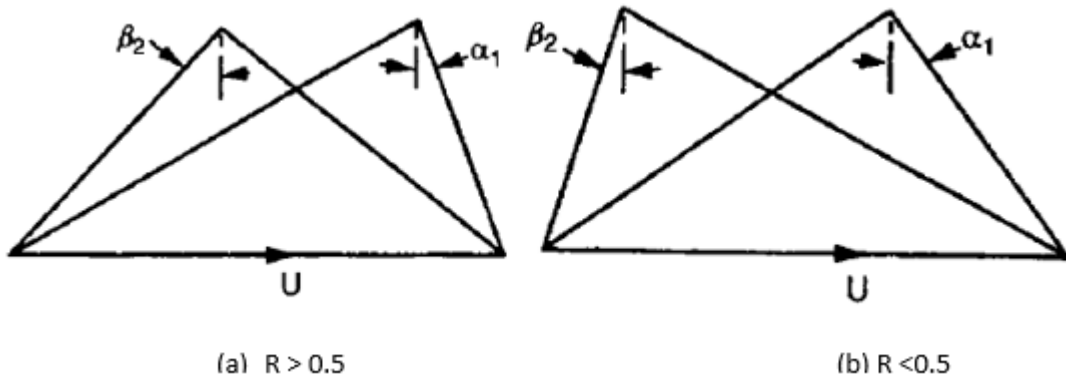


Figure 7: Velocity triangles with different stage reactions

However, the stage reactions are always settled higher in practice, which can help to reduce the whirl for rotors and make it easier to increase the pressure through the rotor. A typical value is in the range 0.5 – 0.8 (Dixon, 2010) [3].

The influence of the stage reaction on the Hyperloop design will be discussed in the later section. In the program, the values of R in all stages will be iterated in a loop to achieve the suitable approximations as the real value of the stage reaction.

### 3.3.7 De Haller number

De Haller number is defined as the rotor deceleration ratio through rotor or stator. It also can be regarded as a simple measure of the amount of diffusion through a row of blades. It can be represented differently in stator and rotor.

$$\text{Stotor: } dH = \frac{W_2}{W_1} \quad \text{Rotor: } dH = \frac{C_2}{C_3} \quad (16)(17)$$

De Haller number is an important parameter in the design of a compressor. Two side effects will greatly influence the deceleration and pressure rise of the flow, which are wall stall and boundary layer growth. To avoid that, de Haller number should be controlled under 0.72, especially for the rotor.

### 3.3.8 Compressor Loss

The compressor losses are due to the unsteady flow and the viscous effects, which can be summarized into profile loss and the end wall loss.

The profile loss is the losses that arise from the blade surface. Because of the effect of blade boundary layer growth, the profile loss causes an increase on entropy and a stagnation pressure loss.

The end wall loss also was called ‘secondary loss’, which is because of the end wall boundary layer, secondary flow and the tip clearance.

The total loss is the summary of the profile and end wall losses. The calculation of the total losses is complicated and far beyond the knowledge that we have. In this design report, the calculation of the compressor loss will use the code of Lund University, which can provide an approximated value of the total losses.

### 3.3.9 Efficiency

To better evaluate the performance of the compressor, isentropic and polytropic efficiencies are calculated here, which are also widely used in the other compressor design and analysis.

#### 3.3.9.1 Isentropic Efficiency

Isentropic efficiency represents the ratio of enthalpy change in an ideal compressor over the actual enthalpy change, where the ideal compressor means both reversible and adiabatic (without any changes in entropy through the compressor). The efficiency can be written as:

$$\eta_{isen} = \frac{h_{02s} - h_{01}}{h_{02} - h_{01}} \quad (18)$$

In practice, because of the entropy increase when the air flow through the compressor, the actually temperature is higher and the power input will be increased to achieve required pressure ratio. As a result, the isentropic efficiency will be lower when we need a high pressure ratio.

#### 3.3.9.2 Polytropic Efficiency

The polytropic efficiency is defined as:

$$\eta_{poly} = \frac{dh_s}{dh} \quad (19)$$

Apply the Gibbs law, and replace the enthalpy with temperature and specific heat. The equation can be rewritten based on temperatures and pressures.

$$\eta_{poly} = \frac{R \frac{1}{p} dp}{C_p \frac{1}{T} dT} \quad (20)$$

After integration:

$$\eta_{poly} = \frac{R \ln(\frac{p_2}{p_1})}{\int_1^2 C_p \frac{1}{T} dT} \quad (21)$$

### 3.3.10 Compressor Type

Three types of axial flow compressors are widely used in the industry and transportations. There are Constant Outer Diameter (COD), Constant Mean Diameter (CMD) and Constant Hub Diameter (CID).

Just as the name, COD has a constant radius of the blade tips. Meanwhile, CMD has a constant root mean square radius and CID has a constant radius of the blade hubs.

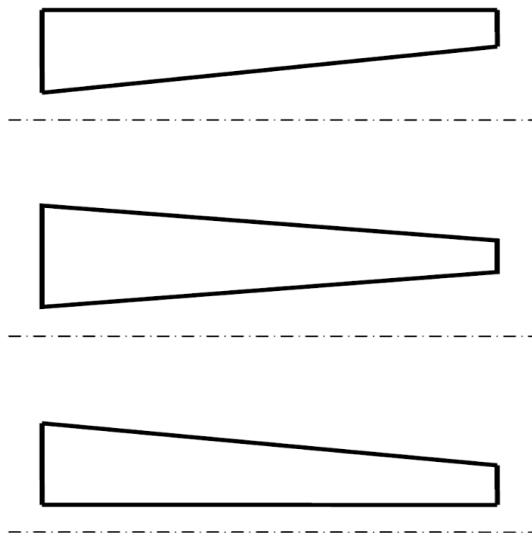


Figure 8: Types of axial flow compressor

Different compressor type will cause the differences in the dimensions, which also influences the compressor performance. In the final result, the performances of these three will be compared, and the one with the best performance and dimensions will be chosen.

### 3.3.11 Mass Flow

In the Hyperloop design, 60% of the air is bypassed, which indicates that 40% of the air in the tube is compressed. The diameter of the Hyperloop tube is known as 2.23 m, which provide a cross-section area  $3.91 \text{ m}^2$ . When the hyperloop reaches the highest speed, the relative velocity of the air to the capsule will be about  $340 \text{ m/s}$ . Consider the truth that the air in the tube is in the condition of  $99 \text{ Pa}$  and  $292K$ , which provide an air density as  $9.69 \times 10^{-4} \text{ kg/m}^3$ . This provide a mass flow for the compressor as:

$$\text{mass flow} = 40\% \cdot \rho A v = 0.57 \text{ kg/m}^2$$

### 3.3.12 Pressure Ratio

As mentioned in the design requirements, the pressure requirement of the outlet air from compressor is  $2.1 \text{ kPa}$ . Compared with the  $99 \text{ Pa}$  inlet pressure, the required pressure ratio is 21.2.

### 3.3.13 Number of Stages

The number of stages depends on the overall pressure ratio need to be achieved through the compressor. The pressure ratio per stage is variable in different use, as shown below [6].

*Table 2: Stage performance in different uses*

Type of Application	Type of Flow	Inlet Relative Velocity Mach Number	Pressure Ratio per Stage	Efficiency per Stage
Industrial	Subsonic	0.4-0.8	1.05-1.2	88%-92%
Aerospace	Transonic	0.7-1.1	1.15-1.6	80%-85%
Research	Supersonic	1.05-2.5	1.8-2.2	75%-85%

In our case, the Mach number of the relative inlet velocity is around 0.99, which is close to the requirement of aerospace application. As a result, the suitable pressure ratio per stage is 1.15-1.6. The stage pressure ratio is increased with the inlet velocity. As the Mach number is 0.99, a suitable stage pressure ratio is assumed to be around 1.4. Based on that, the number of stages is settled as 10 in the program.

### 3.3.14 Rotation Speed

The rotation speed of the blade will influence the blade diameters and compressor efficiency. An initial rotation speed  $5000 \text{ RPM}$  is used. Later the rotation speed will be adjusted to achieve a better design solution.

The rotation speed is the most flexible parameters in the compressor design, which can be in a large range that has a great influence on the performance of the compressor. In the final design section the influence of the rotation speed will be discussed. In the aerospace area, a compressor used on the commercial air jet has a range  $2500 - 5000 \text{ RPM}$ . In the military use, the rotation speed will easily reach  $20,000 \text{ RPM}$ . The rotation speed will be increased gradually in the analysis to achieve a suitable one that can satisfy other requirements.

## 3.4 Blade Geometries

### 3.4.1 Tip Clearance

Tip clearance is the ratio of the gap between the blade tip and the casing over the chord length of the blade tip, which can be written as  $\varepsilon/c$ . To avoid rubbing, this clearance must exist, which links two area with different pressure. As a result, there will be a tip leakage vortex formation. The effect of the clearance will be more significant in the later stages, because the blades will become shorter. Generally, one percent increase of the tip clearance will decrease one to two percent efficiency. In the compressor

design, the tip clearance is settled as 0.02, which is a suitable number to reduce the vortex and also avoid the touches between blade tips and casing.

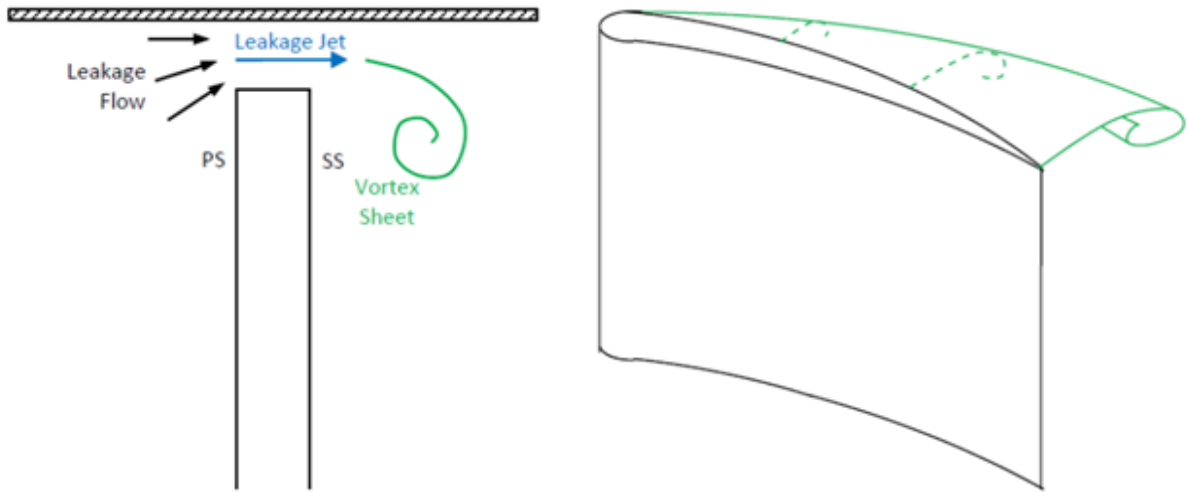


Figure 9: Tip clearance and vortex

### 3.4.2 Aspect ratio

The aspect ratio is defined as the ratio between the blade height and the chord length, which can be written as  $h/c$ . The later stages tend to have a smaller aspect ratio, because the radius of blade tips has a much sharper decrease than the blade hubs, which will reduce the ratio gradually. Meanwhile, the blade of rotor is moving part and being driven by a shaft, which required to be a stronger and has a longer chord, which means a smaller aspect ratio.

In the design, the aspect ratio of rotor is settled to be gradually decreasing in each stage from 2.5 to 1 through the compressor. For the stator this ratio is decreasing from 3.5 to 1.

### 3.4.3 Thickness Chord Ratio

The thickness chord ratio is the ratio between the maximum thickness of the blade and the chord length ( $t/c$ ). As mentioned in the blade geometries section, the blade shape used here is the DCA, in which the thickness, leading and trailing edges is related to the chord length. In the DCA, the thickness and chord ratio should be higher than 5%, lower than that the vibration will increase [3]. In this case the ratio used in the program is chosen as 6%, which can help reduce the vibration and the flutter problems.

### 3.4.4 Axial Velocity Ratio (AVR)

Axial velocity ratio is defined as the ratio of the outlet axial velocity to the inlet axial velocity through a row of blades. This ratio also normally decreases through each rotor. In this design, aiming to achieve a compressor in good performance. This ratio is given as change from 0.99 to 0.97 through the compressor.

### 3.4.5 Blockage Factor (BLK)

The blockage factor here is used to describe the mass flow loss in the compressor through each stage, which also decreases through the compressor. In the design, it is settled to decrease from 0.98 to 0.88 gradually through compressor.

### 3.4.6 Diffusion Factor (DF)

Diffusion factor is usually as an access to the blade loading, which builds a relation between the peak velocities on the suction surface to the velocities of trailing edge.

It can be defined as:

$$DF = \frac{W_{max} - W_2}{W_1} \quad (22)$$

Wright and Miller once built a model to analysis the end wall loss of compressor with diffusion factor, which indicated the typical value of diffusion factor should be around 0.45 for an axial compressor. As a result, DF is settled as 0.45 in the program to achieve better performance in the designed compressor.

## 3.5 MATLAB Coding & Calculation Methods

### 3.5.1 Main Calculation Loop

The calculation theories are based on the work made by Nicals Falck in Lund University. Meanwhile, some changes and adjustments are made to fit our task and design requirements.

The calculation for the whole compressor is complicated and unstable. One change happed in one stage will influence the results of all stages after that. As a result, it is not feasible to calculate the properties and geometries based on one stage. Instead, the program should be able to generate the performances of the whole compressor together, and use a few parameters to restrain the others. To achieve that result, loops and iterations are required to calculate the performance in each stage and also fit the properties of the whole compressor to the settled parameters.

Two parameters used in the design is the stage reaction and the pressure ratio, which must be controlled in required range to satisfy the Hyperloop use and also feasible to be manufactured. The properties and geometries in the rotor will be calculated first in a loop, based on the surrounding temperature, air pressure and the velocity of the Hyperloop. Later the properties will be generate stage by stage, with the rotor loop and stator loop. In the end of the final stage, an OGV loop will be used to generate the outlet results of the compressor. Then the reaction loop will work to iterate until get the approximation of the stage reaction close to reset number. Later the outermost pressure ratio loop will iterate till achieve required pressure ratio. The detailed calculation will be explained in later sections, and the MATLAB code is also shown in the appendix.

The state properties keep changing through the whole compressor, because of the changes of temperature, pressure and flow rate. To achieve the result, the state properties must be easily achieved in the whole calculation. In the program, a MATLAB model according to the Gibbs-Dalton is used.

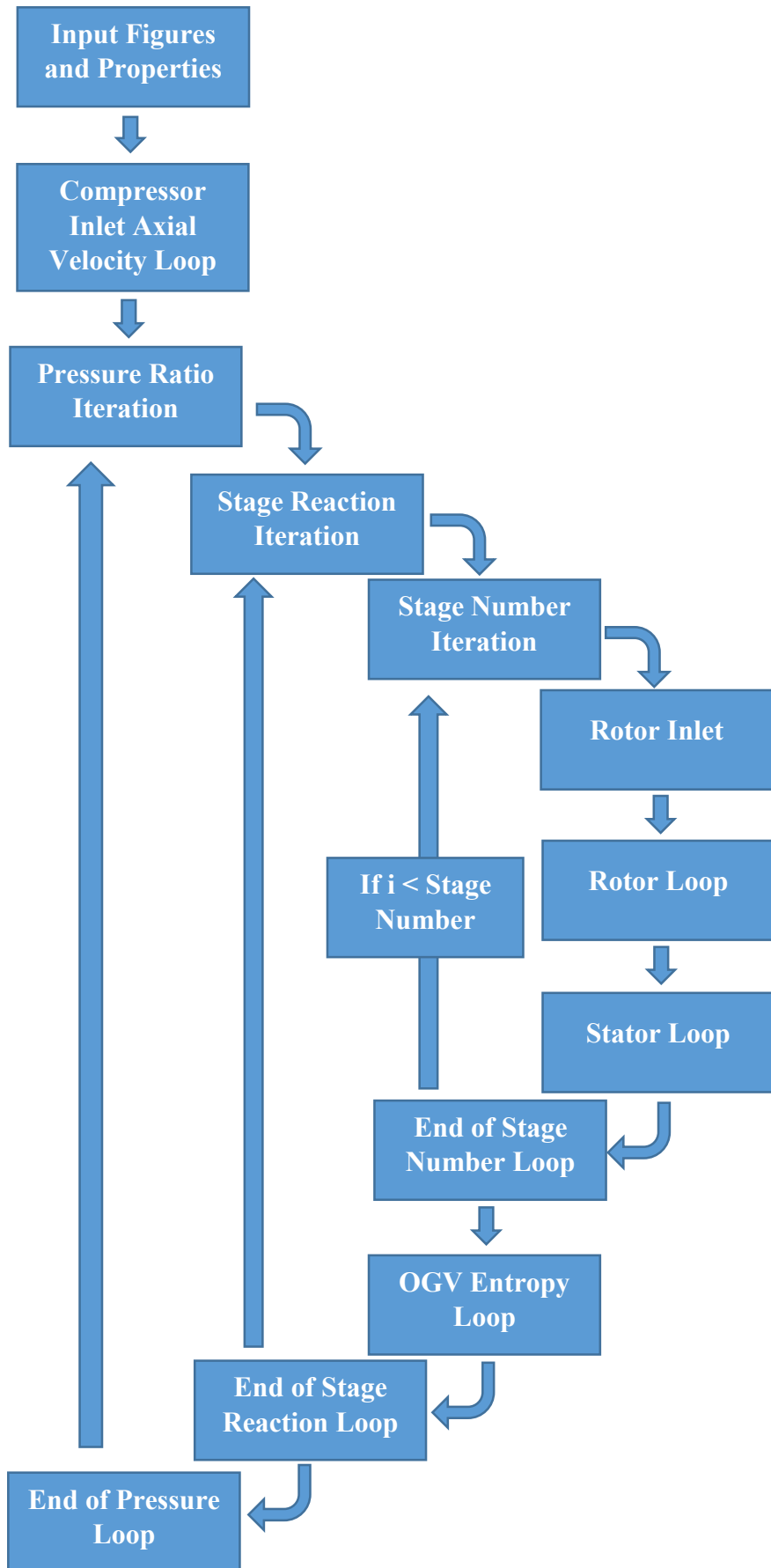


*Figure 10: MATLAB code structure*

### 3.5.2 Input Summary

As discussed in the compressor properties section, several parameters required to design a compressor are settled. The variable parameters include compressor type, number of stages, rotation speed, inlet angle and stage reaction. The details are shown as following.

*Table 3: Input summary*

Compressor Type	CID/CMD/COD	Adjustable
Inlet Pressure	0.00099 [bar]	Settled
Inlet Temperature	19 [Celsius]	Settled
Mass Flow	0.57 [kg/s]	Settled
Pressure Ratio	21	Settled
Number of Stages	9 – 15	Adjustable
Rotation Speed	2500 – 20000 [RPM]	Adjustable
Tip Clearance	0.02	Settled
Aspect Ratio (Rotor)	2.5 → 1	Settled
Aspect Ratio (Stator)	3.5 → 1	Settled
Thickness Chord Ratio	0.06	Settled
Axial Velocity Ratio (AVR)	0.99 → 0.97	Settled
Blockage Factor (BLK)	0.98 → 0.88	Settled
Diffusion Factor	0.45	Settled
Inlet Angle	0 – 35 [degree]	Adjustable
Loading Distribution	1 → 0.8	Auto adjusted
Inlet Hub Tip Ratio (HT)	0.52	Pre set
Stage Flow Coefficient ( $\phi$ )	0.65	Settled
Stage Reaction	0.5 – 0.6	Adjustable

### 3.5.3 Compressor Inlet Calculation

The aim in this section is to figure out the axial velocity of the compressor inlet, based on which we can also calculate out the root mean square (RMS) radius, blade tip radius and blade hub radius of the inlet area.

Flow Properties:

$$\left\{ \begin{array}{l} P_{tube} \\ T_{tube} \end{array} \right. \xrightarrow{\text{state function}} h_{inlet}, s_{inlet}, Cp_{inlet}, \rho_{inlet} \quad (23)$$

In this iteration process, the axial velocity  $C_m$  is given an initial number first. Based on this number, the velocities and radii are achieved, which is used back to achieve a new value for the  $C_m$ . This process is repeated until a suitable value is found.

Velocities and Blade Geometries:

$$area = \frac{\text{mass flow}}{C_m \cdot \rho_{inlet} \cdot BLK} \quad (24)$$

$$r_{tip} = \sqrt{\frac{area}{\pi \cdot (1 - HT)^2}} \quad (25)$$

$$r_{hub} = r_{tip} \cdot HT \quad (26)$$

$$r_{rms} = \sqrt{\frac{r_{tip}^2 + r_{hub}^2}{2}} \quad (27)$$

$$U_{rms} = \frac{2\pi \cdot r_{rms} \cdot RPM}{60} \quad (28)$$

$$C_m(new) = U_{rms} \cdot \phi \quad (29)$$

### 3.5.4 Rotor Inlet

The rotor of the first stage is the first part of the compressor. As a result, the inlet velocities and angles are the same with the inlet specification of the compressor. For the other stages, these properties should be the same with the stator outlet of the stages before that.

First stage properties:

$$\begin{aligned} \text{Compressor Inlet} &\xrightarrow{\text{yields}} r_{1,rms}, C_{m1}, \alpha_1, s_1, h_1 \\ C_1 &= \frac{C_{m1}}{\alpha_1} \end{aligned} \quad (30)$$

$$h_{01} = h_1 + \frac{1}{2} \cdot C_1^2 \quad (\text{stagnation enthalpy}) \quad (31)$$

$$\left\{ \begin{array}{l} h_{01} \xrightarrow{\text{state function}} P_{01}, T_{01} \\ s_1 \end{array} \right.$$

Other stages properties:

$$\text{Stator Outlet of Prior Stage} \xrightarrow{\text{yields}} r_{1,rms}, C_{m1}, \alpha_1, s_1, h_{01}, P_{01}, T_{01}$$

Velocities and flow angles:

$$U_1 = \frac{2\pi \cdot r_{1,rms} \cdot RPM}{60} \quad (32)$$

$$C_{\theta 1} = \tan(\alpha_1 \cdot C_{m1}) \quad (33)$$

$$W_{\theta 1} = U_1 - C_{\theta 1} \quad (34)$$

$$\beta_1 = \arctan\left(\frac{W_{\theta 1}}{C_{m1}}\right) \quad (35)$$

$$C_1 = \frac{C_{m1}}{\cos \alpha_1} \quad (36)$$

$$W_1 = \frac{C_{m1}}{\cos \beta_1} \quad (37)$$

Static properties:

$$\left\{ \begin{array}{l} h_1 \\ s_1 \end{array} \right. \xrightarrow{\text{state function}} P_1, T_1, Cp_1, \rho_1, a_1$$

With the speed of sound  $a_1$  under the pressure and temperature of the rotor inlet, we can get the relative Mach number and axial Mach number.

$$M_{w1} = \frac{W_1}{a_1} \quad (38)$$

$$M_{cm1} = \frac{C_{m1}}{a_1} \quad (39)$$

Relative properties:

For the rotor blade, the dominating velocity is the relative velocity  $W_1$ . To better relate the air flow with the blade work and rotation speed. The relative stagnation properties are required to be calculated, as well as stagnation temperature and pressure.

$$h_{01,rel} = h_1 + \frac{W_1^2}{2} \quad (40)$$

$$\left\{ \begin{array}{l} h_{01,rel} \\ s_1 \end{array} \right. \xrightarrow{\text{state function}} P_{01,rel}, T_{01,rel}$$

As mentioned in the section before, the rothalpy is the only flow properties that does not change through a rotor, which can be written as.

$$I_1 = h_{01,rel} - \frac{1}{2} \cdot U_1^2 \quad (41)$$

Geometries:

$$area_1 = \frac{\text{mass flow}}{C_m \cdot \rho_{inlet} \cdot BLK} \quad (42)$$

Depends on different compressor types, the calculation of the tip, hub and RMS radius will be different. All of them follow the equations down here, and have some changes based on the difference of the constant diameter.

$$r_{rms}^2 = \frac{r_{tip}^2 + r_{hub}^2}{2} \quad (43)$$

$$height_1 = r_{1,tip} - r_{1,hub} \quad (44)$$

$$chord_1 = \frac{height_1}{\text{aspect ratio}} \quad (45)$$

### 3.5.5 Rotor Loop

Rotor loop is used to calculate the properties, velocities and geometries of rotor outlet, which is also the same to the stator inlet, because in our calculation the property changes between blade rows are ignored.

The rotor loop is consisted of two loops. One is the outer enthalpy loop, another is the inner RMS loop. The RMS radius of the rotor inlet can be used as the initial radius of the rotor outlet, which is essential to calculate the velocities and static properties. After that, by calculating the area of the cross-section, a new value of RMS radius will be generated.

Then we can achieve the geometries of the rotor and flow properties through the whole rotor. Wright and Miller's compressor loss model is used here to calculate endwall-losses and profile-losses of the rotor. Then the pressure loss can be achieved, which can also be expressed with an entropy change. The achieved number then is compared with the old one, and replace the old to repeat the iteration. Finally, a suitable number entropy rise number is achieved, and the properties to achieve this number were recorded as the properties of the rotor.

In the first step of the loop, the radius of the rotor inlet is given as the initial value of the rotor outlet, which will be replaced during the iteration of the inner radius loop

$$r_{2,rms} = r_{1,rms} \quad (46)$$

Velocities and flow angles

$$C_{m2} = C_{m1} \cdot AVR_{rotor} \quad (47)$$

$$U_2 = \frac{2\pi \cdot r_{2,rms} \cdot RPM}{60} \quad (48)$$

$$C_{\theta2} = U_2 \cdot \Psi + C_{\theta1} \frac{r_{1,rms}}{r_{2,rms}} \quad (49)$$

$$W_{\theta2} = U_2 - C_{\theta2} \quad (50)$$

$$\alpha_2 = \arctan \left( \frac{C_{\theta2}}{C_{m2}} \right) \quad (51)$$

$$\beta_2 = \arctan \left( \frac{W_{\theta2}}{C_{m2}} \right) \quad (52)$$

$$C_2 = \sqrt{C_{m2}^2 + C_{\theta2}^2} \quad (53)$$

$$W_2 = \sqrt{C_{m2}^2 + W_{\theta2}^2} \quad (54)$$

$$dH_{rotor} = \frac{W_2}{W_1} \quad (55)$$

Where  $\Psi$  is the stage load distribution, and  $dH$  is the De Haller number

Static properties:

An initial number will be given to the entropy rise in the first step, which will be replaced by a more accurate value until the result accurate enough.

$$s_2 = s_1 + \Delta s_{rotor} \quad (56)$$

$$I_2 = I_1 \quad (57)$$

$$h_2 = I_2 - \frac{1}{2} \cdot W_2^2 + \frac{1}{2} \cdot W_1^2 \quad (58)$$

$$\begin{cases} h_2 \\ s_2 \end{cases} \xrightarrow{\text{state function}} T_2, P_2, Cp_2, \rho_2, a_2$$

Mach number:

$$M_{c2} = \frac{C_2}{a_2} \quad (59)$$

$$M_{cm2} = \frac{C_{m2}}{a_2} \quad (60)$$

Relative Properties:

$$h_{02rel} = h_2 + \frac{1}{2} \cdot W_2^2 \quad (61)$$

$$\begin{cases} h_{02rel} \\ s_2 \end{cases} \xrightarrow{\text{state function}} T_{02rel}, P_{02rel}$$

Stagnation Properties:

$$h_{02} = h_2 + \frac{1}{2} \cdot C_2^2 \quad (62)$$

$$\begin{cases} h_{02} \\ s_2 \end{cases} \xrightarrow{\text{state function}} T_{02}, P_{02}$$

Geometries:

$$area_2 = \frac{\text{mass flow}}{\rho_2 \cdot C_{m2} \cdot BLK} \quad (63)$$

$$\begin{cases} \text{compressor type} \\ r_{rms}^2 = \frac{r_{tip}^2 + r_{hub}^2}{2} \xrightarrow{\text{yields}} r_{rms,2} \ (\text{new}), r_{tip,2}, r_{hub,2} \\ area = \pi \cdot (r_{tip}^2 - r_{hub}^2) \end{cases}$$

Rotor Geometries:

$$r_{rotor} = \frac{r_1 + r_2}{2} \quad (64)$$

$$HT = \frac{r_{hub,rotor}}{r_{tip,rotor}} \quad (65)$$

$$height_{rotor} = r_{tip,rotor} - r_{hub,rotor} \quad (66)$$

$$chord_{rotor} = \frac{height_{rotor}}{aspect\ ratio} \quad (67)$$

Reynolds number:

$$Re_{rotor} = \frac{W_1 \cdot chord_{rotor}}{Viscosity_1} \quad (68)$$

Pitch-chord Ratio:

The calculation of the pitch-chord ratio is using diffusion factor method, which can be written as

$$\frac{s}{c} = \left( DF - 1 + \frac{W_2}{W_1} \right) \cdot W_1 \cdot \left( \frac{r_1 + r_2}{|r_2 W_{\theta 2} - r_1 W_{\theta 1}|} \right) \quad (69)$$

Diffusion ratio & Losses:

Diffusion ratio is defined as the ratio of the maximum relative velocity of air flow to the outlet relative velocity.

$$DR = \frac{W_{max}}{W_2} \quad (70)$$

The calculation of this part is using the code made by Niclas Falck and Magnus Genrup of Lund University in 2008. [1]

Meanwhile, the compressor loss calculation here uses the Wright & Miller Compressor Loss Model. The code of this part also used the code from Lund University.

The total loss can be written as:

$$\omega = \frac{\Delta P_0}{P_{01} - P_1} \quad (71)$$

Entropy Increase:

$$\Delta P_{rotor} = \omega_{rotor} \cdot (P_{01rel} - P_1) \quad (72)$$

$$\Delta s_{rotor} (new) = -R \cdot \left( 1 - \frac{\Delta P_{rotor}}{P_{01}} \right) \quad (73)$$

The new value of entropy rise is put back to the calculation of the entropy in the rotor outlet. And the above calculations repeats, until the new entropy is the close enough to the old one from last iteration.

### 3.5.6 Stator Loop

The calculation process of the stator loop is basically same as the rotor loop, where the start properties are the rotor outlet of the stage. There are also two inside loops, as the inner RMS radius loop and the outer enthalpy loop.

The biggest difference between the stator and rotor loop is that the rotation speed of the stator is 0. As a result, the relative velocities will be different as well.

$$velocity_{inlet,rel} = C_2 = C_{m2} \cdot \cos \alpha_2 \quad (74)$$

$$velocity_{outlet,rel} = C_3 = C_{m3} \cdot \cos \alpha_3 \quad (75)$$

Because of the differences on velocity, the calculation of pitch-chord ratio and diffusion ratio are also changed. The relative velocity is equal to the absolute velocity of the air flow.

$$\frac{s}{c} = \left( DF - 1 + \frac{C_3}{C_2} \right) \cdot C_1 \cdot \left( \frac{r_2 + r_3}{|r_3 C_{\theta 3} - r_2 C_{\theta 2}|} \right) \quad (76)$$

$$DR = \frac{C_{max}}{C_3} \quad (77)$$

Meanwhile, the air flow does not receive any energy from the compressor in the stator section. Instead of rothalpy that is not useful in stator anymore, the stagnation enthalpy will be stable through stators, which builds a connection between the inlet and outlet.

$$h_{03} = h_{02} \quad (78)$$

$$h_3 = h_{03} - \frac{1}{2} \cdot C_3^2 \quad (79)$$

Except the changes above, the calculations and loops are basically the same with the ones in the rotor loop. The detail of the calculation can be seen in the MATLAB model in appendix.

### 3.5.7 Outlet Guide Vane (OGV) Entropy Loop

An OGV can be regarded as an extra stator after the final stage of compressor, which is used to change the flow rate to axial, because the whirl velocity will cause disturbance in the latter intercooler system of the Hyperloop.

The OGV Loop only contains an entropy loop, because the dimensions of the whole vane are the same with the outlet dimensions of the stator in final stage.

$$r_{OGV} = r_3 \quad (80)$$

A well designed OGV will eliminate the whirl velocity, which means the outlet velocity of the OGV is only axial and can be written as

$$C_{OGV} = C_{m,OGV} = C_{m3} \cdot AVR_{OGV} \quad (81)$$

Most calculations of OGV are also the same with the ones of stator, except the change that

$$C_{\theta OGV} = 0 \quad (82)$$

More detail can be achieved from the MATLAB model in the appendix.

### 3.5.8 Stage Reaction Loop

The stage reaction is used to represent the ratio of the work done by rotor to the work done by the whole stage, which is also strongly related to the inlet and outlet flow angle. Because the work is related to the enthalpy, as shown in the equations below, which is dependent on the absolute velocity. As calculated before, the absolute velocity is decided by the absolute flow angle. As a result, the stage reaction can be adjusted to the desired number by the convergence of outlet angle,  $\alpha_3$ .

In the following calculations,  $(i)$  represents the stage number.

$$R(i) = \frac{h_2(i) - h_1(i)}{h_{03}(i) - h_{01}(i)} \quad (83)$$

To converge the stage reaction, by using the Newton-Raphson Method, the slope can be related to the flow and blade velocities.

$$slope(i) = \frac{C_{m1}(i)}{U_1(i)} \cdot AVR(i) \cdot \frac{\pi}{180 \cdot \cos(\alpha_3^2(i))} \quad (84)$$

$$error(i) = R(i) - R_{desired} \quad (85)$$

$$\alpha_3(i-1) = \alpha_3(i-1) + 0.8 \cdot \frac{error(i)}{slope(i)} \quad (86)$$

The new value of the outlet angle will be achieved for each stage. The new angles are put back the properties of each stages. This process repeats until the reaction stage close enough to the desired value.

### 3.5.9 Pressure Ratio Loop

The pressure ratio loop works in the similar way as the stage reaction loop. The difference is the pressure ratio is adjusted by the convergence of stage load coefficient. Because the load coefficient is settled in the beginning, to achieve the slope, the whole system is supposed to have two different value for the stage load coefficient through the whole calculation. However, this difference should be very small to achieve more correct result.

$$\Psi(2,:) = 1.01 \cdot \Psi(1,:) \quad (87)$$

$$PR = \frac{P_{OGV}}{P_{inlet}} \quad (88)$$

$$slope = \frac{PR_1 - PR_2}{average[\Psi(1,:) - \Psi(2,:)]} \quad (89)$$

$$error = PR_{desired} - PR_1 \quad (90)$$

New values of stage load coefficient for iteration

$$\Psi(1,:)_{new} = \Psi(1,:) + 0.95 \cdot \frac{error}{slope} \quad (91)$$

$$\Psi(2,:)_{new} = 1.01 \cdot \Psi(1,:)_{new} \quad (92)$$

### 3.5.10 Blade Angle Loop

In the above calculation, flow properties and most of the blade dimensions are calculated, except blade angles. Incidence angle and deviation angle are two main geometries that relate the blade angle to the inlet and outlet flow angle.

Incidence angle is the angle difference between the inlet flow angle and blade angle, which can be represented as

$$i = K_{sh} \cdot K_{it} \cdot i_{010} + 10 \cdot (M_{rel} - 0.7) + n \cdot \theta$$

As mentioned before, the chosen blade type is DCA, which means  $K_{sh} = 0.7$ .

$$K_{it} = -0.0214 + 19.17 \cdot \frac{t}{c} - 122.3 \cdot \left(\frac{t}{c}\right)^2 + 312.5 \cdot \left(\frac{t}{c}\right)^3$$

In this case,  $\frac{t}{c}$  is known as the thick-pitch ratio, which is an input parameter that can be used directly.

$$i_{010} = (0.0325 - 0.674\sigma) + (-0.002364 + 0.0913\sigma) \cdot \alpha_1 + (1.64 \times 10^{-5} - 2.38 \times 10^{-4} \cdot \sigma) \cdot \alpha_1^2$$

$$n = (-0.063 - 0.02274 \cdot \sigma) + (-0.0035 + 0.0029 \cdot \sigma) \cdot \alpha_1 - (3.79 \times 10^{-5} + 1.11 \times 10^{-5} \sigma) \alpha_1^2$$

where  $\sigma$  is the solidity, as the reverse of pitch-chord ratio

Deviation angle is the angle difference between the outlet flow angle and the blade angle of the trailing edge, which can be represented as

$$\delta = K_{sh} \cdot K_{\delta t} \cdot \delta_{010} + m \cdot \theta$$

$$K_{\delta t} = 0.0142 + 6.172 \cdot \frac{t}{c} + 36.61 \cdot \left(\frac{t}{c}\right)^2$$

$$\delta_{010} = (-0.0443 + 0.1057\sigma) + (0.0209 - 0.0186\sigma) \cdot \alpha_1 + (-0.0004 + 0.00076\sigma) \cdot \alpha_1^2$$

$$m = \frac{m'}{\sigma^b}$$

$$b = 0.9655 + 0.002538\alpha_1 + 4.221 \times 10^{-5} \cdot \alpha_1^2 - 1.3 \times 10^{-6} \cdot \alpha_1^3$$

$$m' = 0.249 + 7.4 \times 10^{-4} \cdot \alpha_1 - 1.32 \times 10^{-5} \alpha_1^2 + 3.16 \times 10^{-7} \alpha_1^3$$

## 3.6 Final Design and Final Result Analysis

As mentioned in the design requirement section, the Hyperloop Alpha made some expectations on the pressure, temperature, compressor dimensions and required power. However, the real design may not totally fit these expectations, considering there will be energy loss during the whole compressor that includes the profile losses of the compressor itself and the end wall losses. These side effects will greatly reduce the compressor efficiency and also produce more heat, which will change the outlet temperature and the flow rate through the compressor.

However, comparing all of the expectations, there are several figures that is necessary to satisfy, which will be considered first in the final compressor design. These parameters includes the maximum diameters of the compressor, mass flow and the outlet pressure.

The diameters of the compressor and the mass flow is decided by the dimensions of the whole capsule and the dimensions of the tube, which are settled by the Hyperloop Alpha design. In this report, our test is to generate a robust aero dynamic system that is suitable in the Hyperloop Alpha. So these figures must be fixed.

The outlet pressure also needs to be fixed, because the air flow is later used in the air cushion section, which must be enough to support the weight of the capsule. So the pressure cannot be smaller than the requirement of the air cushion.

Meanwhile, there are some parameters that might be able to adjust in the further design to meet the requirements. The outlet flow will be cooled in the inter-cooling system. As a result, even the outlet temperature is higher than expectation, it is still feasible by changing the cooling system. However, that may cause the change of the dimensions of the whole system.

To meet the other requirements, the input power is not considered as a parameter in the compressor design. However, the required power will be discussed after the design and try to approach the expectation, which is extremely small in for the Hyperloop design.

### 3.6.1 Property Optimization

There are several adjustable figures in the compressor model that can be adjust to generate a higher effective compressor. This section will discuss the influences of them each on the design requirements, which helps us to come out the final design in the next section.

In the later discussion, one input parameter is changes when the others are given a settled number, which will show the relations between the changeable parameters and the design requirements.

#### 3.6.1.1 Number of Stages

As discussed in the input figure section, the number of stages should be around 9 in the Hyperloop design. However, trying to achieve the best design, the number of stages is also adjusted from 7 to 15, which provide a bigger choice range and help us to make a better choice.

The first consideration is the diameter of the compressor. However, after calculations from the program, the diameter is not influenced by the change of the stage number as long as the compressor type is not changed. So the diameter does not need to be considered in this section.

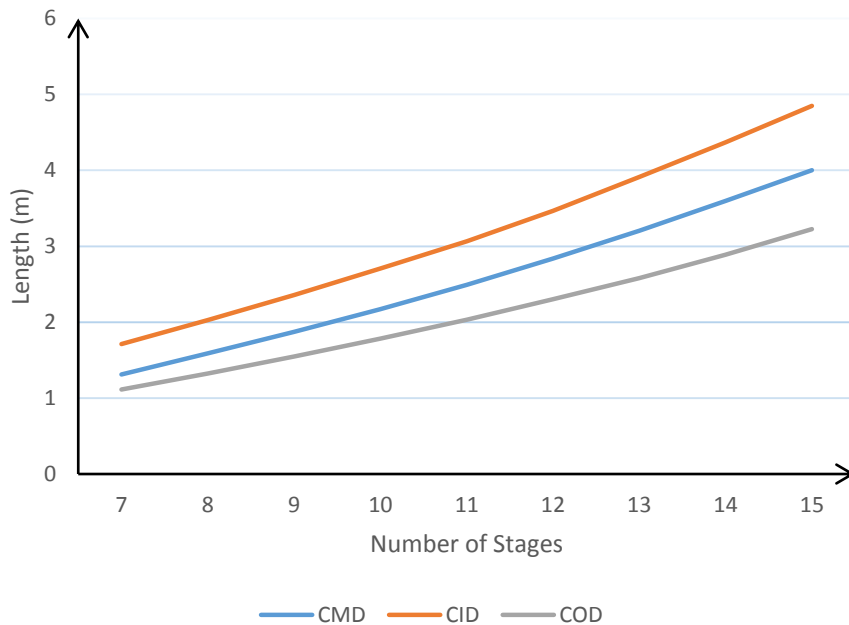
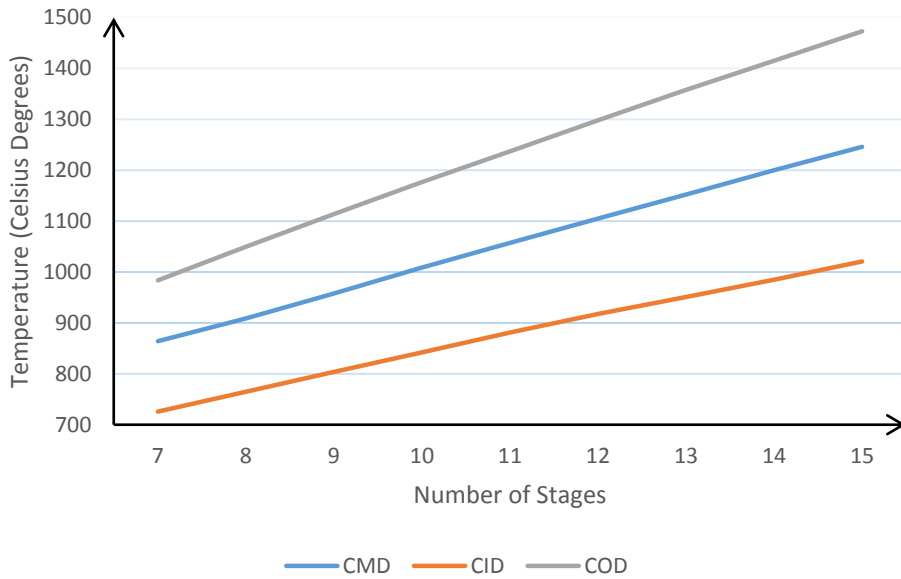


Figure 11: Compressor Length Vs the Number of Stages

In the Hyperloop design, the length of the capsule is designed to be as short as possible, which can help to reduce the overall weigh, simplify the design of the air cushion and also make it easy when the tube is bend in an angle. As a result, the length of the capsule is also an important design parameter in the design. As shown in the Figure 11, with the increase of the stage number, the required length for the compressor will increase, which will cause the increase of the overall length of the capsule. For this consideration, the number of stages should be controlled as small as possible.



*Figure 12 Outlet Temperature of the Compressor Vs the Number of Stages*

As shown in the Figure 12, the outlet temperature will increase with the stage number. A smaller outlet temperature is preferred, which can reduce the complication and the dimension of the intercooling system after compressor.

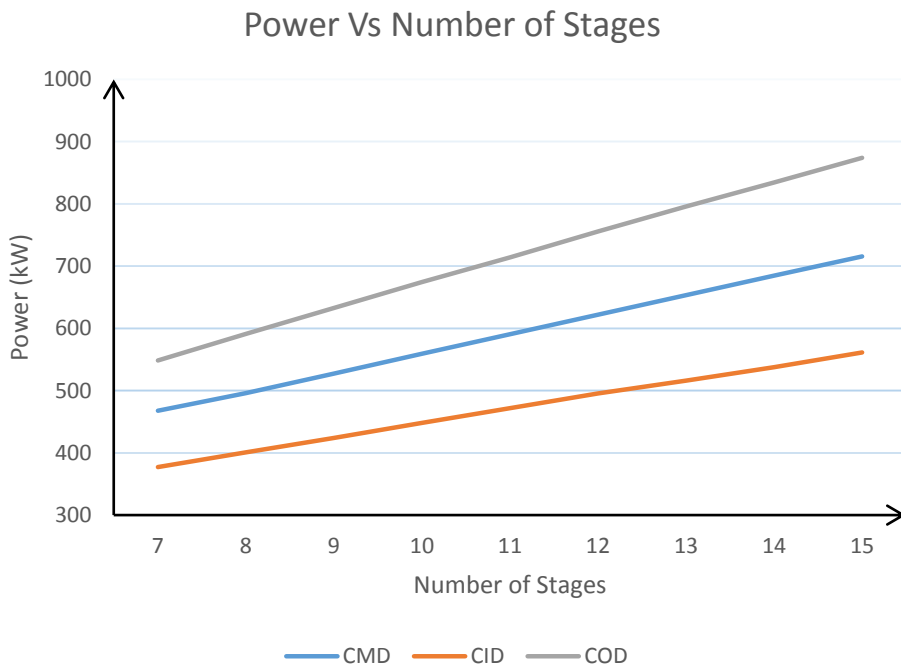


*Figure 13 Power Input of the Compressor Vs the Number of Stages*

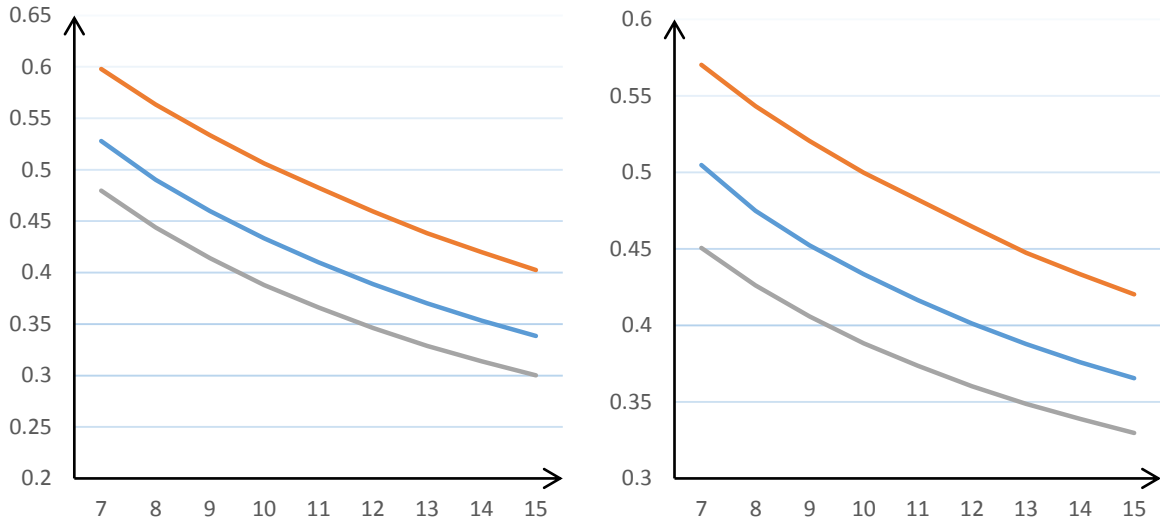


*Figure 14 Isentropic and Polytrophic Efficiency Vs the Number of Stages*

The Figure 13 and Figure 14 shows the changes of the power, isentropic efficiency and polytrophic efficiency with the stage number. It is easy to be understood that the increase of the power also means the decrease of the efficiency, because the pressure ratio is equal.

In a sum, considering from the all requirements, a smaller number of stages is preferred. However, for the realistic consideration of the pressure rise each stages and the blade angles requirements, the number of stages cannot be unlimited small. To achieve the overall pressure ratio around 21 as the Hyperloop design required, the number of stages is chosen as 7.

### 3.6.1.2 Rotation Speed

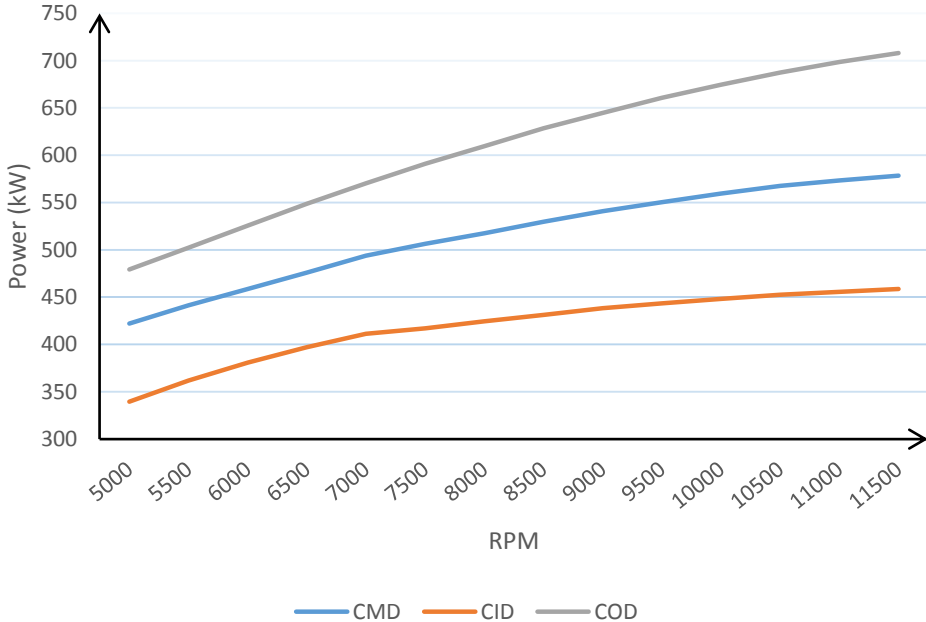


*Figure 15 Input Power Vs Rotation Speed of the Compressor*

As shown in the Figure 15, the required power for the compressor is reduced when the rotation speed is lower. In the consideration about the energy, lower rotation speed is preferred.

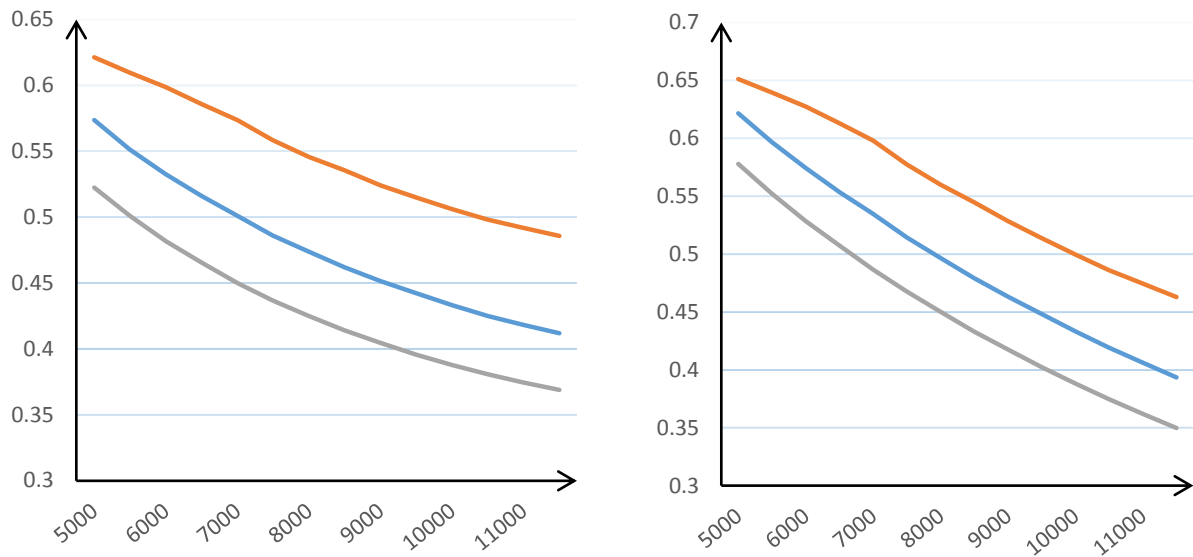


Figure 16 Isentropic and Polytrophic Efficiency Vs Rotation Speed

As expected, the efficiencies work in the counter way with the input power, which will decrease with a higher rotation speed.

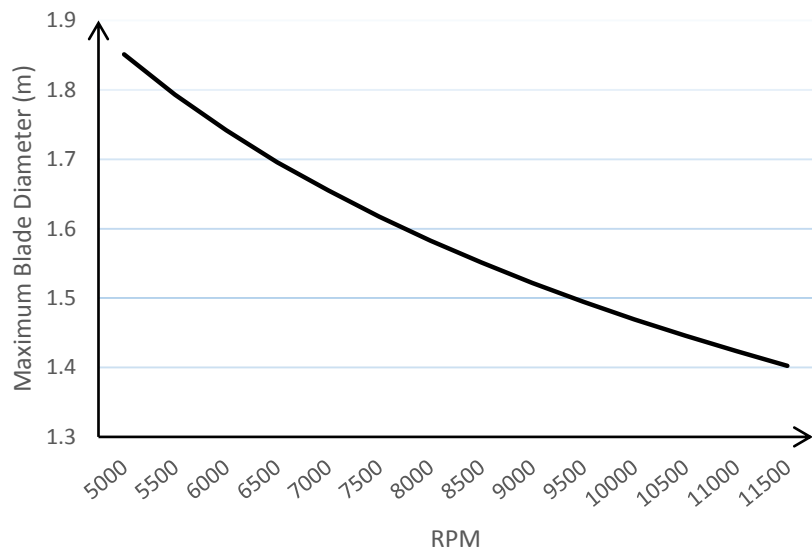


Figure 17 Diameter of the Compressor's Cross-section Vs Rotation Speed

As indicated in the Figure 17, the diameter will be bigger with a smaller rotation speed to help the air flow achieving required speed increase. So only consider from the diameter, the higher rotation speed will reduce the compressor dimension.

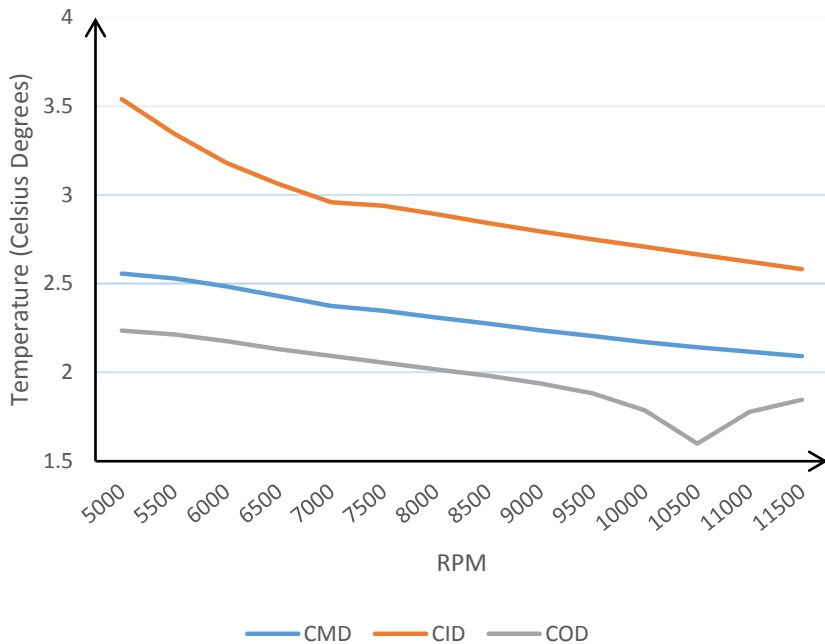


Figure 18 Outlet Temperature Vs Rotation Speed

As shown in Figure 18, a higher rotation speed will generate less heat, which can reduce the dimensions of the intercooling system.

Overall, a smaller Rotation speed can reduce the energy loss. However, the speed must be high enough to keep the diameter of the compressor smaller than 1.1 m.

### 3.6.1.3 Inlet Angle

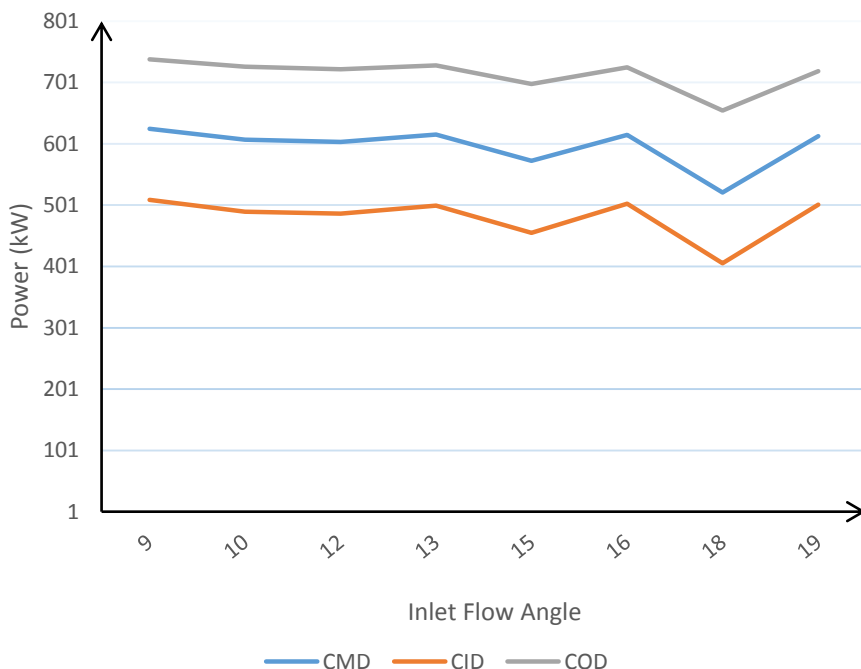


Figure 19 Input Power Vs Inlet Flow Angle

As shown in the Figure 19, the influence of the inlet angle is not regular. Also the main result of this change is the first stage. In the later stages, the inlet flow is decided by the stage before. Even the best inlet angle cannot be find out, a smaller angle is preferred because this angle is achieved ab the Inlet Guide Vane (IGV). A smaller angle can reduce the demands on IGV and also make the system more stable. So the inlet flow angle is chosen as 15 degrees.

### 3.6.1.4 Stage Reaction

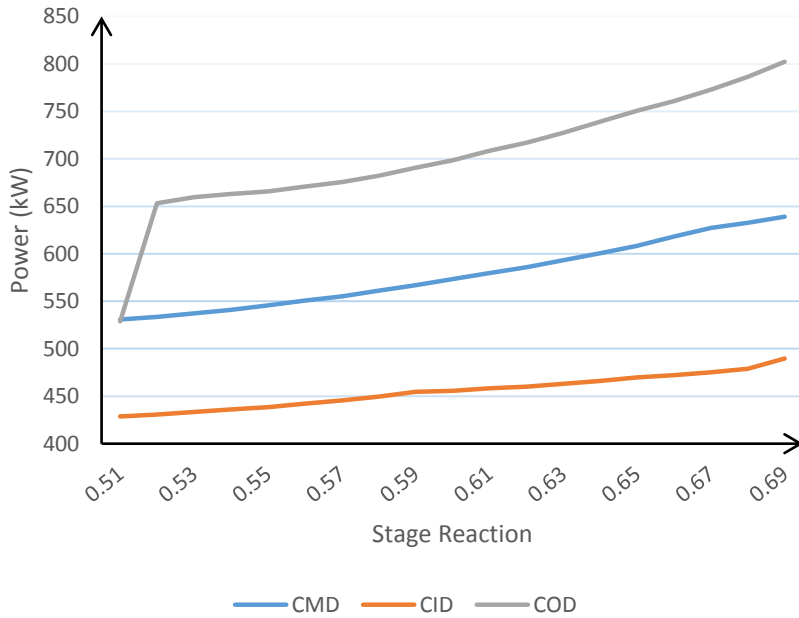


Figure 20 Input Power Vs Stage Reaction

As shown in Figure 20, smaller stage reaction can save the input energy, which is preferred for this consideration. In sum, a smaller stage reaction is preferred, mainly because the consideration of energy, which is extremely limited in the Hyperloop Alpha design.

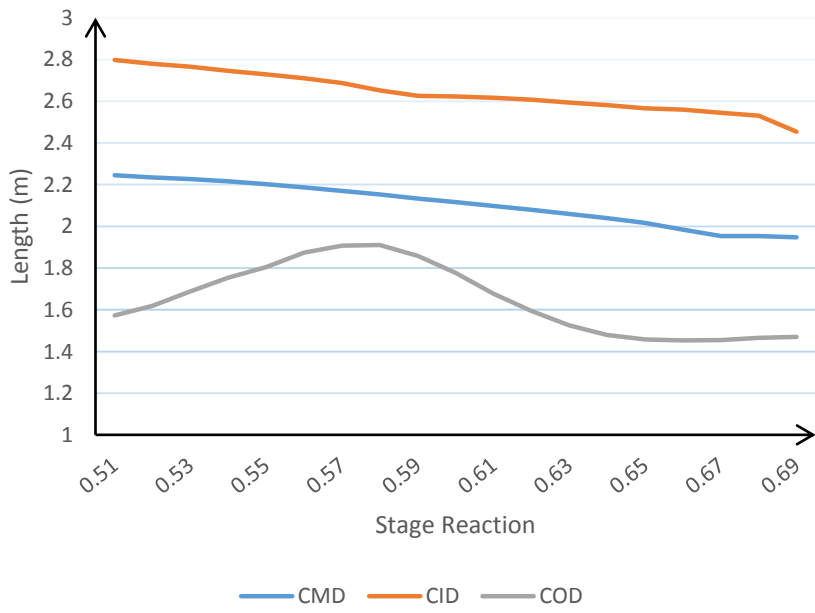


Figure 21 Length of the Compressor Vs Stage Reaction

After simulating in the program, the diameter is not influenced by the stage reaction. However, the length of the compressor is basically reduced with increase of stage reaction, which is also important to reduce the compressor dimension.

### 3.6.1.5 Compressor Type

The influence of the compressor types is already shown in the graphs of the sections above. The Constant Hub Diameter (CID) seems to be the best choice, which has less power requirements, higher efficiencies and smaller diameters in the similar condition. Even though CID design has a bigger length and higher output temperature, the main requirements as the diameter and input power suggest that CID is the best compressor type choice here.

### 3.6.2 Final Design

#### 3.6.2.1 Overall Input Parameters

As discussed above, in the Hyperloop compressor design, CID is the compressor type. The rotation speed must be high enough to keep the diameter smaller than 1.1m. Meanwhile, the stage reaction and number of stages is better to be smaller.

After simulating several times, to achieve the required diameter, the rotation speed should be around 13000 RPM at least. Under this speed, the pressure ratio and stage reaction cannot be too smaller for the considerations of the blade geometry. Smaller stage number will increase the pressure ratio per stage, which will increase the difficulty of manufacturing the blade angles and reduce the intensity of the compressor. As a result, the stage reaction is chosen as 0.56, and the number of stages is 10. The optimized input parameters as shown following:

*Table 4: Input parameters*

Compressor Type	CID
Inlet Pressure	0.00099 [bar]
Inlet Temperature	19 [Celsius]
Mass Flow	0.57 [kg/s]
Pressure Ratio	21
Number of Stages	10
Rotation Speed	13000 [RPM]
Tip Clearance	0.02
Aspect Ratio (Rotor)	2.5 → 1
Aspect Ratio (Stator)	3.5 → 1
Thickness Chord Ratio	0.06
Axial Velocity Ratio	0.99 → 0.97
Blockage Factor	0.98 → 0.88
Diffusion Factor	0.45
Inlet Angle	15 [degree]
Loading Distribution	1 → 0.8
Inlet Hub Tip Ratio	0.52
Stage Flow Coefficient	0.65
Stage Reaction	0.56
Overall Length	2.644]

### 3.6.2.2 Design Performance

After the calculation the program, a few important design properties are as shown below. Meanwhile, the detail design geometries and properties was put in appendix.

As we can see, to achieve the required pressure under the small diameter. The power input will be much larger than the expectation in the Hyperloop Alpha.

*Table 5: Design performance*

Diameter of the Compressor	1.0868 [m]
Outlet Pressure	20.8 [kPa]
Outlet Temperature	1133.68 [K]
Power	432.5531 [kW]
Isentropic Efficiency	48.24%
Polytrophic Efficiency	43.02%
Outlet Flow Velocity	322.54 [m/s]

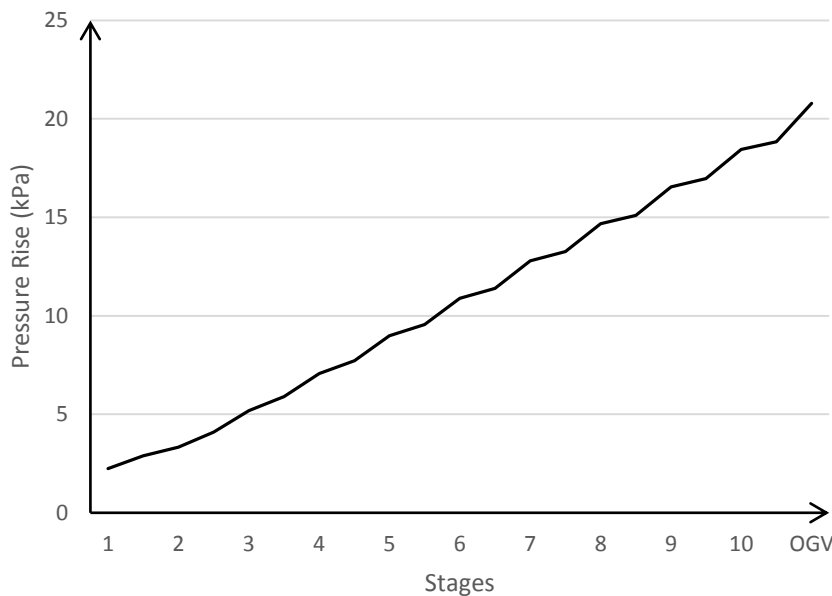


*Figure 22 Pressure of Air Flow through the Compressor*

The pressure rise is as shown in the Figure 22. The pressure rise is steeper through a stator than the rotor, because the rotor do more work on increase the kinetic energy, which later is converted into the potential energy of the air with higher pressure through stator.

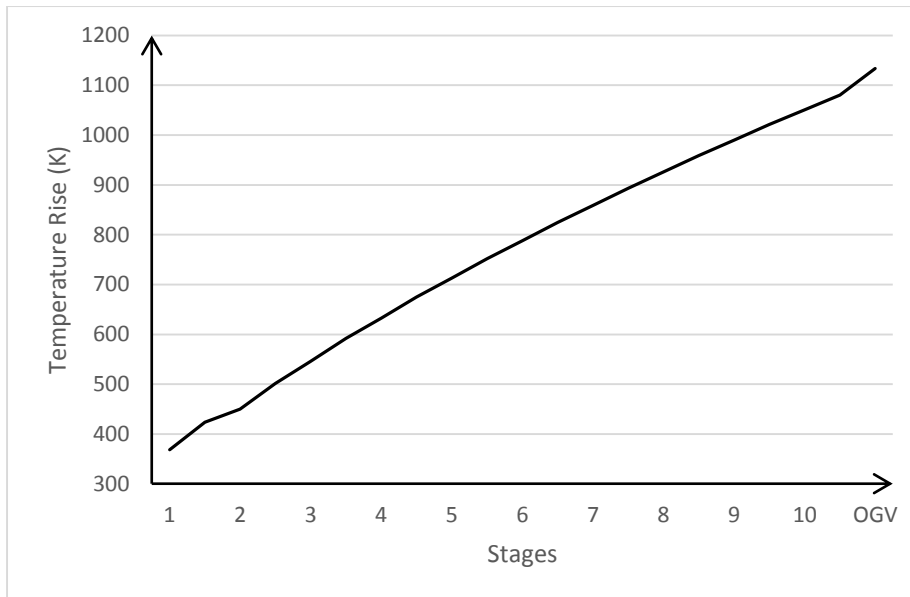


Figure 23 Temperature Rise through Compressor

The temperature will keep increasing through the whole system to 1133.68 K, because of the entropy increase.

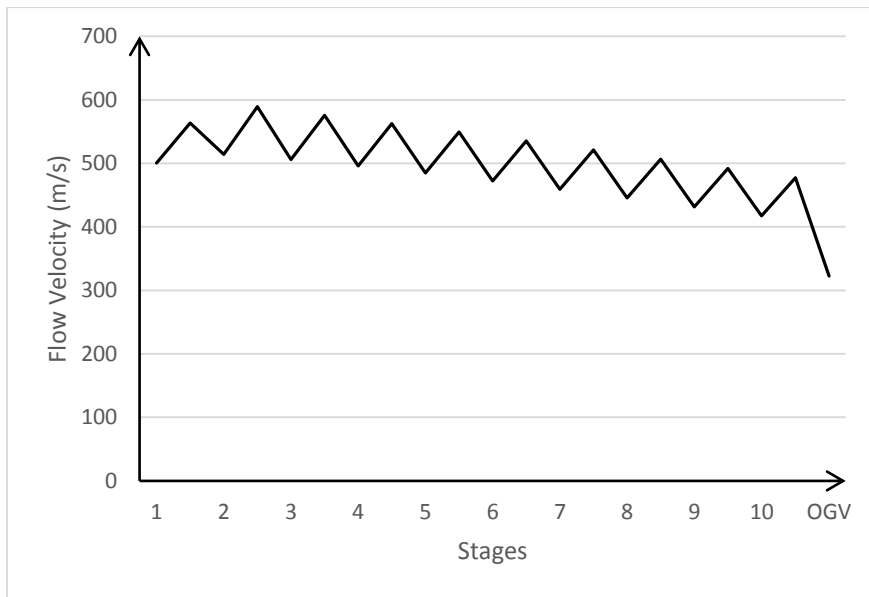


Figure 24 Absolute Flow Velocity through the Compressor

Even though the rotor will increase the flow velocity, which is later converted into potential energy by the stator, the axial flow velocity will still decrease through the compressor by loss, which is represented by the Axial Velocity Ratio (AVR). As a result, the flow velocity tends to decrease overall. The outlet flow velocity will be 322.54 m/s.

### 3.6.2.3 Discussion

The power consuming of the final design is much higher than the expectation in the Hyperloop Alpha design. The main reason is the high rotation speed. As discussed in the design optimization, to keep the diameter within the range, a high rotation speed is necessary, which will decrease the efficiency because of the increase of profile losses and end wall losses. As a result, the power input must be increased as well.

The first possible solution here is to design a better performance on-board battery that is enough to drive the compressor with 432 kW power input. However, this solution maybe not feasible because this change may also increase the overall capsule weight, which might be not fitted with the air suspension system.

Another solution is redesign the dimensions of the tube and the capsule. A bigger cross-section will reduce the rotation speed and increase the efficiency of the compressor. However, as mentioned, this will also increase the weight of the capsule.

If this problem is solved, the Computational Fluid Dynamics (CFD) can be used to generate the fully detailed compressor.

## 4. Heat Exchange System

The compression system proposed by Musk makes use of intercoolers, these cool down the air in between the different compression stages. This cooling of the air reduces its specific volume meaning that the second stage of compression deals with less air, effectively reducing the power consumption. The more heat that can be extracted from the air, the lower the power consumption of the compressor. The design of this system therefore can have a very significant effect on the energy economics of the hyperloop over its lifetime.

According to Kakaç and Liu (1998) [7], heat exchangers can be classified in terms of four different aspects:

- Regenerator vs recuperator
- Direct vs indirect contact
- Single phase vs two phase
- Tube and shell vs plate

The first bullet point is related to the exchanger's heat transfer mechanisms. In a regenerator, the hot fluid first transfers its heat to a thermal mass, this is then followed by the cold fluid which absorbs the heat from the mass, two distinct operations. A recuperator allows for continuous heat transfer from the hot fluid to the cold as a single ongoing operation.

Heat exchangers can also be classified into direct or indirect contact and single or two phase flow. Direct contact heat exchangers involve the physical mixing of the two fluids during the heat exchange. This can be done by, for example, spraying hot air with a mist of water droplets in a cooling tower. The main advantage this form of heat exchange has is that the resistance to heat transfer is much lower. Indirect contact exchangers involve transferring heat through a conducting material separating the two fluids, this is obviously useful when the two fluids need to be separate.

The transfer of heat can occur over one phase which remains constant from one end of the exchanger to the other, or it can occur over two separate phases in one or both of the fluids. Phase changes are advantageous in the cold fluid because heat transfer and temperature drop in the hot fluid occur while the cold fluid remains at constant temperature. This is useful because the exit temperature of the hot fluid cannot be lower than the exit temperature of the cold fluid. However, if the cold fluid temperature were to remain constant, instead of rising, as the hot fluid cools down, the hot fluid's temperature has the potential to drop even further than would've otherwise been possible.

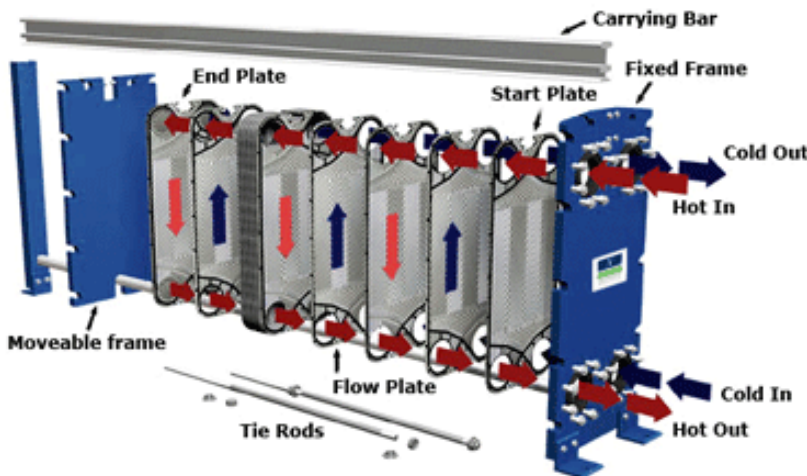


Figure 25: Plate heat exchanger [8]

due to their increased contact surface area and increased turbulence allowing for more exchange of energy. The heat transfer path between the fluids also has a much smaller thermal resistance due to the minuscule thickness of the plates. For these reasons, they also take up much less space as they're more effective. They are also more suited to lower pressure differences between the fluids and environment.

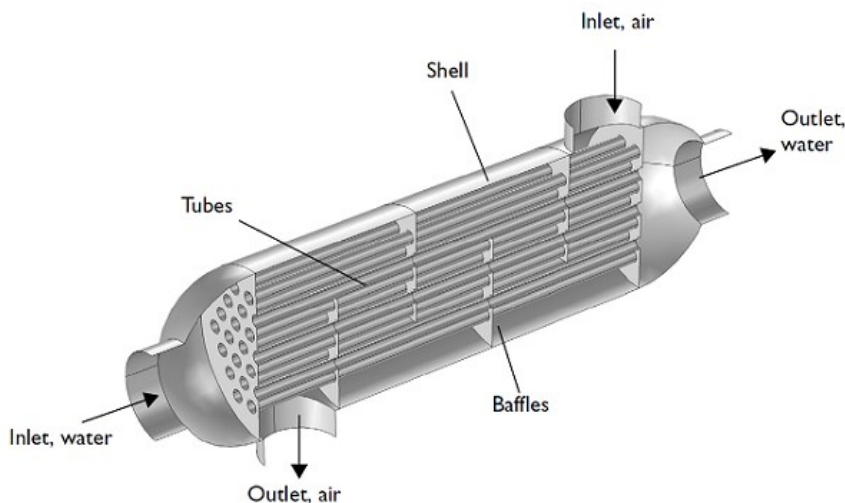


Figure 26: Shell and tube heat exchanger [9]

The remaining classification is to do with the geometry of the exchanger; it can either be a tube and shell or a plate exchanger. Plate heat exchangers consist of several tightly packed plates where the hot and cold fluids flow in an alternating pattern through the plates and in opposite directions. This can be seen in figure X. They are much more efficient than their shell and tube counterparts

Shell and tube heat exchangers on the other hand consist of several tubes carrying cold fluid inside a shell carrying the hotter fluid or vice versa. The tube arrangement, number of fluid passes and amount of baffling are some of many variables that affect the exchanger's heat transfer efficiency and will be discussed individually in the next section.

## 4.1 Specification

In the case of the hyperloop pod, the spatial considerations as well as the very short time it takes the air to move through the compression system means that the regenerator's mechanism of storing the heat in a thermal mass for consequent transfer to the water isn't an option; the recuperator mechanism will be used instead. Heat will be transferred via indirect contact because cooling the dry air by getting it in direct contact with water will increase the air's humidity. This would be a problem as not only is the air used to levitate the pod on skis, it is also used to maintain atmospheric pressure inside the pod. Over time the damp air released in the hyperloop tube would degrade the compressor's rotor blades, the vacuum pumps and the linear induction motor rails.

The water will experience a change of phase during the heat transfer cycle, this can be proved by making a rough calculation of the numbers from the proposal. If we assume the air cools down from 857K to 293K in the exchanger after the first compression, the energy lost by it can be calculated using:

$$Q = C_p m(T_{hot} - T_{cold}) \quad (93)$$

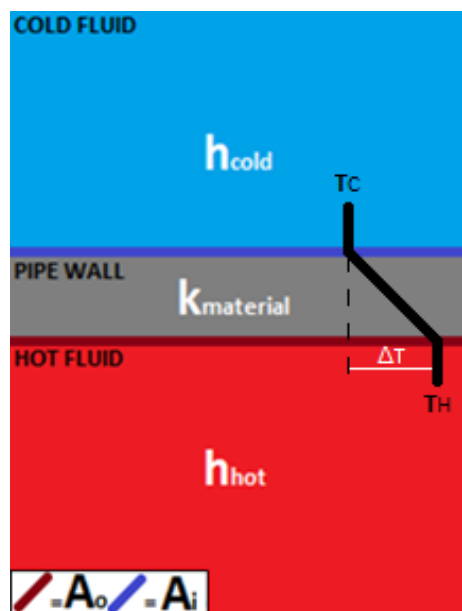
This gives an energy loss of 332 kJ/s if we assume air to have a specific heat capacity of 1.2. In order for water to reach its boiling temperature from 293K, it must absorb 47 of the 332 kJ/s leaving 285 kJ/s to be absorbed as it boils. In order for 0.14 kg of water to boil it needs to absorb another ( $0.14 \times 2257$ ) 315.98 kJ/s which is more than the 285 kJ/s left from the air. This means that in the extreme case where the water absorbs all of the heat from the air, it would exit the heat exchanger as a saturated mixture of liquid and vapour.

Plate heat exchangers would be a huge advantage for this application due to their smaller size and efficiency, however the same reasons that make it a more effective exchanger also make it unsuitable for this task. The very thin plates mean thermal resistance is significantly reduced but the air would be moving at several times the speed of sound in such a small cross sectional area which would again result in choked flow. This time however a compressor cannot be installed to fix the problem. A well designed shell and tube heat exchanger will have to do.

## 4.2 Shell and Tube Heat Exchanger Design

Before discussing the variables which affect heat transfer rates, it would help to go through the mathematical and thermodynamic theory behind heat exchangers. The most important number associated with heat exchange is the overall heat transfer coefficient  $U$ . This is found by considering the convective heat transfer coefficients of each fluid flow, the thermal resistance of the material separating them as well as the heat exchange surface areas. The different resistances are added together much like those in an electrical circuit, this can be seen in equation 94 below.

$$\frac{1}{UA_o} = \frac{1}{R_{Total}} = \frac{1}{R_{cold}} + \frac{1}{R_{pipe}} + \frac{1}{R_{hot}} = \frac{1}{h_{cold}A_i} + \frac{\ln\left(\frac{r_o}{r_i}\right)}{2\pi kL} + \frac{1}{h_{hot}A_o} \quad (94)$$



Where  $A_i$  is the inner surface area of the pipe,  $A_o$  is the outer surface area,  $k$  is the thermal conductivity of the pipe material,  $L$  is the pipe length and  $r_i$  and  $r_o$  are the inner and outer radii of the pipe respectively.

The surface areas  $A_o$  and  $A_i$  depend on the pipe diameter and length, the longer the pipes the more surface there is for heat exchange. The relationship isn't as easy with pipe diameter however as increasing the diameter means more pipe surface area, but fewer pipes that can fit within the exchanger as each pipe occupies more space. Increasing the thickness of the pipe increases the available surface area, but also increases the thermal resistance from the pipe material. In general, it is good to minimise the pipe thickness as this reduces the insulation between the two fluids. Logically, the pipe material itself will therefore also affect the resistance depending on its conductive capabilities.

Figure 27: Resistance in heat

The more tubes inside the shell, the better the heat transfer coefficient as the surface area gets multiplied by the amount of tubes available. The number of tubes depends on the way they are arranged together and the gap between the pipes. The pipes can either be arranged in a triangular 30°/60° layout or in a

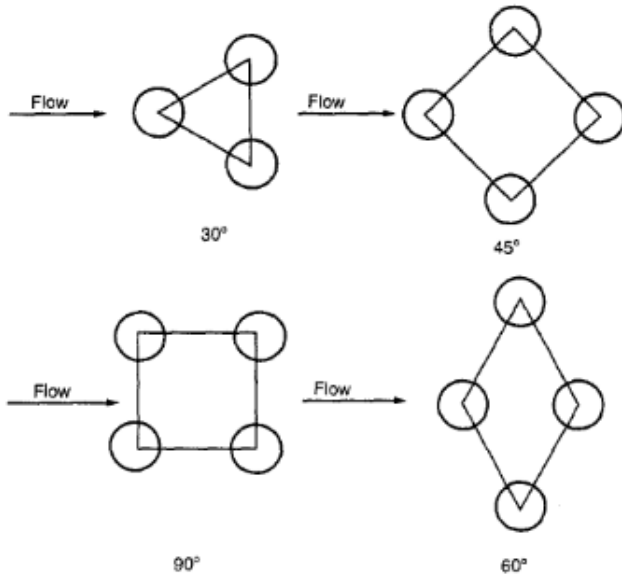


Figure 28: Tube configurations [7]

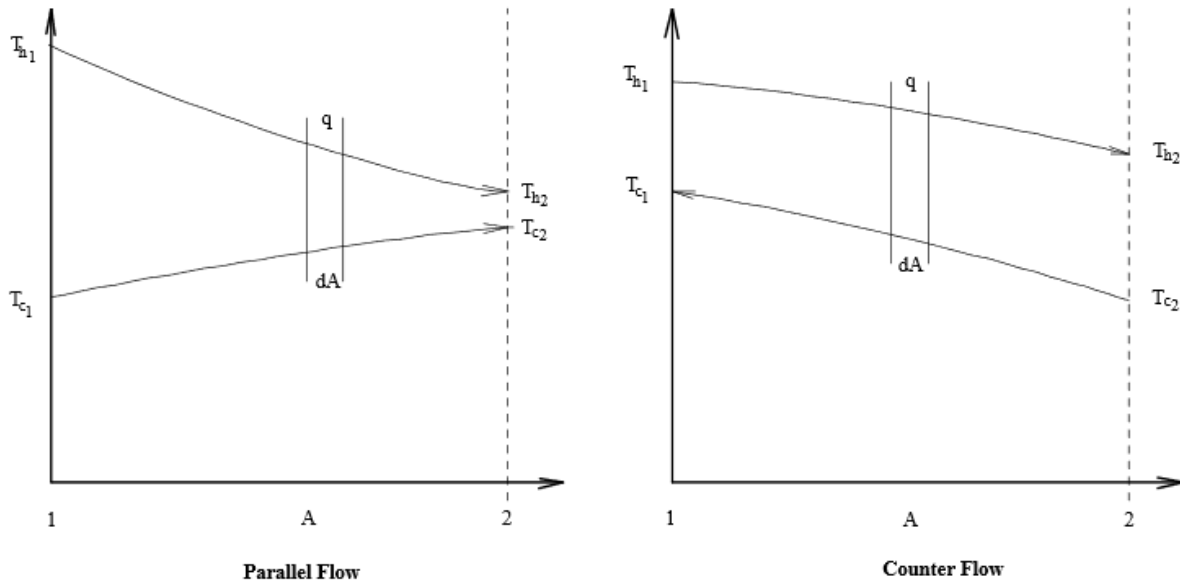


Figure 29: Parallel flow and counter flow temperature drops [10]

As well as the actual pipe dimensions and arrangements, the flow pattern has a significant effect on the heat exchange coefficient. The number of times the cold fluid passes over the hot fluid means more heat can be transferred. The two fluids can also flow in the same direction in parallel flow, in opposing directions in counter flow or perpendicularly to each other in cross flow. All else equal, a parallel flow exchanger will exchange the least heat, followed by counter flow and then cross flow exchangers. To explain this, the inlet hot temperature will be referred to as H<sub>1</sub>, inlet cold temperature will be C<sub>1</sub> and the exit temperatures will be H<sub>2</sub> and C<sub>2</sub>. In an infinitely long parallel flow exchanger, H<sub>2</sub> and C<sub>2</sub> will be the same as all the heat will have been transferred. In a counter flow exchanger however, it is possible for H<sub>2</sub> to be even lower as it exchanges heat with water at temperatures closer to C<sub>1</sub> rather than C<sub>2</sub>. Cross flow heat exchangers offer a lot more turbulence as the tubes act like obstacles in hot fluid's path, resulting in more heat loss.

square 45°/90°, both with their advantages and disadvantages. The triangular layout offers a higher tube density meaning that more heat can be exchanged within the same shell volume. The tradeoff however is that as a result of the increased contact with tubes, the pressure drop in triangularly arranged tube heat exchangers is higher. The pressure drop is caused by energy losses in the fluid due to the geometry of the flow passage, friction with the tube walls as well as features in the path such as pipe entrances, exits and bends. A larger pressure drop in the exchanger means more power required from the pumps to overcome these losses.

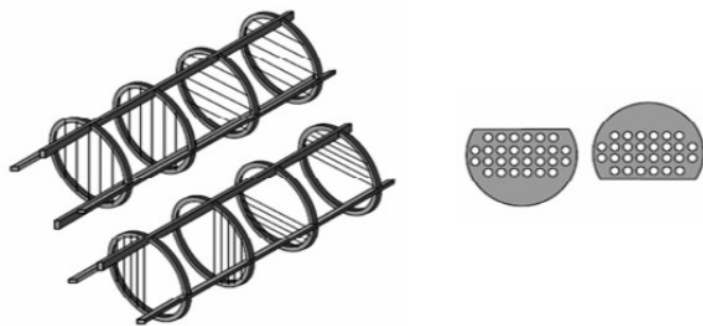


Figure 28: Rod baffle (left) Plate baffle (right) [11]

segmented configurations are the ones that best divert the flow around the tubes. The triple segmented arrangement is more commonly associated with low pressure and velocity situations.

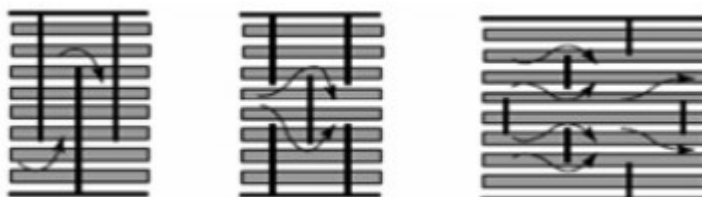


Figure 29: (Right to left) Single segmented, double segmented, triple segmented [11]

Baffling is another feature which can be implemented in heat exchangers to increase the turbulence experienced by the hot flow. Baffles can either be plates or rods which can be inserted in the hot fluid's flow path, disturbing its flow and causing it to come into more contact with the tubes. They can also be arranged in different ways: single, double or triple segmented configurations. Single and double

Last but not least the outer surface area of the heat exchanger affects the heat loss to the environment from both fluids. This is not something that can easily be planned and is more of a result of the design of other aspects of the exchanger, nevertheless it should be considered in calculations.

### 4.3 Theory and Calculations

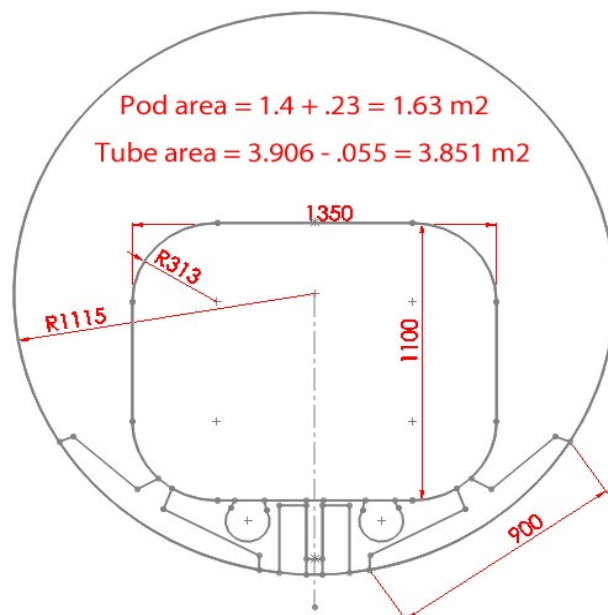


Figure 30: Pod dimensions

At a certain speed, the displaced air entering the gap between the pod and the wall reaches sonic speed as explained by the equation of continuity. This speed can be found to be 706 km/h. What this means is that the air compressor will need to be activated at or slightly before this point in order to prevent the choked flow condition. To design for the worst case scenario, the volume of air displaced when the pod is moving at its top speed (1220 km/h) is 552 m³/s. If we divide this by the area of the gap between the pod and tube, we find that the air would be moving at 588 m/s which is around mach 1.7.

The first thing that needs establishing is the minimum compressor intake flowrate of air required to avoid the Kantrowitz limit. The Hyperloop Alpha proposal includes some dimensions for the pod and tube, we are told that the pod will be 1.35 m in width and 1.1 m in height with a frontal area of 1.4 m<sup>2</sup> and the tube will have a diameter of 2.23 m. Given also the dimensions of the air bearing skis and the linear induction motor's rails and by making reasonable assumptions for missing dimensions, some simple calculations can help find the full frontal area of the moving pod. Some of these dimensions can be seen in figure X.

The amount of air that gets displaced by the pod as it moves through the tube is equal to the speed of the pod multiplied by its frontal area.

The density of the air in the tube can be found by rearranging the ideal gas equation and taking into account its relative humidity as shown in equation X:

$$\rho = \frac{P(1+x)}{R_a T(1 + \frac{R_w}{R_a}x)} \quad (95)$$

where  $R_a$  and  $R_w$  are the individual gas constants for air and water respectively,  $P$  is the pressure,  $T$  is the temperature and  $x$  is the relative humidity of the air. Using humidity figures for the different times of day and year from the National Climatic Data Center [12] for the state of California, an average relative humidity can be calculated and is found to be 0.6164. Using equation X, the air density is found to be 0.00096883 kg/m<sup>3</sup>.

Multiplying the volume flowrate found earlier (552 m<sup>3</sup>/s) by the air density gives us the mass flowrate which is found to be 0.535 kg/s. If the compressor bypasses 0.49 kg/s of air as suggested by Musk, that leaves 0.0452 kg/s going to the gap between the pod and tube walls. The area of the gap is 2.221 m<sup>2</sup>, multiplying this by the speed of the pod gives the volume of air which does not get displaced by the pod. If we convert the remaining mass flowrate of displaced air (0.0452 kg/s) back to volume flowrate, add it to the volume of air which does not get displaced and divide by the area of the gap, we can calculate the speed of the air entering the gap. What we find is that with a compressor intake of 0.49kg/s, the air entering the gap is travelling at mach 1.09 which is still not adequate.

This process was reversed to find the minimum intake flowrate to avoid the Kantrowitz limit; a flowrate of 0.54 kg/s was found to make the air travel at mach 0.99. However, a margin should be added as the intake flowrate will vary slightly throughout the trip which may result in passenger discomfort. A flowrate of 0.57 kg/s makes the air in the gap travel at mach 0.95, this is a reasonable safety margin if we assume the air density is constant throughout the tube and the linear induction motor provides a stable speed.

By looking at axial compressor manufacturers' catalogues, a good estimate of the dimensions of a compressor can be produced, allowing us to proceed in the heat exchanger design. The main applications of axial compressors are in oil and gas power plants and the aerospace industry. The compressors used in power plants are extremely large and heavy, they would not fit in the front section of a hyperloop pod and so will not be considered. The ones that are more suitable for this application would be aircraft jet engine compressors, these vary in diameters and length depending on whether they power commercial airliners or military fighter jets. The diameters of commercial airliner compressors lie in the range 1-3 m on average which is still too large for this pod.

*Table 6: Comparison of jet engine specifications*

Manufacturer	Model	Flowrate (kg/s)	Pressure Ratio	Length (m)	Diameter (m)
General Electric	F-414	77.1	30:1	3.91	0.89
General Electric	CF-700	38		1.918	0.838
General Electric	CFE-738	108	30:1	1.73	0.902
General Electric	CJ-610			1.15	0.45
Eurojet	EJ-200	77.1	26:1	4	0.7
Sneecma	M-88	65	24.5:1	3.538	0.696

The compressors in military aircraft deal with air at almost the same conditions as the hyperloop; very low pressures and densities and a very high flowrate. Table 6 compares several models of jet engines, mainly from General Electric who possess a large market share of compressor technology.

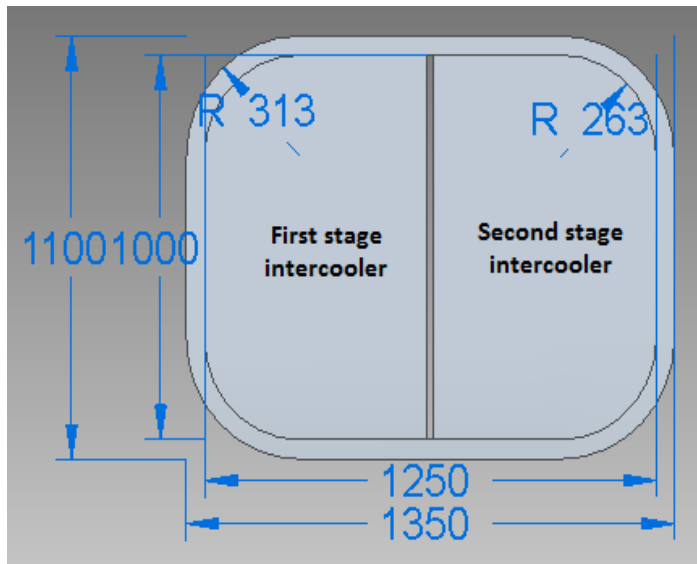


Figure 31: Intercoolers inside the pod

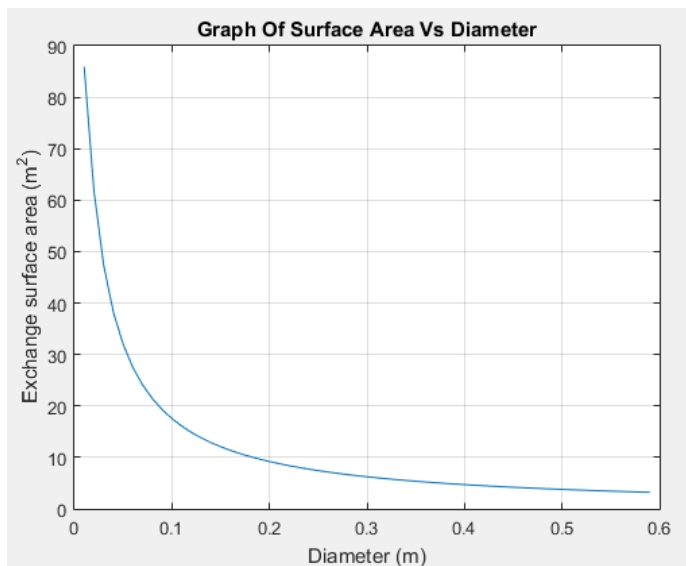


Figure 32: Graph of surface area vs diameter

The first stage of compression proposed by Musk has a ratio of 21:1 (100 to 2100 Pa), while the second stage compressor is only 5.2:1. The compressors shown in the table above have roughly the same pressure ratios as the first stage in the hyperloop; the lengths and diameters can therefore be assumed to be representative of the given situation. Given that the pod height is 1.1 m, the diameter of the compressor inlet should be around 0.8 – 1 m. This means there isn't enough space for the intercoolers to fit on either side of the compressor and so will have to be pushed back. To fill the given space taking into account the pod's body, each intercooler will have a cross sectional area of 0.595 m<sup>2</sup>.

The next step in the process is to determine the optimal tube diameter, number of tubes and the tube clearance. The graph in figure 34 suggests that the smaller the pipe diameter, the more pipes available and therefore more surface area for exchange. However the pipes must also be able to withstand the pressure requirements, the water inside will be at 101000 Pa while the surrounding air will be at 2100 Pa in the first intercooler and 11000 Pa in the second. A suitable pipe thickness can be found by considering the axial, circumferential and radial stresses experienced by the pipe. A safety factor of 1.3 is reasonable as the conditions inside and outside the pipe will not change for the duration of the trip.

To proceed, a pipe material must be selected for yield stress considerations; the ideal choice would be copper as it has excellent thermal conductivity allowing for lots of heat exchange. The minimum thickness of the pipe can now be determined using the following equation from the International Association of Classification Societies' "Requirements For Pipes And Pressure Vessels" [13]:

$$t = t_0 + b + c \quad \text{where } t_0 = \frac{PD}{20Ke + D} \quad (96)$$

In these equations,  $b$  is the bending allowance,  $c$  is the corrosion allowance,  $K$  is the maximum permissible stress,  $e$  is the efficiency factor and  $P$  and  $D$  are the pressure inside the pipe and its outside diameter. The pipes in this heat exchanger will have no bends meaning  $b = 0$  and the efficiency factor  $e = 1$  as the pipes are seamless without any joints/welds. The corrosion allowance  $c$  can be looked up in the IACS handbook and is found to be 0.8 mm for 'Copper, brass and similar alloys'. The value for

K can be worked out by dividing copper's yield stress by the chosen safety factor leaving K = 90 MPa. Finally, the value of t can be calculated giving t = 0.8006 mm for an outer diameter of 10 mm.

The tube pitch is the distance between the centres of two adjacent pipes and should be at least 1.25 times the outer diameter of the pipes according to the Tubular Exchanger Manufacturers Association standards [14]. This implies a pitch of 12.5 mm and therefore a clearance of 2.5 mm, however this is too small a gap between the tubes and will result in a large pressure drop due to the friction. A gap of 30 mm will allow the air to move between the tubes with ease. Using this information, equation 97 gives the maximum number of tubes that can fit within the given cross sectional area.

$$N_t = CTP \frac{A}{CL P_t^2} \quad (97)$$

Where CTP is a factor which accounts for the decrease in available area depending on the number of tube passes, CL is a factor which accounts for the tube configuration and P<sub>t</sub> is the tube pitch. To increase packing efficiency for more heat transfer, a triangular configuration will be selected giving a value of CL of 0.87. The number of passes should be even as the water will need to enter and exit at the same end of the intercooler. This is because the water and steam tanks will be located together and so the water must go through the intercooler and return back the way to enter the steam tank. The first intercooler will need to exchange more heat than the second as the temperature of the incoming air will be higher, for this reason the first intercooler will have 4 passes with a CTP value of 0.78 while the second will have only 2 with a CTP value of 0.9. The maximum number of tubes in the first intercooler is 333 while the second has 384.

Having defined the size and number of tubes, the flow regimes and states for both air and water can now be calculated to find the thermal resistances in the design. Dividing the mass flowrate of water by the cross sectional area of the tubes gives the average flow speed which can be used to determine the Reynolds number of the flow. The Prandtl number can be worked out from the average dynamic viscosity, specific heat capacity and thermal conductivity of water within the intercooler. These values, as well as the density of water needed for the Reynolds number, can be approximated by averaging the values at the initial and final temperatures of the water.

The Nusselt number can be calculated from the Prandtl and Reynolds numbers as follows:

$$N_u = 0.023 R_e^{0.8} P_r^n \quad (98)$$

Where n = 0.3 if the fluid is cooling down and n = 0.4 if the fluid is heating up. In this case the water is heating up so n = 0.4. The convective heat transfer coefficient can then be calculated according to:

$$h_u = \frac{N_u k}{D_i} \quad (99)$$

The TEMA standards suggest that the shell side heat transfer coefficient will not vary much from an initial prediction and that a value of 5000 W/m<sup>2</sup>K is suitable. These values can now be substituted into equation 94 with a k value of 385 W/mK [15] for copper and L = 1 to give the thermal resistance of a 1 m section of the intercooler. This yields an overall heat transfer coefficient U of 1730 W/K for the first intercooler and 2342 W/K for the second.

The heat lost Q by the air as its temperature drops from 857 K to 300 K in the first intercooler, as proposed by Musk in the Hyperloop Alpha whitepaper, can be found using equation 93 and is equal to 327 kJ. The same method shows that the air loses 92 kJ of heat in the second intercooler. Equation 100 below can be used to calculate the length of tubing required for those temperature drops.

$$L = \frac{Q}{LMTD \cdot U \cdot \pi \cdot D_o} \quad \text{where } LMTD = \left| \frac{(T_{h1} - T_{c1}) - (T_{h2} - T_{c2})}{\ln \left( \frac{T_{h1} - T_{c1}}{T_{h2} - T_{c2}} \right)} \right| \quad (100)$$

Where the h/c subscripts refer to the hot/cold flows and the ½ subscripts refer to the entry/exit points. The first intercooler needs to have roughly 25 m worth of tubing while the second needs 15 m. This means the first intercooler needs to be 6.25 m long as it consists of three tube passes, while the second intercooler needs to be 7.5 m.

## 4.4 Analysis

The LMTD (logarithmic mean temperature difference) method was used to calculate the required length, however this method is an iterative one where the output length allows us to calculate the output temperatures. This affects the exchange surface area which in turn affects the overall heat exchange coefficient and so on and so forth. The method brings us closer and closer to the actual values for this specific heat exchanger for the specified temperature difference. Another method can be used to give the actual temperature drop for a given overall heat transfer coefficient and exchange surface area.

The NTU (number of transfer units) method is one where the maximum theoretical heat transfer is multiplied by the efficiency of the heat exchanger to give the actual heat transferred. The first step is to determine the heat capacity rates for both fluids; the specific heat ratio multiplied by the mass flowrate. The maximum possible heat transfer is equal to the smaller of the two heat capacity rates multiplied by the difference in inlet temperatures of the fluids. In this case, the air and water have heat capacity rates of 0.633 and 0.588 kJ/K respectively meaning that the water has the lower heat capacity rate. However, as the water experiences a phase change its heat capacity rate approaches infinity, this means that air has the smaller heat capacity rate  $C_{minimum}$ . The efficiency is calculated differently according to the flow pattern (parallel/counter flow etc.) and depends on the ratio of heat capacity rates as well as the number of transfer units, which are directly correlated to the surface area available for exchange.

The NTUs and efficiency can be calculated as follows:

$$NTU = \frac{UA}{C_{minimum}} \quad (101)$$

$$\text{effectiveness} = \frac{1 - e^{-NTU(1-Cr)}}{1 - Cre^{-NTU(1-Cr)}} \quad (102)$$

The equation for efficiency above includes a term Cr which is the ratio of heat capacities. This number approaches 0 when there is a phase change reducing the equation to:

$$\text{effectiveness} = 1 - e^{-NTU} \quad (103)$$

The effectiveness of the first intercooler has been found to be 0.883 while that of the second is 0.993. These can then be used to calculate the actual heat transfers which occur and therefore the final output temperatures which are found to be 359 K in the first stage and 374 K in the second. These are slightly different from the target temperatures (300 K and 400 K), however the result is a lower temperature in the final stage.

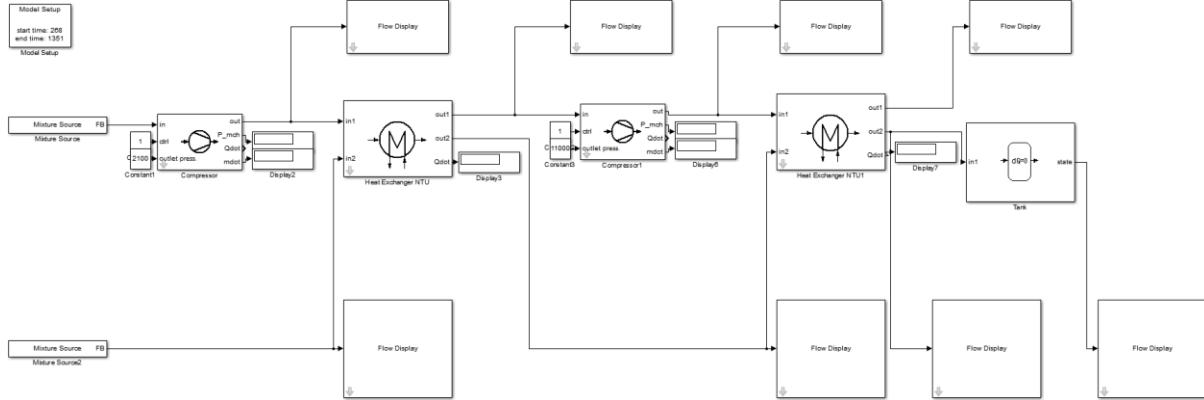


Figure 33: Simulink model of air compression system

To verify these results, a Thermolib Simulink model was created. Thermolib is a Simulink expansion which incorporates libraries of data for the properties of the most commonly used substances in thermodynamics. It also contains processes which simulate commonly used components such as heat exchangers, compressors, pumps etc.

The initial temperatures and pressures for air and water can be specified as well as their flowrates. The compressor can either be isentropic or polytropic in which case a value for the polytropic coefficient must be input. As this number is not given in Musk's proposal, it was found by trial and error until a temperature of 857 K was achieved by the compressor. The heat exchanger block can accommodate different flow patterns and takes the overall heat transfer coefficient as an input. Thermolib uses the NTU method to give an output temperature.

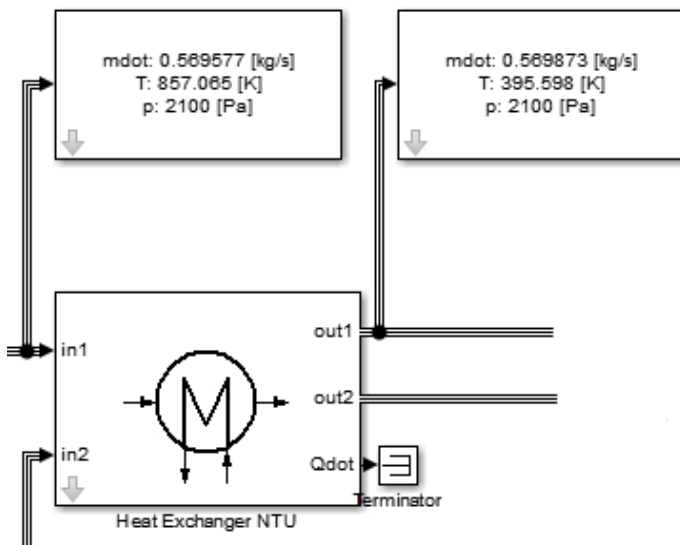


Figure 34: Input and output temperatures for first intercooler

The resulting output temperature is 395 K as shown. This is higher than the 359 K calculated earlier, but is most likely more accurate as the properties of both fluids such as specific heat, thermal conductivity, density and dynamic viscosity all change as the temperature changes. Thermolib takes this into account and updates these values iteratively throughout the cycle. The heat transfer calculation is therefore an integral over the range of temperatures for incremental changes in all the other values, this is bound to produce more precise results.

The same polytropic coefficient was input into the second stage compressor, however as the incoming air from the first intercooler has a different temperature than Musk's proposal, the output temperature

is now 710 K. Updating the air inlet temperature for the second intercooler in the NTU method carried out earlier gives an expected output temperature of 375 K. The Simulink model produces a result of 471 K for the output of the second intercooler. The discrepancy is most likely due to the compounding effects of fluid property value errors carried forward from the first intercooler.

The effect of baffles on the temperature drop could not be accurately calculated as the literature on the effect of baffles is empirical rather than theoretical. The available data comes from studies where certain variables to do with baffles were changed and their effects documented. Unfortunately this could not be analysed qualitatively either as the shape of the designed intercoolers is adapted to the pod shape and not cylindrical like most shell and tube heat exchangers. This would have too large an effect on the fluid flow inside and so the two cannot be compared.

Another effect which could not be quantified correctly is the heat loss from the intercooler surface to the environment. This is because the material of the pod walls as well as the ambient temperature around the intercoolers are unknown. Both these effects when taken into account, should reduce the temperature of the air even further and would probably mean that the intercoolers would be shorter in length, reducing the overall weight and length of the pod.

## 4.5 Storage Tanks

As well as water, the pod will need to carry air for the parts of the trip where the compressor isn't running. The capacities of the air, water and steam tanks need to be determined to finalise the pod design. For very low speeds the pod will be moving on wheels as mentioned in the proposal, however this should only last for a few seconds as the pod accelerates and picks up speed quite fast. Once a threshold speed has been exceeded, the air skis will activate allowing the pod to levitate. For simplification, it will be assumed that the air skis will be active throughout the duration of the trip.

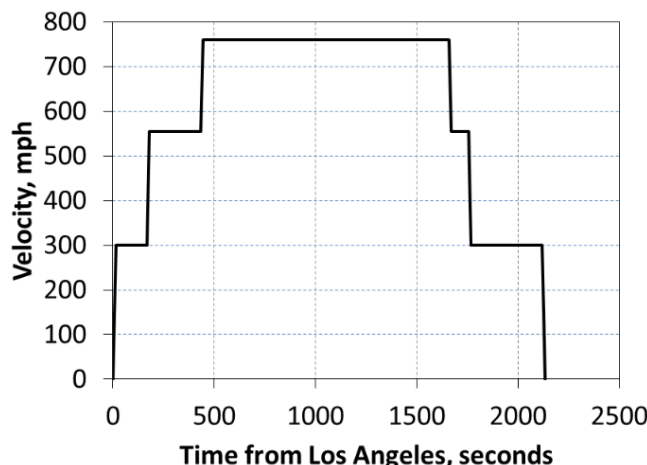


Figure 35: Velocity vs time graph of complete trip [X]

For simplicity again, it will be assumed that the compressor will activate at the very beginning of the second acceleration and turn off at the very end of the second deceleration.

According to the proposal, the pod will begin its second acceleration 167 seconds into the trip and stop its second deceleration 1750 seconds in. This leaves a period of 551 seconds during which the compressor will not be active and compressed air will have to come from the storage tank instead. As calculated in the air bearings section, the skis will need to eject around 0.2362 kg of air every second to keep the pod levitating, a total of 130.15 kg for the 551 seconds.

Assuming strict weight requirements for luggage will be in place and control systems will continuously manage the pod height off the ground, speed and acceleration, a safety factor of 1.3 can again be used

The compressor gets activated as soon as the pod exceeds 706 km/h as explained previously. The Hyperloop Alpha proposal suggests three distinct speeds for the pod to maintain in different sections of the track. These speeds take into account the radii of bends along these three sections to ensure the lateral acceleration experienced by passengers does not exceed 0.5 g, the maximum lateral acceleration experienced comfortably by humans. These speeds can be seen in the graph shown and are 300, 555 and 760 mph or 480, 890 and 1220 km/h. The compressor will therefore activate at some point during the second pod acceleration. For

simplicity again, it will be assumed that the compressor will activate at the very beginning of the second acceleration and turn off at the very end of the second deceleration.

as the conditions remain relatively stable every trip. This means there should be 170 kg ( $130.15 \times 1.3$ ) of air on board the pod at the beginning of every trip. If the compressor fails at any point, the pod will have to travel on its emergency wheels until it reaches its destination. Periodic maintenance of the hyperloop systems and quality control of the air inside the pod should ensure that the likelihood of air compressor failure remain very low. For the remainder of the trip, air will leave the compressor and enter the tank at the same rate as the air leaving the tank. Increasing the flowrate from 0.2 to 0.24 kg/s should not be a problem as the bypass flowrate can be controlled by valves at the nozzle expander. The air leaving the tank will have varying pressure throughout the trip as the tank empties. Pressure regulator should be used near the air bearings system inlet to keep the pressure at a fixed value.

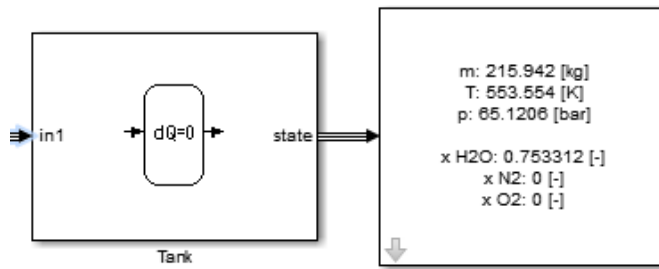


Figure 36: Steam tank simulation

The water needed initially is estimated to be around 221.62 kg, a safety factor of 1.3 can be used once more to bring the total water required to 288.106 kg or 300 kg for simplicity. This can be stored in a tank small enough to fit in the gap formed due to the first intercooler's shorter length. If all 221.62 kg of water were to completely turn to steam inside the exchanger, the steam

would occupy a volume of  $378 \text{ m}^3$ . The steam will need to be stored in a high pressure vessel on board the pod to reduce its volume. An arbitrarily chosen volume of 5000 L would occupy 4.42 m of pod length if the vessel were to have a diameter of 1.2 m. The pressure inside the tank after all the steam has entered will be 76.4 bar through simple rearranging of the ideal gas equation. To verify this, the Simulink model was run once more with the output steam entering a tank. At the end of the 1583 seconds of compressor run time, the pressure inside the tank reached 65.1 bar as shown. The discrepancy is again due to the continuous updating of the pressure and temperature incrementally instead of in one calculation.

The air tank will be at its maximum pressure at the very beginning of the trip and will continuously lose mass and pressure until the compressor is activated. At that point the mass and pressure will vary little due to the differences in inlet and outlet flowrates from the tank and the heat input from the air. After the compressor is turned off, the tank's mass and pressure will continue to drop until the pod arrives at its destination. A 250 L tank would need to be at a pressure of 60 bar in order to contain the necessary 170 kg of air.

High pressure steam and air vessels are readily manufactured according to the clients' specifications with several companies advertising their standard tank sizes but also accommodating specific requirements from clients. One such company is Shandong Pulilong Pressure Vessel Co. Ltd, which advertises its ability to manufacture vessels ranging from 1 to 100 bar [16].

## 4.6 Improvement and Future Work

As the compressor is powered by batteries on board the pod, reducing its energy consumption is crucial in minimising the weight of the pod and cost of the trip. One way to do this would be to correlate the compressor flowrate with the pod speed. This would mean that as soon as the pod begins its second acceleration, the compressor would activate at a lower intake of 0.2362 kg/s without bypassing any of the air to the nozzle expander. When the pod accelerates for a third time to 1220 km/h, the compressor flowrate can then be increased to 0.57 kg/s with 0.2362 kg/s making it to the air bearings and the rest being bypassed through the expander. Upon decelerating to 890 km/h once more, the compressor can reduce its intake again to 0.2362 kg/s. This would make a significant difference to the energy consumption for the trip. The expander only produces thrust when the pod moves at 1220 km/h, the effect of this force should be looked into further to establish whether it makes a significant difference

on the power consumption of the linear induction motor. If the difference is not great, it may be a better idea to store the excess air on board the pod for use in the air bearing system. This would reduce the weight of the air tank required initially as more air is available for storage along the way.

Another way to reduce the power consumption of the second stage compressor would be to bypass the air before allowing it through the first intercooler instead of after. This would mean the air entering the intercooler now has less heat to exchange due to the lower flowrate. The air leaving the intercooler would be at a lower temperature and therefore smaller volume, reducing the power input in the second compression. This may also mean the water's flowrate can be reduced, bringing the weight and size of the water and steam tanks down. The only problem would be that air is now re-entering the tube at a higher temperature. With the number of pods going through the hyperloop every hour, this can cause the air inside the tube to heat up over time. The temperature inside the pod will eventually reach a new equilibrium, however more research needs to be done on the heat loss from the tube walls to the environment and the rate of heat addition to the tube.

The water should also be pumped into both intercoolers separately and their output should fill the steam tanks separately. This would increase the power requirements of the pump, however the resulting reduction in both air and water temperatures would mean that the work done by the compressor as well as the sizes and pressures of the storage tanks decrease. These two effects would outweigh the extra power input from the pump.

## 5. Suspension

### 5.1 Why Air Suspension System

#### 5.1.1 Wheels & Magnetic Levitation

It is challenging for the capsule to cruise in the tube at transonic velocities. There are several alternative options for the suspension system, but some of these seem impractical in the condition of current technological level.

Conventional wheel and axle suspension system is commonly applied but it is impossible to work at high speeds due to enormous frictional losses (assumed approximately 1200 kilometres per hour from Hyperloop Alpha Design [1]). Actually some special wheels could successfully reach the very high speed, for example 1600 kilometres per hour achieved by aluminium wheels on Bloodhound [17]. However there are still many problems to be solved for the wheel plan, such as the harsh contact between the wheels and tube wall, noise and dynamic instability. In addition, the braking distance would be a long way in consideration of a limited coefficient of friction.

Magnetic levitation is another viable technical solution. With an advantage of low mechanical contact and friction, magnetic levitation would be a good choice applied to Hyperloop's high speed conditions. However this option is not economically viable. The extreme cost associated with material and construction (e.g. the track lined with copper coils) would be prohibitive.

#### 5.1.2 Air Bearing Suspension

Air bearing suspension is chosen due to its stability and low drag at a feasible cost. In Hyperloop Alpha

Design [1], there are two sources for the suspension of the capsule, aerodynamic air bearing and externally pressurized air bearings (Figure 38), which will be introduced in the following parts. The idea is to produce a pressurized air film to make the capsule float at a fixed height. When the gap between skis and tube wall is reduced, the restoring pressure of the flow in the narrowed gap

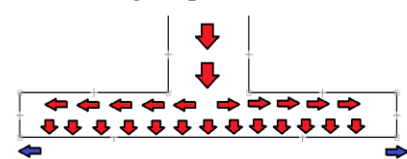


Figure 38: Schematic Air Bearing

would exhibit a highly non-linear increasing reaction, which will push the capsule back to its nominal height. Consequently the air cushion suspension has a superb advantage of stability and reliability. Moreover, the injected air would make use of the pressurized air from compressors. It is a very efficient and energy-saving way to get the air film in required pressure and it is also more economic compared to the cost of magnetic levitation.

## 5.2 Lift Force & Air Cushion Pressure Required Calculation

The preliminary dimensions of suspension from Hyperloop Alpha Design are shown as follows [1]: the suspension of Hyperloop consists of 28 air bearings, the width and length of which are 0.9m and 1.5m respectively. The gap between the suspension ski and tube wall varies from 0.5mm to 1.3mm. The air pressure in the tube is 100 Pa and the assumed weight of the whole system is approximately 15000kg (Table 7).

*Table 7: Capsule weight breakdown*

Capsule Component	Weight (kg)
Capsule Structure & Doors	3100
Interior & Seats	2500
Propulsion System	700
Suspension & Air Bearings	1000
Batteries, Motor & Coolant	2500
Air Compressor	1800
Emergency Braking	600
Passenger & Luggage	2800
<b>Total Weight Assumed</b>	<b>15000</b>

Therefore in consideration of 100 Pa of air pressure in the tube, the effective pressure to lift the capsule is calculated as follows, where  $\Delta_{pressure}$  is the pressure difference between ambient pressure and air cushion pressure,  $A_{effective}$  is effective lifting area,  $A_{total}$  is total lifting area and  $P_{min}$  is the minimum air cushion pressure required.

$$F_{Lift} = \Delta_{pressure} \times A_{effective} = 15000 \times 9.81 = 147150 \text{ N}$$

$$A_{total} = 1.5 \times 0.9 = 1.35 \text{ m}^2$$

$$P_{min} = \frac{m_{total} \cdot g}{A_{total}} + P_{ambient} = \frac{15000 \times 9.81}{28 \times 0.9 \times 1.5} + 100 = 3992.86 \text{ Pa}$$

However in the real condition, the effective lifting area is not exactly equal to the total lifting area due to the curved surface of the ski and the bank angle of the ski distribution. Because the objective of the group project is to give the group design for the Hyperloop and check the feasibility of the idea, the minimum required pressure will be used in the following validation and the influencing factors will be considered in the discussion.

## 5.3 Aerodynamic Air Bearing Investigation

### 5.3.1 Shape Design

The capsule is considered to cruise at a peak speed of 1200 km/h (around 333 m/s). The speed of sound in an ideal gas is obtained as follows:

$$C_{ideal} = \sqrt{\frac{\gamma \cdot R \cdot T}{M}} \quad (104)$$

The temperature T in the tube is assumed as 293K. Molar gas constant R is 8.314 J/(mol · K).

$\gamma$  is heat gap ratio, which is assumed as 1.4 at this air condition and the mean molar mass of the gas is 0.029 kg/mol. Therefore the speed of sound in the tube is calculated as 342.93 m/s and the capsule will achieve subsonic speed during the journey.

The shape design of air bearing has a reference to the Clark Y air foil design [18], which is commonly applied in subsonic condition with a good performance of lift-and-drag ratio. The side view of air bearing ski is shown in Figure 39.

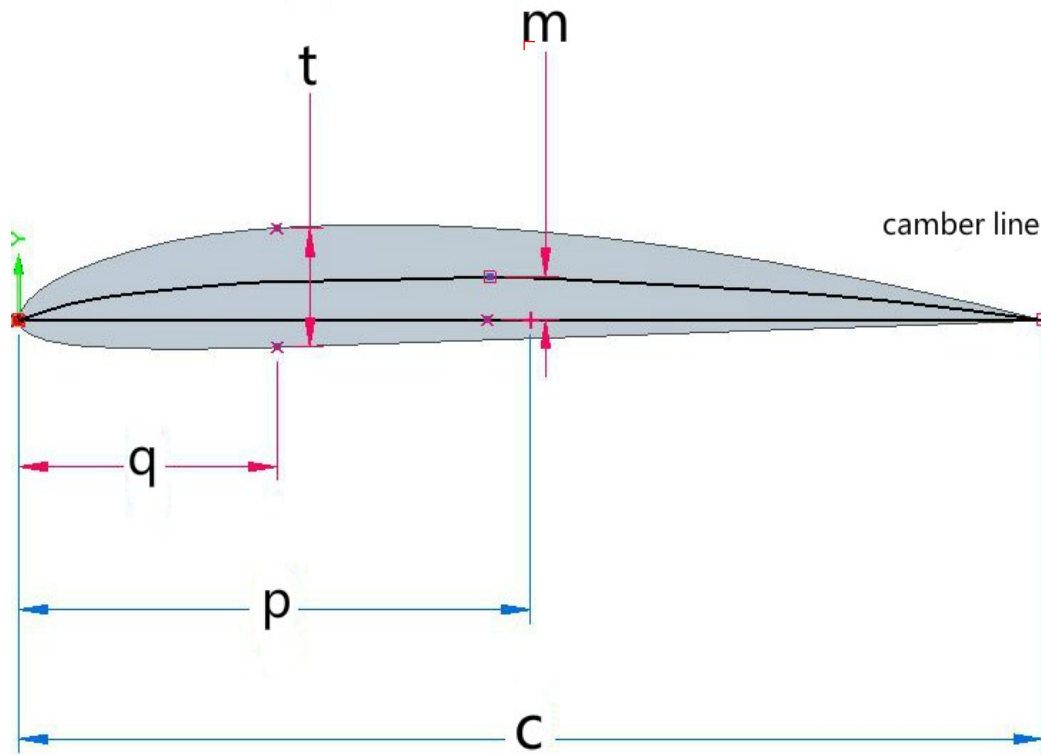


Figure 39: Side view of air bearing

Dimensions of the skis are shown in following table.

Table 8: Main dimension of the air bearing ski side sketch [18]

Dimensions	Percentage	Length
Maximum thickness t	11.7%	175.5 mm
Maximum camber m	3.4%	51 mm
Maximum camber position p	42%	630 mm back from the leading edge
Maximum thickness position q	28%	420 mm back from the leading edge
Length of the ski c	100%	1500 mm

The following formula is used to determine the camber line [19]:

$$y_c = \begin{cases} m \frac{x}{p^2} \left( 2p - \frac{x}{c} \right), & 0 \leq x \leq pc \\ m \frac{c-x}{(1-p)^2} \left( 1 + \frac{x}{c} - 2p \right), & pc \leq x \leq c \end{cases} \quad (105)$$

Where: c is the length of air bearing ski, m is maximum camber and p is maximum camber position in the form of percentage.

The expression of half thickness  $y_t$ , which express the camber line and airfoil surface, is shown as follows:

$$y_t = 5tx \left[ 0.2969 \sqrt{\frac{x}{c}} + (-0.1230) \left( \frac{x}{c} \right) + (-0.3516) \left( \frac{x}{c} \right)^2 + 0.2843 \left( \frac{x}{c} \right)^3 + (-0.1015) \left( \frac{x}{c} \right)^4 \right] \quad (106)$$

Where: t represents the maximum thickness in the form of percentage.

Because the coordinates of the ski side view shape is the sum of the y-coordinate of camber line and the perpendicular y-coordinate of the half thickness, the coordinates  $(x_u, y_u)$  and  $(x_l, y_l)$ , which represents the upper and lower lines of ski side view shape respectively, are calculated as follows:

$$x_U = x - y_t \sin \theta \quad (107)$$

$$y_U = y_t + y_t \cos \theta \quad (108)$$

$$x_L = x + y_t \sin \theta \quad (109)$$

$$y_L = y_c - y_t \cos \theta \quad (110)$$

Where:

$$\theta = \arctan \left( \frac{\frac{dy_c}{dx}}{1} \right) \quad (111)$$

$$\frac{dy_c}{dx} = \begin{cases} \frac{2m}{p^2} \left( p - \frac{x}{c} \right), & 0 \leq x \leq pc \\ \frac{2m}{(1-p)^2} \left( p - \frac{x}{c} \right), & pc \leq x \leq c \end{cases} \quad (112)$$

Based on the aforementioned formulas, the coordinates of points of ski side view shape are generated in an Excel file and then these position data are transferred into a Solidworks sketch as the side sketch of air bearing skis.

Because the upper and lower surface of the skis are well conformed to the shape of the tube wall and the capsule, a circular arc design (Figure 40) is used in the front view sketch of air bearing skis.

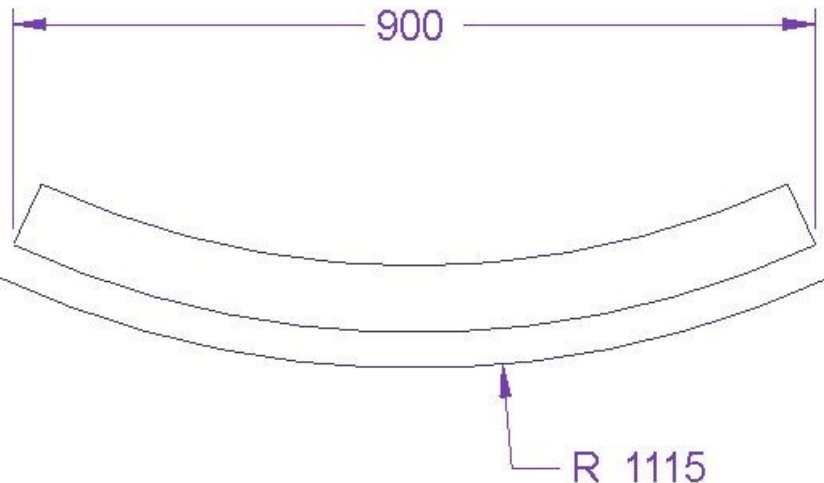


Figure 40: Front view of the air bearing ski

On the basis of the front and side view sketch design, Solidworks Surface tools are employed to generate the 3D shape of the air bearing skis (Figure 41). The features used to create the model are mainly Surface Sweep, Surface Extrude, Surface Fill and Boundary Surface.

The final design of the skis would efficiently help to provide the lifting force and achieve a good balance of the drag force. Moreover, the optimized shape of the air bearing skis would be in favour of the following flow simulation and calculation to some extent and make the verification more accurate.

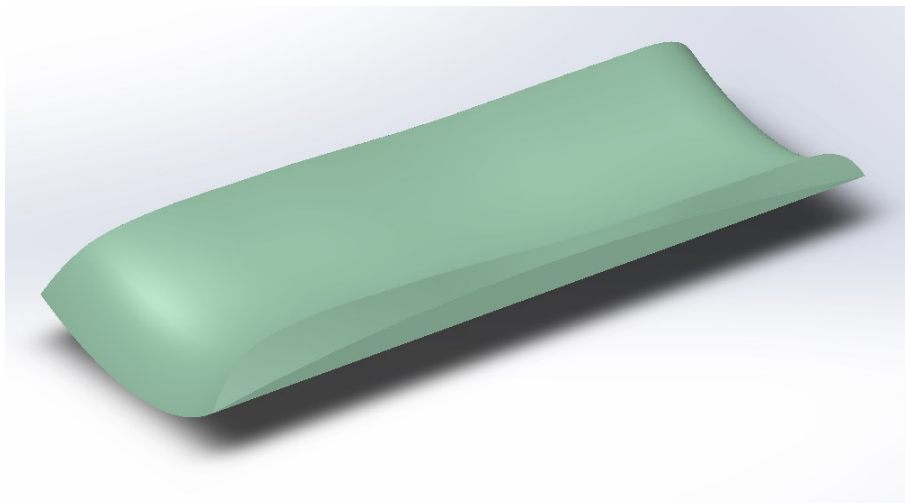


Figure 41: Final Design of Air Bearing Ski

### 5.3.2 Aerodynamic Air Bearing Simulation

Aerodynamics air bearing is applied at moderate to high speeds. The idea is to make the front of skis elevated 0.05° relative to the back tip and a very thin film of air will be trapped in the converging gap between the skis and the tube wall due to viscous forces. The trapped air is pressurized to make fundamental laws of mass and energy conservation satisfied and the net lifting pressure (pressure difference between air cushion and ambient atmosphere) will support part of capsule's weight during the travel.

A preliminary flow simulation is done by Solidworks Flow Simulation to verify the effect of the aerodynamic air bearing and find out what level of lifting pressure the bearing could provide. The model is simplified with only three rows of air bearing skis, each of which has an elevated angle of 0.05° (Figure 42): the inlet air of the first row of skis is directly from the ambient atmosphere while that of the second and the third rows of skis from the outlet air of first and second rows of skis respectively. They are mainly three flow patterns passing through the skis and the flow by the fourth ski is considered similar to the one by the third row of skis.

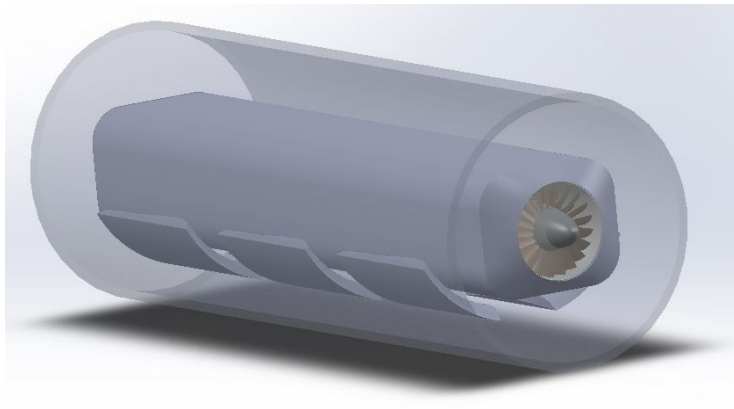


Figure 42: Simplified model for flow simulation

Reynolds number calculation in boundary layer flow (between skis and tube wall):

$$R_e = \frac{\rho \cdot V \cdot L}{\mu} \quad (113)$$

Where:

$$\rho = \frac{PM}{RT} \quad (114)$$

The parameters used are shown in Table.

Table 9: Parameters used in Reynolds number calculation

Pressure under skis P	3992.86 Pa
Temperature under skis T	400 K
Gas constant R	8.314 J/(mol·K)
Molar mass of air M	0.02897 kg/mol
Velocity V	333 m/s
Width of skis L	0.9 m
※Dynamic viscosity $\mu$	$1.45 \times 10^{-5}$ kg/(m·s)

※ Dynamic viscosity  $\mu$  is obtained from gas viscosity graph [19].

Therefore the approximate Reynolds number in the flow between skis and tube wall is around 719280, which is much more than 4000 and thus would be considered as turbulent flow.

The operation steps of the CFD are shown in following chart.

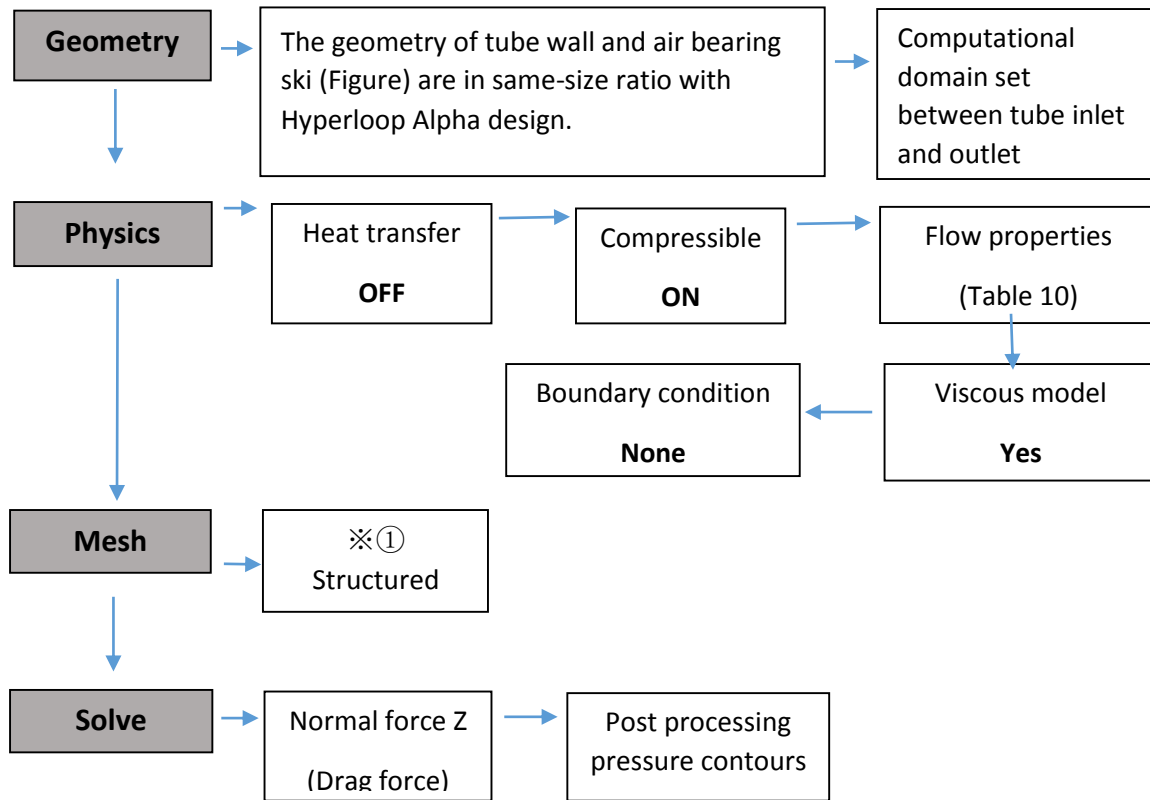


Figure 43 Operation steps

Table 10: Flow properties

Ambient pressure	100.0 Pa
Ambient temperature	293.0 K
Turbulence intensity	5%
Turbulence length	0.112 m

Turbulence intensity in high-turbulence case (high Reynolds number) is typically between 5% and 20%. In the CFD, 5% is assumed as the value of turbulence intensity [19].

It is common to estimate the turbulence length scale to a percentage of the dimension of the problem. In the CFD, the turbulence length is valued as 5% of the channel height (0.112 m) with a reference to a similar analysis [19].

※① Thin boundary layers could be best resolved with high-stretched structured grids.

Figure 44 indicates the pressure distribution under air bearing skis and trajectory and velocity vector of the flow passing through skis.

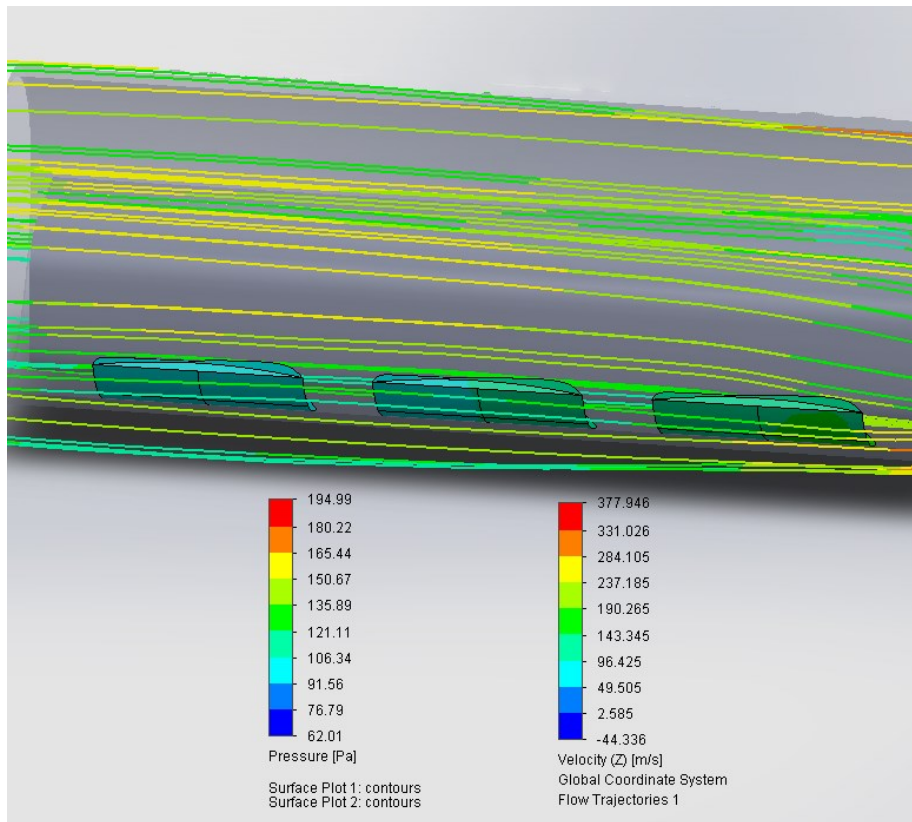


Figure 44: Flow trajectory and pressure distribution on skis

The goal result of the normal force Z (drag force) is output in the Figure 45. The maximum drag force in the simulation would be 149.242 N and the minimum value would be 148.960 N. In consideration of the suction of front compressor, the drag force could not be suitable in the section but for the suspension, the values would be a good explanation. In Hyperloop Alpha design, the predicted drag force generated by the air bearing at the speed of 333 m/s is around 140 N [1].

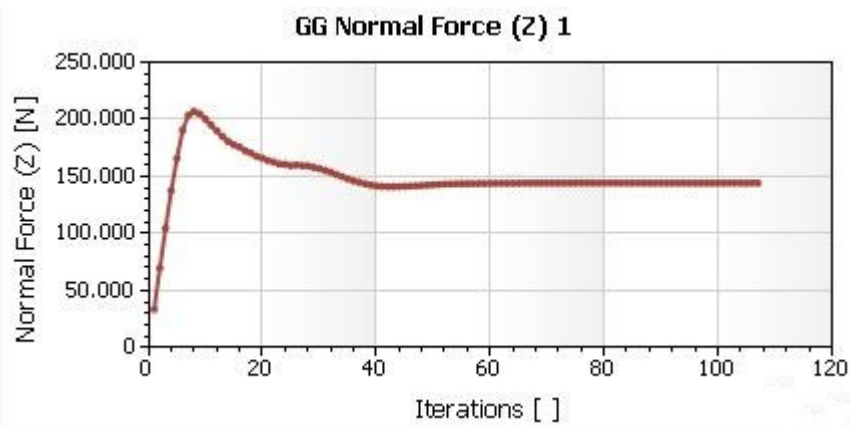


Figure 45: Normal force result output

The following figures show the pressure distribution of three rows of air bearing skis respectively.

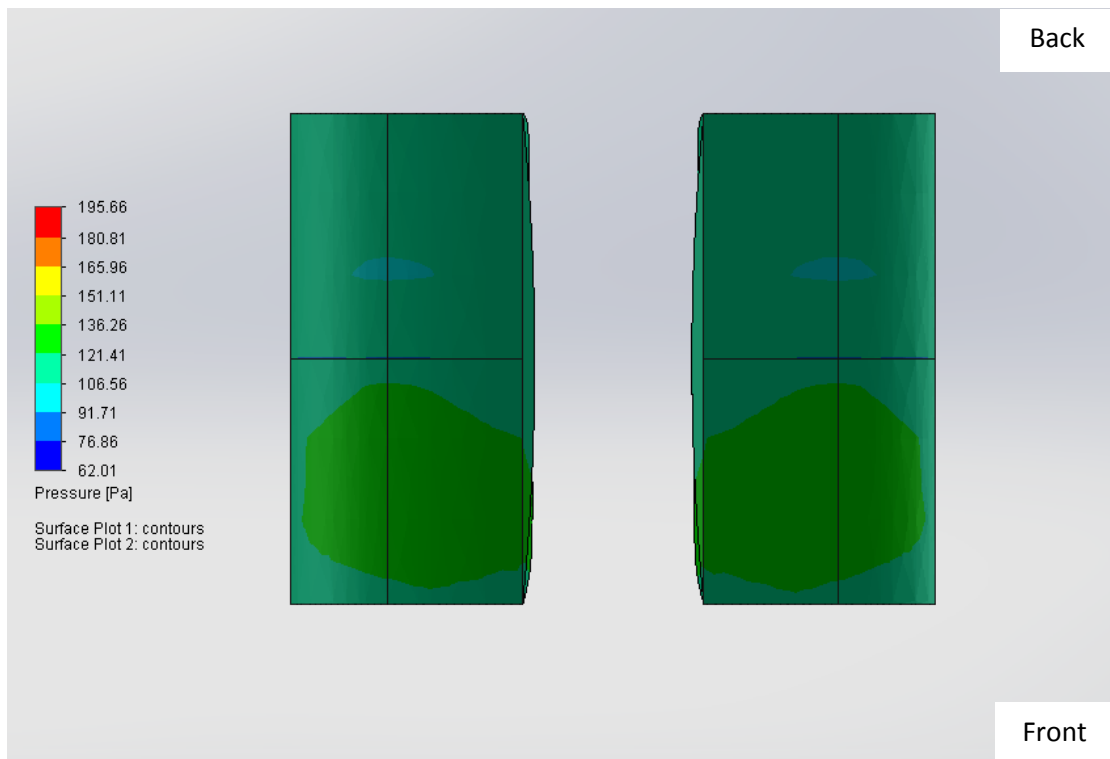


Figure 46: Pressure Distribution on the First Row of Air Bearing Skis

i

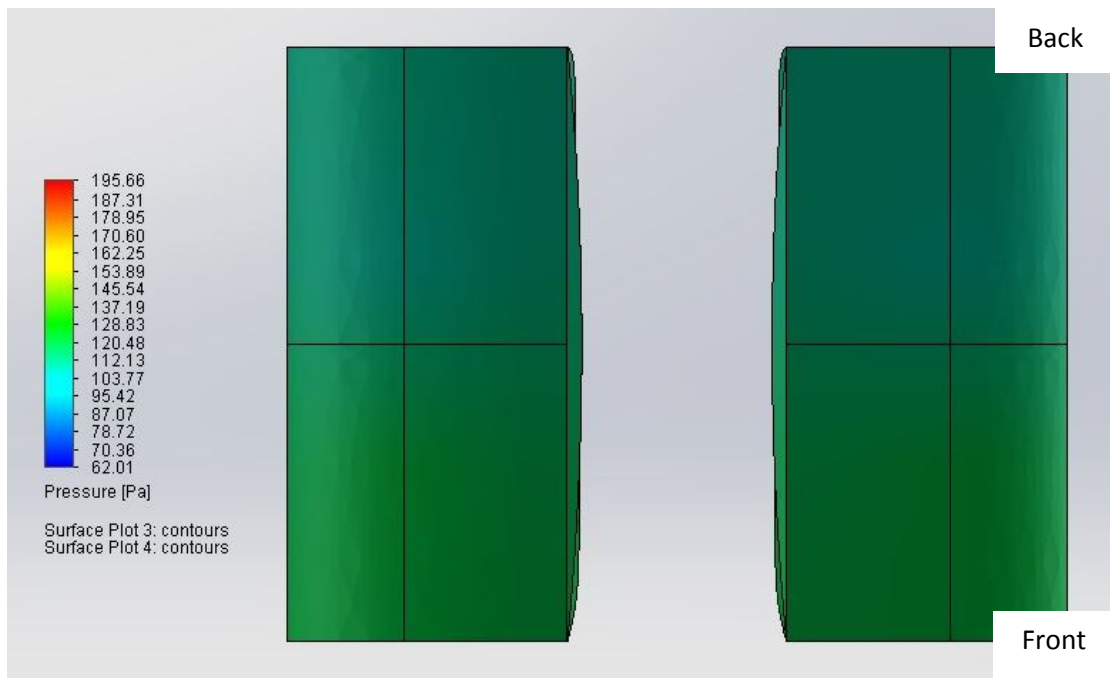


Figure 47: Pressure Distribution on the Second Row of Air Bearing Skis

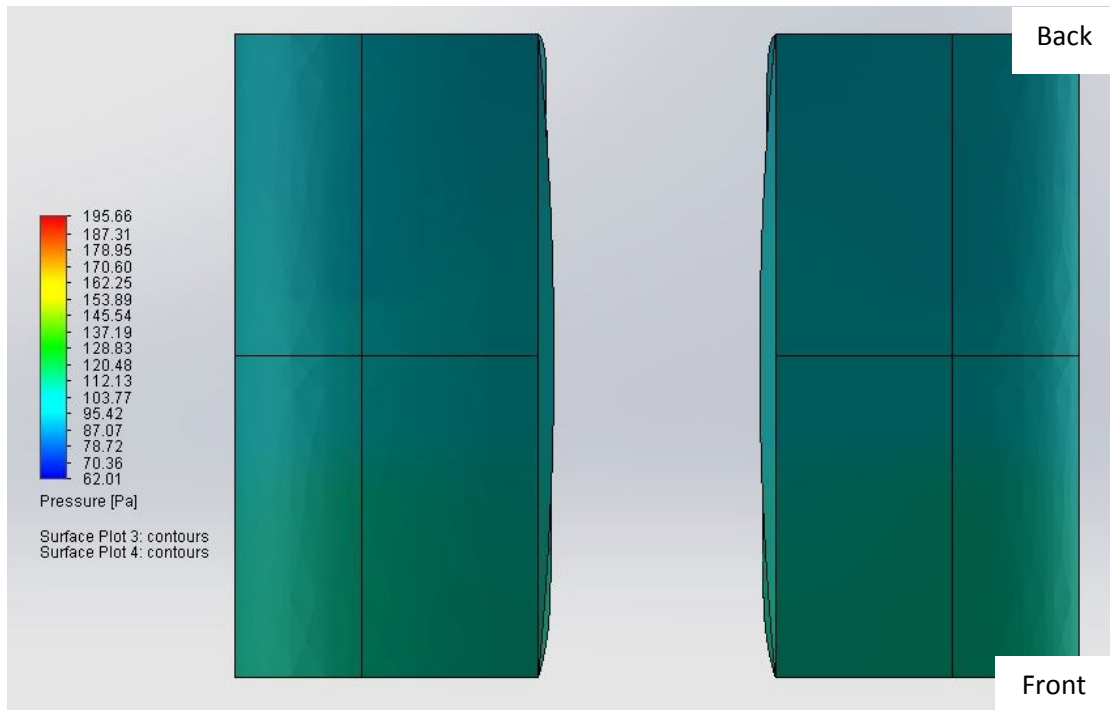


Figure 48: Pressure Distribution on the Third Row of Air Bearing Skis

Based on the three images above, it is clear that the pressure decreases when the flow passes by the skis ahead. The peak lift pressure generated by the flow is around 136 Pa, which is much less than the pressure required. It is concluded that the aerodynamic air bearing actually could help to provide lifting force to push the capsule but it is not the mainly lifting source for the capsule's weight and requires other sources of air supplies.

### 5.3.3 Discussion

The result of the flow simulation would well explain that the aerodynamic air bearing actually works to provide some parts of lifting pressure. And the drag force generated by the air bearing is thought to be close to the predicted value in Hyperloop Alpha design. However, the main sources of the lifting pressure will come from the external bearings, which are both external and aerodynamic bearings in Alpha design. This is attributed to two reasons. The first one is the design of the ski, which is required to be elevated 0.05°. Due to the drag and the gap between tube walls and skis, the elevated angle probably could not be able to be very large but 0.05° seems a very tiny angle for the whole structure. There might be a better angle value for the application of aerodynamics air bearing but this part of elevated angle optimization is not included in the report due to the limit of time. The other reason is the error produced in the process of simulation. In preliminary flow simulation, some of the input parameters are assumed in the analysis, such as turbulence intensity, turbulence length, etc. As a consequence, an error is possible to happen in the process. And when the speed of the capsule is close to the speed of sound, the airflow acts very differently than at lower speeds. Moreover, the actual flow will become more complex because of the suction of the compressor in the front. Consequently the analysis could not simulate the exact flow condition completely.

However, the simulation in the report can well conclude what level of lifting pressure aerodynamic bearing could provide and indicate that the idea of the aerodynamic air bearing is feasible but that would be of limited effect.

In the future, several analysis could be done for more accurate and comprehensive results. Solidworks is a stable and powerful modelling tool with a good performance of surface modelling, but for the flow simulation, ANSYS Fluent is considered as a better CFD tool with advantages of precise and detailed simulation of complex flow (e.g. turbulent flow with very high Reynolds number). A series of CFD

with different ski elevated angle could be carried out to find out the most efficient value. Moreover, the data about the properties of front compressor can be input into the analysis to have a better simulation of a real flow.

## 5.4 External Pressurized Air Bearing Investigation

### 5.4.1 Shape Design

Orifice bearing and porous bearing are two common types of external pressurized air bearing, which are shown in Figure 9.

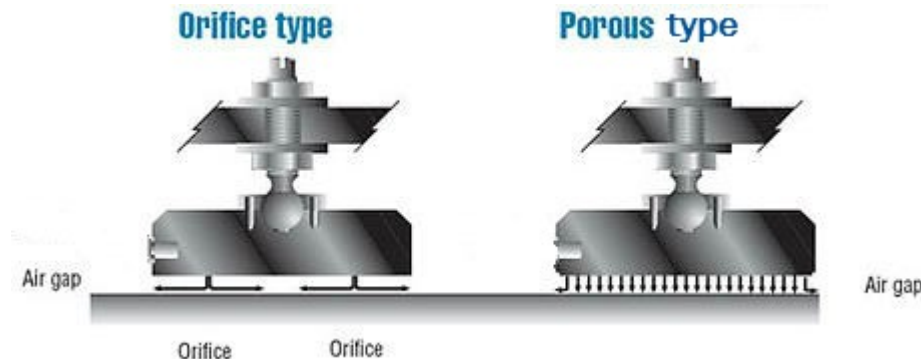


Figure 49: Schematic diagram of orifice bearing and porous carbon bearing [20]

A porous surface has advantages in producing air cushion with well-distributed pressure, but the mechanical strength of the porous surface could be a potential risk. In comparison, orifice type has better precise flow rate control and the technology is more mature. Therefore an orifice type of air bearing is applied in the design.

A schematic diagram of orifice air bearing and air conduction grooves are shown in Figure 50 and Figure 51 respectively. The corresponding dimensions are shown in Table 11.

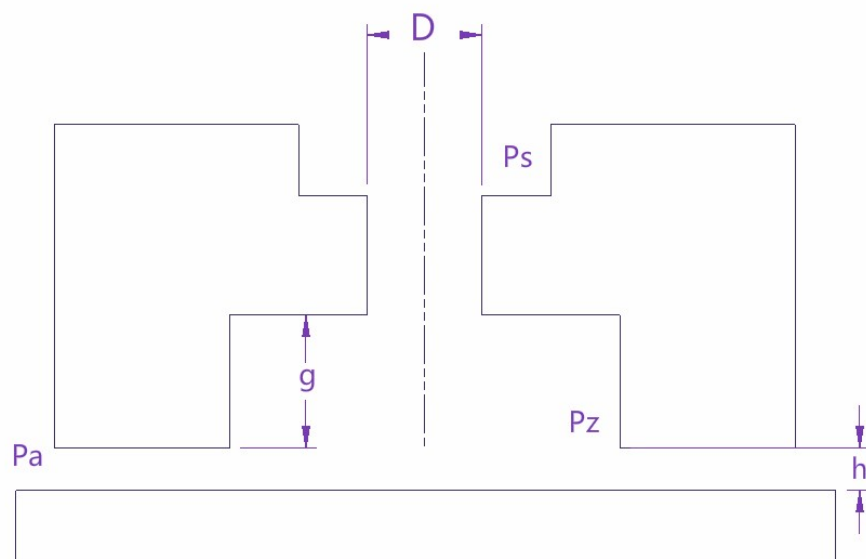


Figure 50: Section View of Orifice Air Bearing

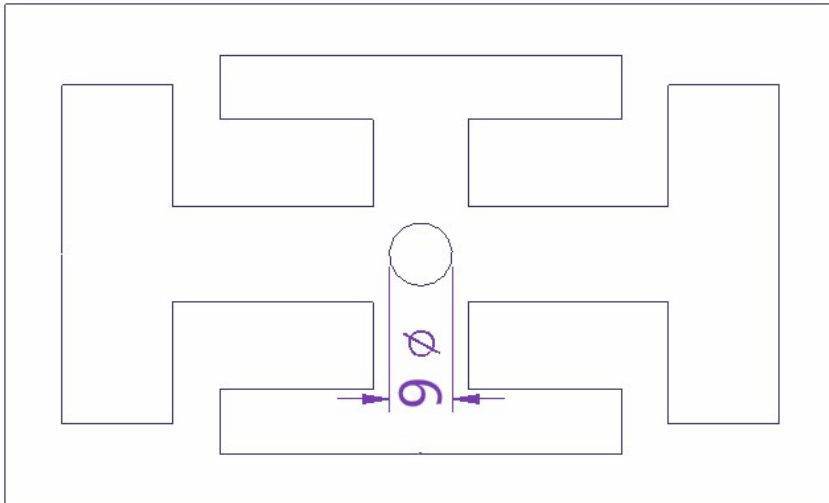


Figure 51: Air Conduction Grooves

Table 11: Air Bearing Parameters

Diameter of the orifice D	0.06 m
Depth of the air conduction grooves g	2 mm
Bearing gap h	1 mm
※Coefficient of the gas viscosity $\mu$	$2.3263596 \times 10^{-5}$
Gas constant R	8.314 J/(mol·K)
Gas temperature T	400 K
Specific heat ratio of bearing gas $\kappa$	1.4

※Coefficient of the gas viscosity  $\mu$  is obtained from gas viscosity graph [19]

#### 5.4.2 External Pressurized Air Bearing Flow Calculation

The flow is assumed to have an adiabatic expansion pass through the orifice. Base on the restriction effect, the mass flow rate of the air injected from the orifice is as follows:

$$M' = \frac{A \cdot P_s}{\sqrt{(RT)}} \cdot \varphi_0 \quad (115)$$

Where,

$$A = \pi D (g + h) \quad (116)$$

$$\varphi_0 = \sqrt{\frac{2\kappa}{\kappa-1}} \cdot \sqrt{\sqrt{\frac{P_z}{P_s}} - \sqrt{\frac{\kappa+1}{\kappa}} \sqrt{\frac{P_z}{P_s}}} \quad (117)$$

In Hyperloop Alpha design, the pressure of air coming from the intercooler is 11000 Pa. And based on the calculation in Section 3.2, the minimum pressure of air cushion in grooves is required as 3993 Pa. According to Toshio MUKA. (2006), the air injection pressure and the air cushion pressure are considered to have following relation:

$$\frac{P_z}{P_s} \geq \left(\frac{2}{\kappa+1}\right)^{\frac{\kappa}{\kappa-1}} \quad (118)$$

$\therefore$  The range of inlet air pressure is  $7562.5 \text{ Pa} \leq P_z \leq 11000 \text{ Pa}$

Based on aforementioned formulas and the formula to calculate air density, a MATLAB script is written to find the mass flow rate, volume flow rate and velocity of the injected air with respect to the variation of the inlet pressure and the graphs plotted are shown in Figure 52.

Density of inlet air:

$$\rho = \frac{P_s \cdot M}{T \cdot R} \quad (119)$$

Where T is the temperature of inlet air, M is molar mass of the air and R is gas constant.

Volume flow rate of the injected air:

$$V = \frac{M'}{\rho} \quad (120)$$

Velocity of injected air:

$$v = \frac{V}{\text{orifice area}} \quad (121)$$

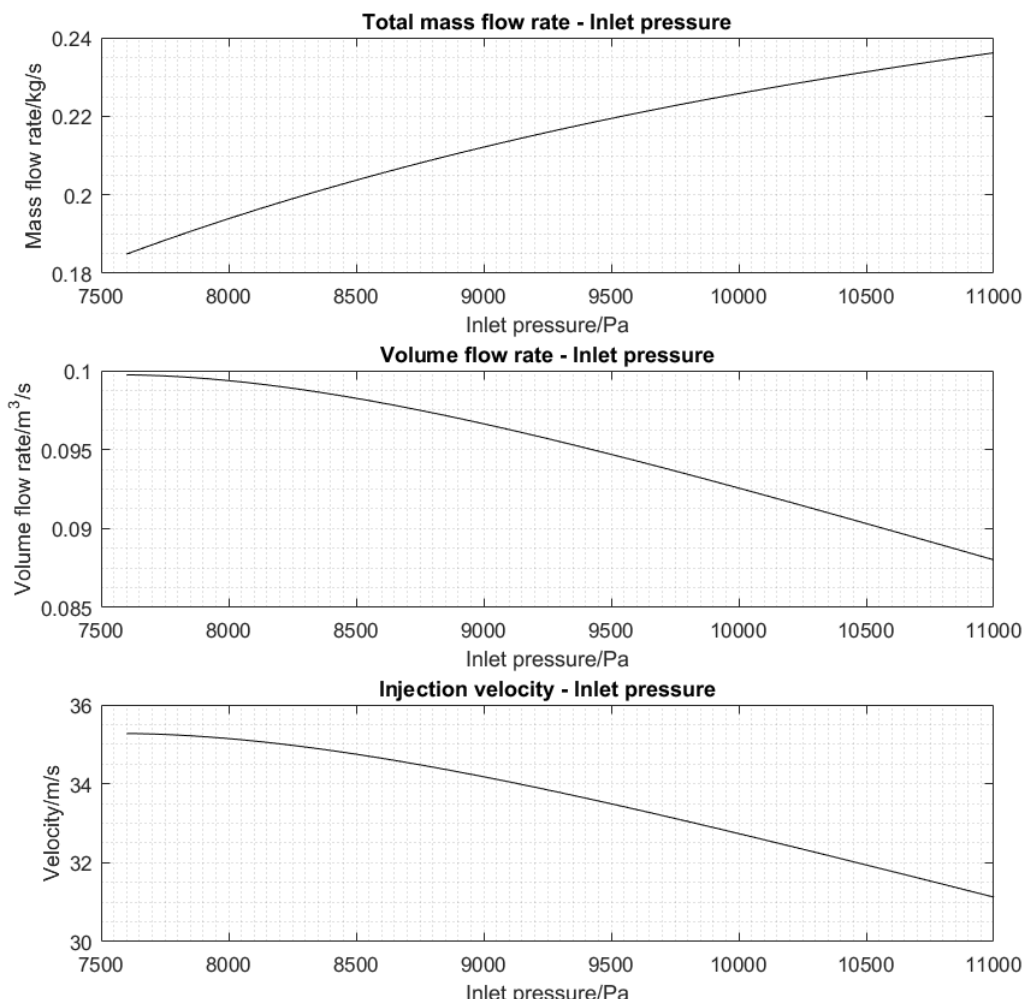


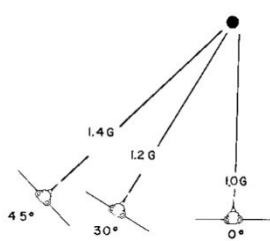
Figure 52: Injection Flow against Inlet Pressure

It is clear from graphs that the mass flow rate is required to be 0.2362 kg/s at the inlet pressure of 11000 Pa. The maximum volume flow rate is  $0.0997\text{m}^3/\text{s}$  when the inlet pressure is 7562.5 Pa and the maximum injected velocity will be 35.2759 m/s.

Therefore technically it is feasible to use external pressurized air bearing to push the capsule up. The value of mass flow rate is reasonable for the air reservoir to provide such volume of air when the capsule is cruising. And the velocity of air injection is also within a reasonable range.

Therefore a flow rate of 0.2362 kg/s at a pressure of 11000 Pa maintains a levitation of the capsule at mass of 15000 kg.

#### 5.4.3 Discussion



Problem①: The aforementioned mass flow calculation happens in the condition that the bank angle of air bearing ski is  $0^\circ$ . The figure might be far more than the values at another bank angle.

In consideration of the lifting efficiency, the bank angle (Figure) of the skis is set between  $0^\circ$  and  $45^\circ$ . the inlet air pressure is set as 11000 Pa. Another MATLAB script is run to find out the impact from the ski bank angle. The result is shown in Figure 13.

Figure 53: Bank angle

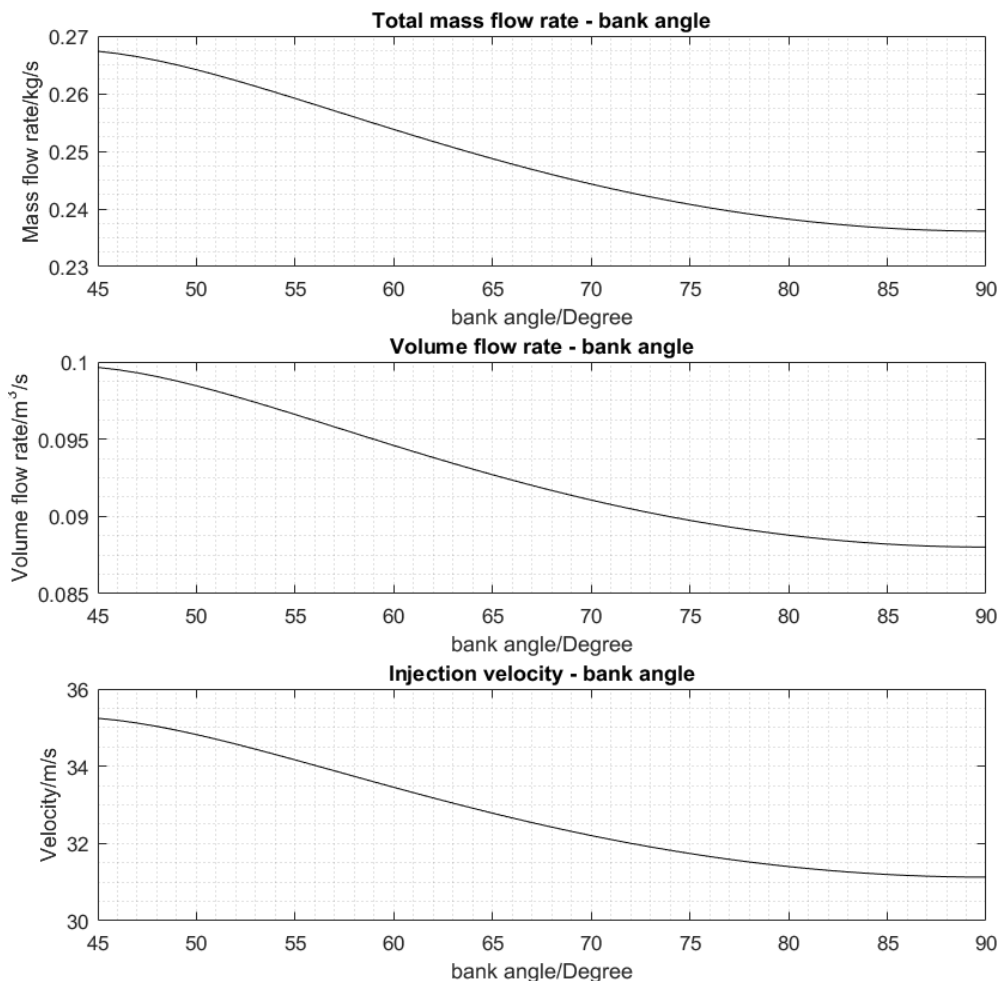


Figure 54: Injection Flow against Bank Angle

From the graphs, it is clear that the mass flow rate will increase as the bank angle goes up, but the result is still feasible to carry out the Hyperloop Project. Therefore in current design of the report, external pressurized air bearing could work and there is also feasibility for other possible design with different bank angles

Problem②: There would be pressure loss when the air is discharged from the grooves to the outside atmosphere. And the flow outside would have impact on the pressure distribution under skis.

In fact, the pressure of air will fall to the atmospheric pressure due to viscous resistance when pass through the tube wall to outside. A feasible solution is to make the area of guided air conduction grooves as much as possible, which could delay the pressure drop and make sure that most lifting areas are under required pressure. For the effect from outside flow, the depth of air conduction grooves is considered to increase for the compensation of the flow impact, which acts like a hovercraft skirt.

Moreover, the elevation of the air bearing skis will produce a larger gap between skis and walls in the front and smaller in the tip, which would also influence the final result. To solve this, a robust flow simulation could be carried out to analyse the flow pattern and then use finite element tools to calculate the pressure of each lattice, which is very accurate to find out the required flow rate.

Generally the externally pressurized bearing is feasible to be used in Hyperloop. By injecting pressurized air into the gap, the capsule could float during the travel. However, there are still some detailed technological programs to be solved. In addition, there are also some challenges to make the plan come true. For example, the current air bearing is use as a lubricant with a gap of several micrometres. The air bearing gap for Hyperloop is assumed as 1 mm at present, but for such a big project, the precise manufacturing of skis and walls must have an enormous cost.

## 5.5 Suspension Safety

It is risky if the capsule can only be supported by the air bearing. In consideration of this, two rows of deployable wheels similar to aircraft landing gears are applied at the low speed condition (160 km/h) and also serve as an emergency component. The wheels are controlled automatically by computers so it could work smartly and be suitable for emergency. For the comfort of travel, traditional mechanism suspension systems are included on the capsule to reduce the discomfort from vibration. The traditional suspension is placed between the skis and the capsule pod. Using aforementioned ways, the suspension of the Hyperloop could be safe as much as possible.

# 6. Vacuum system

## 6.1 Introduction to Vacuum Details

### 6.1.1 Vacuum Proposal

The design area of the partial vacuum system will focus on the feasibility of the design proposed by Elon Musk in the hyperloop alpha. This will include research on the different vacuum pumps available, selecting the most suitable vacuum pump from the information gathered, calculations on how the partial vacuum will operate and potential improvements that can be made to the design.

There is a lot of data that is needed that is taken from the hyperloop design alpha to check the feasibility of the design.[1] Primarily, the most important piece of information is the planned pressure inside the tubing, 100 Pascal's (1mbar). This is vital in the hyperloop design as it decreases the drag force on the hyperloop capsules by 1000 times. This allows the capsules to be able to reach very high speeds with a lot less power than at atmospheric pressure. To maintain and generate this low pressure vacuum, it is proposed that standard commercial vacuum pumps will be used. As no details were given on the type or performance of the proposed vacuum pumps, the different types of vacuum pumps available will be researched with the most suitable chosen for further analysis.

The proposed geometry and structure of the tubing was also proposed in the hyperloop alpha and is vital for calculations in the vacuum feasibility. The tube is also proposed to be made out of steel. Therefore, it is planned that the tube can then easily be welded together by side by side configuration. The following is the geometry given for the tube design:

- The inner diameter of the tube is planned at 2.33 metres.
- The cross sectional area of the tube will therefore be 3.91 metres squared.
- The tube will have an inner wall thickness between 20 to 23 millimetres.
- The tube will have a length of roughly 563 kilometres.

Using the above geometry, the volume of the tube can be calculated. However, it is not stated if the proposed length of the tube is the true distance of the tubing or if it is the displacement between the two hyperloop stations. Therefore, it is assumed that the length given is a rough estimation. The volume calculated will then be treated as the rough volume given from the hyperloop alpha data.

$$V = A \times L \\ V = 2201330m^3 \quad (122)$$

This volume is then used in further calculations in determining the number of vacuum pumps that will be required for the system and the evacuation time of reducing the pressure in the tube.

### 6.1.2 Vacuum Pump Terminology

To compare the different types of vacuum pumps, some key attributes are needed to be known. Primarily, the CFM of the pumps will be compared. The CFM stands for cubic feet per minute and is a measurement of the speed of the vacuum flow (flow rate) [25]. This is key for comparisons as it shows how fast the vacuum pump can create the vacuum. Another important attribute is the Ultimate vacuum of the pump. This is important as the vacuum pumps will cease to work if their ultimate vacuum is exceeded. The efficiency of a vacuum pump will also decrease as the pressure of air climbs towards the ultimate vacuum pressure.

## 6.2 Research on Vacuum Pumps

### 6.2.1 Different Vacuum Pump Types

Vacuum pumps are widely categorised into 2 different types, gas transfer pumps and entrapment pumps. Gas transfer pumps can then be further split into another two types, positive displacement pumps and momentum transfer pumps. These different types can then be evaluated to decide which pump is most suitable for the hyperloop system [26] [27].

The positive displacement vacuum pumps (PDVP) work by increasing the volume of the desired vacuum region with the opening of the pump inlet. As air will expand as it is drawn into the vacuum pump, the pressure will decrease. The air inside the pump is then sealed off from the vacuum and then exits the pump through an outlet into the atmosphere. The process then repeats itself with constant volume of air exiting the vacuum until the desired pressure level is achieved inside the vacuum region. The momentum transfer pumps work in a similar way to PDVPs as air is taken from the vacuum region and displaced into the atmosphere. Gas molecules will enter the pumps and will be forced downwards into the pump by mechanical instruments inside the pump. These instruments can be high speed turbines or jets of fluid turning blades. The air molecules will then exit through the bottom of the pump. The final type of vacuum pumps is entrapment pumps. They work by using chemical reactions to create vacuums. These pumps can work in different ways but always capture the gas in a solid state. An example is the cryogenic pump which condenses the gas onto a cold surface.

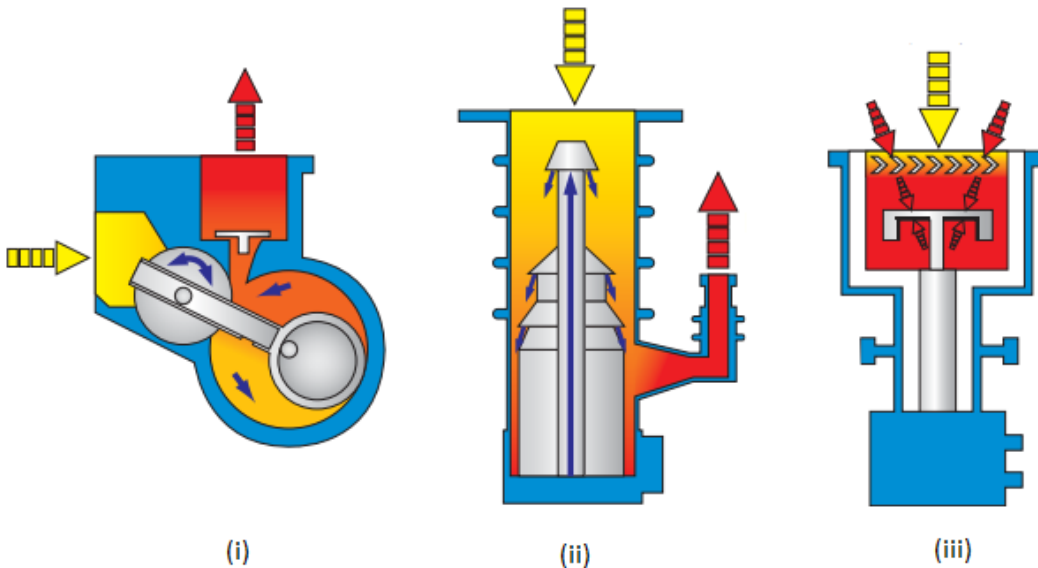


*Figure 55: Diagrams of (i) PDVP (rotary piston), (ii) Momentum transfer pump (Diffusion) and (iii) Entrapment pump (Cryogenic). [30]*

The three types of pumps all have advantages and disadvantages that will affect the hyperloop system. Primarily, the positive displacement pumps main advantage over the other pumps is that they pump at a constant air removal rate. This is useful as it simplifies the calculations needed for determining the level of vacuum in the system. This means the pumps can also be easily corrected for errors and faults. Another important benefit the positive displacement pumps have over the other two is that there are far less vibrations in these pumps. As too many vibrations can disrupt the workings of the hyperloop system, it is ideal if vibrations are kept to the minimum. However, the main drawback with positive displacement pumps, compared to the other 2 pumps, is that they often work at lower flow rates. This means they will take longer to create the desired vacuum in the tubing and may also not be as efficient at keeping the vacuum in equilibrium.

The momentum displacement pumps are very efficient at pumping at very large flow rates. This is very advantageous in regards to the hyperloop system as it means the system can produce and retain the desired pressure with ease. However, there are a few disadvantages with momentum transfer pumps that make them undesirable for use within the hyperloop system. Primarily and most importantly, the momentum transfer pumps, that are available on the market, are mainly designed for high and ultra-high vacuums or designed for very low vacuum levels. With the high performance pumps, the desired pressure of 100 Pascal's for the hyperloop system is at the lower end of the pressure scale of these pumps. This means the pumps will not be competent enough for the desired pressure. This is due to the inlet pressure in the tubing being too high, thus the pumps will easily stall. To overcome this deficiency, the momentum transfer pump will first need a positive displacement pump before it to lower the pressure to an operational pressure value. Therefore, using straight positive displacement pumps will be much easier and straightforward. Other drawbacks of momentum transfer pumps are the high power outputs given by the pumps and also the high vibrations caused by these pumps. The high power outputs of the momentum transfer pumps means that there will need to be a high level of power continuously fed to the pumps, this is not desirable with the long hyperloop system. The high vibrations may transfer over to the tubing, causing serious safety concerns.

The entrapment vacuum pumps main appeal is their use for creating vacuums that are contamination free. As the other vacuum pumps need some sort of lubricant or liquid, there will be small contamination leaks caused by these. This means the entrapment pumps can create the cleanest vacuums. However, there are several disadvantages with the entrapment pumps for the hyperloop system. The main disadvantage is that entrapment pumps are nearly always designed to be placed inside of the area that is to be the vacuum. This is not possible for the hyperloop system as there is no space

for the pumps to be placed in the tubing. This makes the entrapment pumps unavailable for use in this system. The pumps also tend to be large in size and would not be suited to the environment of the hyperloop. Other shortcomings with these pumps are similar to the momentum transfer pumps, there are large vibrations caused by the pumps and the pumps need PDVPs to be used as well to create high vacuums.

The drawbacks of the other two types of vacuum pumps make the positive displacement vacuum pumps the most desirable for the hyperloop system. However, there are still some concerns with these pumps. Therefore, the different types of PDVPs were researched to find the most suitable for the hyperloop system.

### 6.2.2 Different Positive Displacement Vacuum Pumps

There are several different types of positive displacement vacuum pumps that were researched for consideration for use in the vacuum. From the research, it is evident that all the pumps create problems for the hyperloop system and none would be a perfect fit. However, as the design proposal states that standard vacuum pumps were to be used, the pumps are evaluated and the most suitable pump for the system is chosen for further analysis.

The first pump to be considered is the **rotary piston vacuum pump**. These pumps work by a rotating eccentric piston and a sliding vane working in unison to suck the gas into the pump before it is compressed. The gas is then ejected into the atmosphere and the cycle is restarted. The compressed gas is sealed off from the inlet by oil. These vacuum pumps can give quick volume flow rates for pumping gases in comparison to other vacuum pumps. However, these pumps are best suited for vacuums at lower ultimate vacuums than the vacuum required for the hyperloop system. In practical uses, these pumps are usually equipped in backing up diffusion or roots vacuum pumps.

The next vacuum pump that was evaluated was the **diaphragm vacuum pump**. This pump works by having reciprocating materials to draw air at two ends of the pump. The pump is then sealed using different types of valves. The main advantage of this pump is that it is a dry air pump, there is no oil needed as a sealant and therefore has no oil contamination in the air. However, these pumps are not intended for use in a hyperloop type system. They normally have an ultimate vacuum of 1000 Pascal's and therefore do not operate at the required pressure level. This means this pump is not suitable for use.

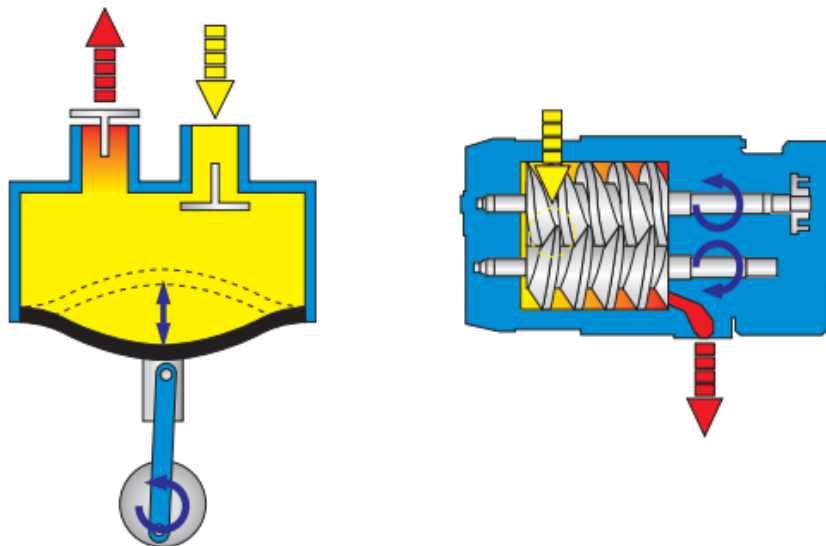


Figure 56: Diagrams of diaphragm pump (left) and rotary screws pump (right). [30]

The **rotary screw vacuum pump** works in several different ways. The pump can have one or more screws rotating, drawing the gas into the pump. The pump draws gas in at a constant rate and the screws

send the gas through the entire structure of the pump, before it exits at the end of the pump. The screw pump can achieve fast flow rates with high ultimate vacuums. However, when achieving the fast flow rates, the screws need to rotate extremely fast. This causes the pump to have a rapid increase in heat. This means the pump will need to be cooled continuously. This increase in speed also increases the rate of vibrations in the pump. This makes the screw pump not as suitable for the hyperloop system as the other vacuum pumps.

There were other vacuum pumps that fall into the positive displacement pump category but are not listed here as they were not evaluated deeply as they were not suitable for the hyperloop system due to not meeting the requirements necessary. The main shortcomings of these pumps were not having the required ultimate vacuum needed or having a much lower flow rate than some of the other vacuum pumps.

The vacuum pump chosen for further analysis is the **rotary vane vacuum pump**. Primarily, the rotary vane pump works by gas entering the pump through the inlet and is trapped between the vanes and the pump body. The gas is compressed down and is moved towards the outlet. Once the gas reaches atmospheric pressure, it is ejected through the outlet. The rotor then moves back and the process is repeated at a constant rate. The pump uses oil for a few different reasons, as a lubricant for the pump for smooth operation, to cool the pump down when the temperature increases and to also act as a sealant for the gas.

There are many different advantages for this vacuum pump in use in the hyperloop system. First and foremost, high flow rates are achieved with this vacuum pump, compared to the other pumps researched. This is a major advantage as it allows the air to be evacuated quicker than the other pumps. This means the rotary vane pump is more efficient than the other positive displacement pumps at the required pressure level. Another benefit of the rotary vane pump is that it has a very simple operation and design. This means that if there are any faults with the pumps during operation, they can easily be fixed or replaced. The rotary vane pumps also operate at very quiet levels. This relates to the low vibration levels of the vacuum pumps compared to the other pumps considered, especially the rotary screw pump. This is important as the greater number of vibrations in the pumps, the likelihood of this affecting the vacuum tube increases. Therefore it is vital that vibrations are kept to a minimum. The quiet operation also reduces sound pollution. The cost of a rotary vane vacuum pump suitable for the hyperloop system is also lower than the cost for the other vacuum pumps. This is important as several vacuum pumps will be needed to maintain the vacuum as it is an extremely large volume. When using more vacuum pumps, the overall cost will also increase. Therefore, the rotary vane pumps are suitable for the lower expenditure on vacuum pumps.

However, one consideration that is needed with the rotary vane vacuum pumps is the oil that is needed inside the pump. This oil will need to be correctly upheld for the vacuum pumps to be run at maximum efficiency. The rotary vane pumps will also have a maximum life expectancy that will need to be considered if the hyperloop system is to be a long term transport solution.

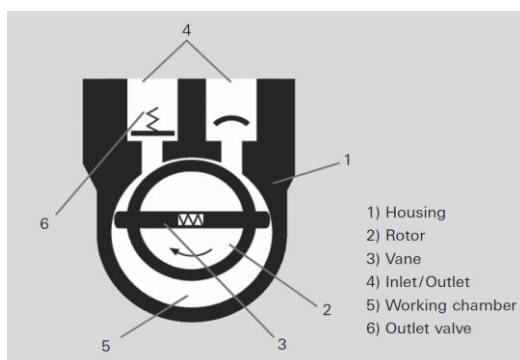


Figure 57: Diagram of rotary vane pump [31]

### 6.2.3 Market Research of Rotary Vane Pumps

For the rotary vane pumps that were researched and are available on the market, there were several factors that need to be taken into account when choosing the vacuum pump. The best possible flow rate for the pumps is extremely important but the environment will be an issue for larger more powerful pumps. Therefore the vacuum pumps researched were focused on pumps that were small and light, easily fitting into the tubing. The vacuum pumps must have a suitable maximum vacuum and be able to withstand the tube conditions. The table below shows different rotary vane vacuum pumps found online and the mass flow rates for each. There were also other vacuum pumps found online but had slower mass flow rates and consequently were not listed as they did not offer any further insight.



Figure 58 Rotary vane pump [32]

Table 12: Market vacuum pumps comparison

Vacuum Pump Model (company)	Ultimate Vacuum for pump (mbar)	Working mass flow rate ( $\text{m}^3/\text{s}$ )
PFPE RV12 (Edwards) [33]	$2 \times 10^3$	0.004719
Pascal 2063, C2 version (Pfeiffer) [32]	$1 \times 10^3$	0.01833
DS 602 (Agilent Technologies) [34]	$2 \times 10^3$	0.010083
7893R28 (Direct Drive) [35]	$5 \times 10^4$	0.005333

From the table, the Pascal 2063 vacuum pump was selected as the most suitable for further analysis. The pump has the greatest mass flow rate from the different pumps that were found on the market and can use this flow rate at the desired pressure. The following figure is the company's characteristic curve of how the flow rate varies with pressure. This curve shows the efficiency of the flow rate starts to decrease once the pressure goes below 100 Pascals. The curve also takes a sharp decline once the pressure is approaching the maximum vacuum level. Therefore the pump is suitable and works best for a vacuum of 100 Pascals.

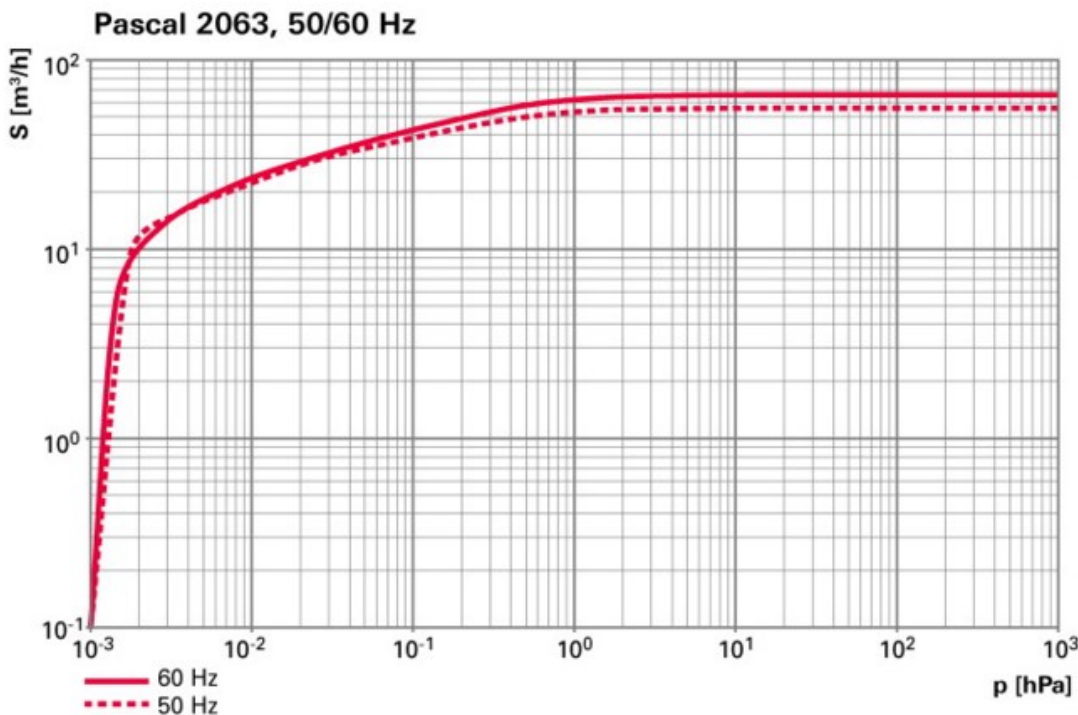


Figure 59 Pascal 2063 performance curve [32]

## 6.3 Calculations for Hyperloop Vacuum Pumps

### 6.3.1 Initial Design Calculations

The number of vacuum pumps used in the hyperloop system is evaluated based on how long it takes to create the vacuum. The following formula was used in MATLAB to find the optimum number of vacuum pumps needed in the hyperloop system [36].

$$t = \frac{V}{q \times \ln\left(\frac{P_{atm}}{P_{req}}\right)} \quad (123)$$

Where:

- $t$ = the time taken in seconds for the vacuum pump to reduce the volume of air to the required pressure.
- $V$ = total volume of air that is being reduced by the vacuum pump, in  $\text{m}^3$ . This volume is varied in MATLAB. When the volume decreases in size, there will be more vacuum pumps in operation and will reduce the volume that one vacuum pump will need to reduce the pressure in.
- $q$ = the volume flow rate of the vacuum pump that has been chosen for analysis, in  $\text{m}^3/\text{s}$ .
- $P_{atm}$ = the atmospheric pressure of air in the tubing, in mbar.
- $P_{req}$ = the required final pressure that is needed inside the tubing, in mbar.

The volume is varied to get different times for the number of vacuum pumps used. From this, a suitable value for the number of vacuum pumps can be chosen. However, this is just for the start up in creating the vacuum. Further calculations are needed to find how many vacuum pumps are required to keep the vacuum in equilibrium when it is running.

There are several different factors that affect the equilibrium of the vacuum while it is running. There

will be small leaks in the tubing from where the vacuum pumps are placed. Vacuum seals are used to reduce this pressure leak. If these seals are used correctly, it makes this value of pressure leakage so small it can be ignored for this consideration. Nevertheless, if the vacuum seals were to fail, the leakage would be very important. However, the geometry and conditions of the vacuum seals with the vacuum pumps is not known and therefore this cannot be calculated. There could also potentially be air leakage from the entrances and exits to the hyperloop tubing when the pods enter and exit the tube. However, the station geometry and how this air leakage will be dealt with is not currently known. This means this cannot be calculated for air loss.

The air that exits the pod and is left behind could also affect the equilibrium of the tubing pressure. There is one consideration however that this air will be of higher pressure and will succumb to sudden expansion in the low pressure tubing. However, to make sure this air cannot build up and affect the tube pressure, the vacuum pumps will be used to quickly pump this air out of the tube. The worst case scenario for this will take place where the hyperloop will be running and the tube will be full of capsules. To find the amount of air that has to be removed, the following data is taken from the suspension section.

- Density of air at 400 kelvin=  $0.887 \text{ Kg/m}^3$ .
- Maximum mass flow rate of air exiting the pod=  $0.2362 \text{ Kg/s}$ .
- Maximum pressure of air exiting the pod= 11000 pascals.
- 

To find the volume of air in the tube left by the pods, the mass flow rate must first be changed into the volume flow rate. This is done in the following calculation.

$$q_{pod} = \frac{\dot{m}}{\rho} \quad (124)$$

$$q_{pod} = \frac{0.2362}{0.887} = 0.2663 \text{ m}^3/\text{s}$$

With this flow rate, the volume of air that is released into the tube by one pod over its total journey is as follows:

$$V_{1pod} = q_{pod} \times \text{time of journey} \quad (125)$$

$$V_{1pod} = 0.2663 \times 2134 = 568.2647 \text{ m}^3$$

For the worst case scenario, the tube will be full of pods. As the pods are planned to be released every 2 mins, the total volume of air will need to account for all the pods at the different stages of their journeys. Therefore, the volume of air that a pod will release will simply be calculated as the time the pod has been in the tube over the total volume of air released. With the pods released every 2 minutes, the true total volume will take the volumes of the pods from 2 minutes into the pod all the way up to a pod completing a full journey. This total volume was calculated in excel and can be seen in the appendices. The value of total air released by the pods for the worst case scenario is  $5398.51465 \text{ m}^3$ . The calculations for the optimum number of vacuum pumps can now be completed. The formula [insert number] can be used again with the new data to find the time taken to remove gas released from the pods, with the volume varied to get the ideal number of vacuum pumps.

### 6.3.2 Decision on Numbers of Vacuum Pumps

As the total volume of air released calculated above takes place over 2134 seconds [1], the time taken to remove this air must be below this number, otherwise the tube will continuously fill with high pressure air. Therefore, any values above 2134 seconds can be instantly ignored. This still leaves several values of time left to be evaluated. As there is nothing given on the design brief on the number of vacuum pumps used, the analysis is evaluated to find a set of values that will give a reasonable set of values for time taken to create the vacuum and also for the vacuum to be kept in equilibrium. This comparison is simply checking and comparing the evacuation times for several different volumes. The value for the volumes were then interpolated to get a round number for the number of vacuum pumps used. After comparing the different sets of values, it is decided that 772 vacuum pumps will

give the best operation for the hyperloop system, based on the information gathered.

With the use of 772 vacuum pumps, it will take 22473.5 seconds to initially create the vacuum from scratch. This is removing all of the air from the tubing. This equates to 6.24 hours. As this is the start-up time and the vacuum will be kept continuously at the low pressure, this is quite a reasonable time. The only time this process will need to repeat itself is if the vacuum will need to restart after a failure of some sort. However, this means there is not a long down time if the hyperloop does fail. The use of 772 vacuum pumps also means that each pump will have to cover a volume of 2851.5m<sup>3</sup> of operation. The time it will take 772 vacuum pumps to remove the air from the pods, is 81.172 seconds. This is a very quick time as the high pressure air should be removed as soon as possible. However, there are quite a few inaccuracies with this number. As previously stated, there will be air leaks in the tubing that will also increase the air pressure. However, as the removal rate of these air leaks are unknown, they are not included. In theory, this time value will also be inaccurate. As the high pressure gas is left in the tube, it will in theory rapidly expand due to the density of the air. Therefore, it should be quicker to remove the high pressure air from the pod. This means the value of 81.172 seconds can be taken as the worst case scenario based on the information gathered.

The 772 vacuum pumps recommended for the hyperloop system will not all necessary be running when the hyperloop is in operation. As the vacuum pumps are commercial standard pumps, they will need a lot of maintenance to be able to work for a long period of time. This was considered when choosing the optimum number of pumps. If there are some pumps not in operation, this has a minimum effect on the efficiency of the vacuum.

### 6.3.3 Power Calculations

The vacuum pumps will need some sort of power source connected to be able to constantly run when needed. This power source can come from different sources available but as the local power capabilities for the route in California are unknown, there cannot be a recommendation for how to get the power at this time. However, the total power output of all of the vacuum pumps can be easily found. The total power output of 1 vacuum pump running at full operating capacity is 2.6kW [32]. This is given in the vacuum pump technical data section of the supplier's website. To find the total power output, the power output should be multiplied by the number of pumps, 772, in the system.

$$P_T = P \times N \\ P_T = 2.6 \times 772 = 2007.2kW \quad (126)$$

This is an extremely large number for the power output. For the practical application of the hyperloop, this power output should be looked at to be reduced.

## 6.4 Sustaining the Vacuum

### 6.4.1 Vacuum Seals

The hyperloop system cannot afford any leakages that may disrupt the operational capabilities of the system. Therefore, vacuum seals should be used to maintain the pressure level in the tubing. There are different types of vacuum seals that are suited to different types of connections used for securing the vacuum [37]. Depending on the connections used, vacuum seals can be installed through two different arrangements, static and dynamic. For the tube, the different tube parts are welded together in the construction. Therefore, the tubing falls into the non-detachable connections. For all non-detachable connections, static arrangements are necessary. Therefore, the different vacuum seals in this type can be compared in table 13. The outgassing rate displayed in the table is the pressure of the rate of gas that the seal will leak every second.

*Table 13: Vacuum seals*

Seal Material	Maximum working Temperature (°C)	Outgassing rate
Synthetic rubber	90	$1 \times 10^{-7} Pa.m^3/s$
Fluoroelastomer	150	$1 \times 10^{-9} Pa.m^3/s$
Perfluoroelastomer	200-250	$1 \times 10^{-10} Pa.m^3/s$

The synthetic rubber vacuum seals have a maximum working temperature of 90 degrees Celsius. Due to the higher temperatures that will be experienced, this vacuum seal is not appropriate for use. The Fluoroelastomer and Perfluoroelastomer vacuum seals will work in the temperature range. The outgassing rate for these seals is very low. However, the Perfluoroelastomer seal is a lot more expensive than the Fluoroelastomer seal and is also suited for higher vacuums. Therefore, the Fluoroelastomer is the most suitable vacuum seal for the hyperloop system. For the calculations of air leakage, the leakage is so small that it is not added to the vacuum pump calculations as it has no effect on the values achieved.

#### 6.4.2 Maintenance of Pumps

There are several tasks that will need to be done to ensure that the vacuum is treated with proper maintenance. The first major task that is required is to maintain the oil levels in the vacuum pumps. The vacuum pumps need the oil levels maintained to keep the seal inside the vacuum pump. The oil levels will need to be checked on a regular basis. This can be done by placing oil level gauges in the vacuum pumps. These gauges can then be connected to a control centre that will monitor the oil levels in every pump. To refill the oil levels, there are two possibilities that can be undertaken. Primarily, a mechanical filling system could be designed to automatically refill the oil. If this system cannot be designed, the oil levels will simply be refilled by human workers employed for hyperloop maintenance. As there is not enough data for the oil level reduction rates, no system can be designed to control this.

The next maintenance task that is required for the vacuum pumps is to insert gauges into the pumps to check the current vacuum level in the pumps. These would again be fed back into a control station. These are vital as they can alert operators of any pressure changes that may happen due to leakages. The vacuum pumps themselves will also need to be continuously checked to make sure there are no failures with the pumps. However, as the pumps have a life expectancy of a minimum of 5 years of continuous use, they will eventually need replacing. Yet, the vacuum pumps will not all be running at once, so they should last longer than this life expectancy. However, workers will need to be employed to ensure these pumps are still in proper working state.

#### 6.4.3 Future Improvements

There are some further improvements that were conceived for the hyperloop but cannot be done due to insufficient information. Firstly, the hyperloop station design has not yet been finalised and leakages from the entrances and exits to the tube cannot be found. Therefore the subsequent leakage calculations cannot be done. The leakages at the stations may be caused by not being properly sealed or proper operation is not used. Therefore, for the stations, an air lock system is proposed to maintain the low pressure vacuum in the tubing. This would involve creating another small vacuum for the pods at the station so the air is not leaked. This would require more vacuum pumps for the air lock [38]. The air lock system proposal would work with the passengers entering the pods at atmospheric pressure. Once all passengers are inside and the pod is sealed, it would move to an area before the tube to be depressurised. Then, once this areas pressure level matches the pressure level in the tubing, the tube will open and the pod can then be transported in the main tube. However, there was insufficient data and information to even conduct small calculations on this proposal.

## 7. Conclusion

As shown in the compressor final design, the further development should be focusing on solving the problem of power input. In the limited diameter as 1.1 meter, the power cannot be controlled lower than 400 kW, which is far higher than the expectation. In this situation, a more powerful batteries might be the best breakthrough for this problem, considering the truth that the battery capacity is developing very fast in recent years. Meanwhile, the outlet temperature of the compressor is a bit higher than the expectation that may require some adjustment of the length of the intercooler system to achieve the expected temperature.

The intercoolers were designed by following industry standards and considering the properties of both fluids at the beginning and end of each heat exchange process separately. The heat exchange coefficient was determined for both intercoolers and the expected temperature change calculated using the logarithmic mean temperature difference (LMTD) method. The two intercooler designs were then tested using the number of transfer units (NTU) method to give the final output temperatures. The data from this method showed that there would be a 498 K temperature drop in the first intercooler and a 183 K temperature drop in the second. These results were compared against a Simulink model with live updating of fluid properties. The results from this model were also produced using the NTU method but are more accurate due to the iterative process in the solution. The simulation gave a temperature drop of 462 K in the first intercooler and 239 K in the second. There is an error of 7.23% in the first value and 23.4% in the second; this has been found to be caused by the accumulating errors in the fluid properties over the duration of the simulation.

With regards to the hyperloop system, the output air temperature from the second intercooler was 71 K higher than the proposed output from the Hyperloop Alpha whitepaper. The output value of 471 K from the Simulink model however, does not take into account the effect of the baffles or heat loss to the environment. This should cause a significant temperature drop in the final output value, it cannot however reduce the temperature below 373 K as this is the temperature of the water inside the second exchanger. The completed intercoolers occupy 7.5 m in the front of the pod while the air and steam pressure vessels occupy a further 4.46 m. With an assumed compressor length of 4 m, the front of the pod takes up roughly 16 m. Further research needs to be done taking the passengers, luggage compartments and batteries into account to give a full length for the pods in order to determine the feasibility of the compression system's design with respect to pod length. It may be that the pods are too long to turn inside the hyperloop tube, in which case further options such as flexible joints should be considered.

Generally the air bearing suspension is considered to be feasible for the Hyperloop. The air bearing shape is optimized and a flow simulation is run to find out the flow pattern. Based on these, the maximum drag force on the air bearing skis is small and the value found in the report is very close to the one from Hyperloop Alpha design. However the maximum lifting pressure aerodynamic air bearings provide is limited so according to the simulation, it could not be the main source of lifting force. An orifice type is used in the external pressurized air bearing and by the calculation, a flow rate of 0.24 kg/s at the pressure of 11000 Pa would maintain the levitation of the whole capsule. In this condition, the volume flow rate and the injection velocity is within a practical range, so this scheme is feasible. However the flow rate calculated is slightly different from the ones in Hyperloop Alpha design, which could be caused by some changes in the shape design. Overall, the idea of air bearing suspension is feasible and more work is supposed to be done in the future to make the design more efficient.

For the vacuum system, the vacuum pumps used to create the vacuum in this design are rotary vane vacuum pumps. The recommended rotary vane pumps used is the Pascal 2063, C2 version rotary vacuum pump available from Pfeiffer. This vacuum pump has a working volume flow rate of 0.01833m<sup>3</sup>/s. These vacuum pumps should be very efficient for the hyperloop tube with many

connected in series. After calculations, the optimum number of rotary vane pumps for the hyperloop system is 772. The Time taken to create the vacuum from atmospheric pressure, using all the vacuum pumps, is 6.24 hours. These values mean the vacuum will be created and maintained very capably. The vacuum will also be sealed by Fluoroelastomer vacuum seals which have an outgassing rate of  $1 \times 10^{-9}$  Pa.m<sup>3</sup>/s. This is a very tight vacuum seal that will not give any problems with air leakages.

## 8. Reference

- [1] SpaceX, 2013. Hyperloop Alpha. [pdf] SpaceX. Available at: <[http://www.spacex.com/sites/spacex/files/hyperloop\\_alpha-20130812.pdf](http://www.spacex.com/sites/spacex/files/hyperloop_alpha-20130812.pdf)>
  - [2] Falck,N. (2008) 'Axial Flow Compressor Mean Line Design'. Lund University
  - [3] Funda Ersavas.(2011) Multidisciplinary Conceptual Design of a Transonic Higher Pressure. Chalmers University of Technology
  - [4] Grote, Karl-Heinrich, Antonsson, Erik K. Springer Handbook of Mechanical Engineering
  - [5] S. L. Dixon. (1998) Chapter 5: Axial-flow Compressors and Fans. Fluid Mechanics, Thermodynamics of Turbomachinery
  - [6] Meherwan P. Boyce '2.0 Axial-Flow Compressors'
- 
- [7] Kakaç, S and Liu, H, 1998. Heat Exchangers: Selection, Rating and Thermal Design. 2<sup>nd</sup> ed. CRC Press: United States.
  - [8] JiaWei, 2013. [Plate heat exchanger] Available at: <<http://www.jiawei-phe.com/Gasket-Plate-Heat-Exchanger.html>>
  - [9] Comsol, 2015. [Shell and tube heat exchanger] Available at: <<https://www.comsol.com/blogs/how-model-shell-and-tube-heat-exchanger/>>
  - [10] [Temperature drop in parallel flow and counter flow] n.d. Available at: <<http://www4.ncsu.edu/~doster/NE400/Text/HeatExchangers/HeatExchangers.PDF>>
  - [11] Professor John R.Thom, 2004. [Wolverine Tube Heat Transfer Data Book III]. Wolverine Tube Inc. Available at:  
<[https://www.academia.edu/5223501/A\\_STUDY\\_BASED\\_ON\\_DESIGN\\_OF\\_AIR\\_COMPRESSOR\\_INTERCOOLER](https://www.academia.edu/5223501/A_STUDY_BASED_ON_DESIGN_OF_AIR_COMPRESSOR_INTERCOOLER)>
  - [12] National Climatic Data Center, NOAA, 2011. Comparative Climatic Data – United States. Available at: <<http://ggweather.com/ccd/avgrh.htm>>
  - [13] International Association of Classification Societies, 2001. Requirements Concerning Pipes And Pressure Vessels. [pdf] Available at: <[http://www.iasc.org.uk/document/public/Publications/Unified\\_requirements/PDF/UR\\_P\\_pdf157.PDF](http://www.iasc.org.uk/document/public/Publications/Unified_requirements/PDF/UR_P_pdf157.PDF)>
  - [14] TEMA, 1988. Standards of the Tubular Exchange Manufacturers Association. TEMA: New York.
  - [15] Young, H.D., Freedman, R.A. and Ford, A.L., 2011. University Physics, 7th Ed. Table 15-5. Addison-Wesley: United States.
  - [16] Shandong Pulilong Pressure Vessel Co. Ltd, 2015. Available at: <[http://www.alibaba.com/product-detail/high-pressure-steam-tank-of-pressure\\_1833610264.html?spm=a2700.7724857.29.12.wB16mg&s=p](http://www.alibaba.com/product-detail/high-pressure-steam-tank-of-pressure_1833610264.html?spm=a2700.7724857.29.12.wB16mg&s=p)>

- [17] Bloodhound Team. (2015). the BLOODHOUND Project. Available: <http://www.bloodhoundssc.com/>. Last accessed 16th Nov 2015.
- [18] Marzocco, Pier. "The NACA airfoil series" (PDF). Clarkson University. Retrieved 07-03-2009.
- [19] Hyperloopdesign team. (2014). The Problems with Air Bearing Skis. Available: <http://www.hyperloopdesign.net/#!air-skis/cgkx>. Last accessed 25th Oct 2015.
- [20] Moran, Jack (2003). *An introduction to theoretical and computational aerodynamics*. Dover. p. 7. ISBN 0-486-42879-6.
- [21] Toshio MUKAI. (2006). Analysis of Dynamic Characteristics of Air Bearing. NIPPON STEEL TECHNICAL REPORT. 3 (1), p15-16.
- [22] J.Y.Wong (2001). THEORY OF GROUND VEHICLE. 3rd ed. Canada: John Wiley & Sons, Inc . . p485-519.
- [23] Westwind Air Bearings (2007). AIR BEARING TECHNOLOGY. 2nd ed. Dorset: Westwind Air Bearings. p2-16.
- [24] Edinburgh University Hyperloop Team. (2015). Hyperloop Pod Competition. Hyperloop Pod Competition. 30 (3), p20-21.
- [25] Vacuumchuck.com, 'Vacuum Pumps Explained'. Website. Accessed 14 Nov. 2015.
- [26] Pumpscout, Mackay, Ross. 'Understanding Positive Displacement Pumps'. Pumpscout.com. N.p., 2015. Website. Accessed 3 Nov. 2015.
- [27] Gastmfg.com, 'Vacuum Pumps'. Website. Accessed 29 Oct.2015.
- [28] Oerlikon leybold Vacuum. 'Fundamentals of Vacuum Technology'. 3.nd.edu. Accessed 22 Nov. 2015.
- [29] PPIPumps.com, 2009, 'Types of Vacuum Pumps' Website. Accessed 22 Oct.2015.
- [30] Lesker.com, 'Pump Classifications', Website. Accessed 2 Nov.2015.
- [31] Pfeiffer Vacuum, 'Rotary Vane Vacuum Pumps', Website. Accessed 25 Nov.2015.
- [32] Pfeiffer Vacuum, 'Pascal 2063 C2', Website. Accessed 2 Nov.2015.
- [33] Edwards Vacuum, 'PFPE RV12 Two Stage Rotary Vane Pump' Website. Accessed 2 Nov.2015.
- [34] Agilent Technologies, 'DS 602 rotary vane pump', Website. Accessed 2 Nov.2015.
- [35] Thomas Scientific, 'Direct Drive Vacuum Pumps', Website. Accessed 2 Nov.2015
- [36] engineeringtoolbox.com, 'Vacuum - Evacuation Time', Website. Accessed 16 Nov.2015
- [37] VAT, Sonderegger Kurt, 2006, 'Vacuum SealingTechnology', Website. Accessed 12 Nov.2015
- [38] HyperloopDesign, 2015, 'Station layouts, airlocks and passenger loading' Website. Accessed 27 Nov.2015

# Appendix

## Appendix A. Compressor geometries and Flow Properties

### Overall Properties

Compressor Type	CID
Inlet Pressure	0.00099 [bar]
Inlet Temperature	19 [Celsius]
Mass Flow	0.57 [kg/s]
Pressure Ratio	21
Number of Stages	10
Rotation Speed	13000 [RPM]
Tip Clearance	0.02
Aspect Ratio (Rotor)	2.5 → 1
Aspect Ratio (Stator)	3.5 → 1
Thickness Chord Ratio	0.06
Axial Velocity Ratio	0.99 → 0.97
Blockage Factor	0.98 → 0.88
Diffusion Factor	0.45
Inlet Angle	15 [degree]
Loading Distribution	1 → 0.8
Inlet Hub Tip Ratio	0.52
Stage Flow Coefficient	0.65
Stage Reaction	0.51
Diameter of the Compressor	1.0868 [m]
Outlet Pressure	20.8 [kPa]
Outlet Temperature	1133.68 [K]
Power	432.5531 [kW]
Isentropic Efficiency	48.24%
Polytrophic Efficiency	43.02%
Outlet Flow Velocity	322.54 [m/s]

## Stage 1

Flow Properties

Pressure Ratio	1.3164
Temperature Rise	91.57
Enthalpy Increase	82857
Entropy Increase	89.77
Load Distribution (psi)	0.2670
Stage Flow Efficiency (phi)	0.7028
Stage Reaction	0.6256
Isentropic Efficiency	44.64%
Polytrophic Efficiency	46.93%
Mass Flow	0.57

Velocity [m/s]							
Section	$C_m$	$U$	$C$	$C_\theta$	$W$	$W_\theta$	Sound Speed
R In	483.33	743.59	500.38	129.51	781.48	614.08	384.54
R Out	478.50	624.98	563.59	297.77	579.68	327.21	411.89
S Out	473.72	N/A	514.07	199.66	N/A	N/A	424.09

Section	Flow Angles [degree]		Pressure [Pa]		Enthalpy [kJ/kg]		Entropy [J/K]	Specific Heat	Density	Viscosity
	$\alpha$	$\beta$	Total	Static	Total	Static				
R In	15	51.79	620	220	221.24	96.044	2058	1010.9	0.0021	0.0111
R Out	31.89	34.37	880	290	311.04	152.22	2126	1017.6	0.0024	0.0109
S Out	22.87	N/A	820	330	311.04	178.90	2148	1021.6	0.0026	0.0106

Section	De Haller	Diffusion Ratio	Critical Mach
Rotor	0.7418	1.6464	1.3683
Stator	0.9121	1.5543	1.2122

Blade Geometries

Section	Pitch/Chord	Thickness/Chord	Aspect Ratio	Tip/Chord	Number of Blades
Rotor	1.0063	0.06	2.5	0.02	18
Stator	4.0240	0.06	3.5	0.02	14

Blade Angles [degree]						
Section	Inlet	Outlet	Camber	Stagger	Incidence	Deviation
Rotor	38.78	31.91	6.87	48.36	13.01	2.46
Stator	41.55	-54.53	96.08	-16.15	-9.66	77.40

section	Radius [m]		
	Tip	RMS	Hub
Rotor In	0.5435	0.4525	0.3380
Rotor Out	0.5260	0.4421	
Stator Out	0.5161	0.4362	

## Stage 2

Flow Properties

Pressure Ratio	1.3205
Temperature Rise	95.74
Enthalpy Increase	98644
Entropy Increase	72.79
Load Distribution (psi)	0.2580
Stage Flow Efficiency (phi)	0.7694
Stage Reaction	0.5603
Isentropic Efficiency	50.28%
Polytrophic Efficiency	52.10%
Mass Flow	0.57

Velocity [m/s]							
Section	$C_m$	$U$	$C$	$C_\theta$	$W$	$W_\theta$	Sound S
R In	473.72	616.65	514.07	199.66	631.10	416.98	424.09
R Out	467.93	607.22	589.31	358.24	530.04	248.98	446.94
S Out	462.21	N/A	505.77	205.35	N/A	N/A	465.42

Section	Flow Angles [degree]		Pressure [Pa]		Enthalpy [kJ/kg]		Entropy [J/K]	Specific Heat	Density	Viscosity
	$\alpha$	$\beta$	Total	Static	Total	Static				
R In	22.85	41.36	820	330	311.04	178.90	2147	1021.6	0.0026	0.0106
R Out	37.44	28.02	1160	410	405.45	231.80	2198	1030.8	0.0028	0.0103
S Out	23.98	N/A	1080	520	405.45	277.55	2220	1039.9	0.0033	0.0095

Section	De Haller	Diffusion Ratio	Critical Mach
Rotor	0.8399	1.5888	1.3186
Stator	0.8582	1.5795	1.0867

Blade Geometries

Section	Pitch/Chord	Thickness/Chord	Aspect Ratio	Tip/Chord	Number of Blades
Rotor	2.1064	0.06	2.3333	0.02	9
Stator	2.2743	0.06	3.2222	0.02	24

Blade Angles [degree]						
Section	Inlet	Outlet	Camber	Stagger	Incidence	Deviation
Rotor	38.32	16.49	21.82	30.44	3.04	11.53
Stator	37.56	6.82	30.73	22.07	-0.12	17.15

Radius [m]			
section	Tip	RMS	Hub
Rotor In	0.5173	0.4370	0.3380
Rotor Out	0.5048	0.4295	
Stator Out	0.4871	0.4192	

## Stage 3

Flow Properties

Pressure Ratio	1.2179
Temperature Rise	86.69
Enthalpy Increase	90996
Entropy Increase	65.95
Load Distribution (psi)	0.2490
Stage Flow Efficiency (phi)	0.7759
Stage Reaction	0.5604
Isentropic Efficiency	44.45%
Polytrophic Efficiency	46.47%
Mass Flow	0.57

Velocity [m/s]							
Section	$C_m$	$U$	$C$	$C_\theta$	$W$	$W_\theta$	Sound S
R In	462.21	592.64	505.77	205.35	603.01	387.28	465.42
R Out	455.53	590.09	575.72	352.06	513.97	238.04	483.79
S Out	448.95	N/A	495.89	210.60	N/A	N/A	499.24

Section	Flow Angles [degree]		Pressure [Pa]		Enthalpy [kJ/kg]		Entropy [J/K]	Specific Heat	Density	Viscosity
	$\alpha$	$\beta$	Total	Static	Total	Static				
R In	23.96	39.96	1080	520	405.45	277.55	2219	1039.9	0.0033	0.0095
R Out	37.70	27.59	1400	590	491.50	325.77	2267	1050.2	0.0035	0.0095
S Out	25.14	N/A	1310	710	491.50	368.54	2285	1059.8	0.0039	0.0089

Section	De Haller	Diffusion Ratio	Critical Mach
Rotor	0.8523	1.5825	1.1900
Stator	0.8613	1.5780	0.9933

Blade Geometries

Section	Pitch/Chord	Thickness/Chord	Aspect Ratio	Tip/Chord	Number of Blades
Rotor	2.4134	0.06	2.1667	0.02	8
Stator	2.4540	0.06	2.9444	0.02	23

Blade Angles [degree]						
Section	Inlet	Outlet	Camber	Stagger	Incidence	Deviation
Rotor	41.19	8.55	32.64	23.64	-1.23	19.04
Stator	40.73	2.65	38.08	18.66	-3.03	22.49

		Radius [m]		
section		Tip	RMS	Hub
Rotor In		0.4882	0.4199	0.3380
Rotor Out		0.4840	0.4174	
Stator Out		0.4722	0.4106	

## Stage 4

Flow Properties

Pressure Ratio	1.1639
Temperature Rise	80.27
Enthalpy Increase	85840
Entropy Increase	59.92
Load Distribution (psi)	0.2401
Stage Flow Efficiency (phi)	0.7668
Stage Reaction	0.5602
Isentropic Efficiency	40.44%
Polytrophic Efficiency	41.97%
Mass Flow	0.57

Velocity [m/s]							
Section	$C_m$	$U$	$C$	$C_\theta$	$W$	$W_\theta$	Sound S
R In	448.95	580.45	495.89	210.60	581.67	369.85	499.24
R Out	441.47	580.73	562.64	348.81	498.68	231.92	514.74
S Out	434.11	N/A	484.64	215.46	N/A	N/A	528.21

Section	Flow Angles [degree]		Pressure [Pa]		Enthalpy [kJ/kg]		Entropy [J/K]	Specific Heat	Density	Viscosity
	$\alpha$	$\beta$	Total	Static	Total	Static				
R In	25.13	39.48	1310	710	491.50	368.54	2284	1059.8	0.0039	0.0089
R Out	38.31	27.71	1620	770	571.82	413.54	2328	1069.9	0.0040	0.0090
S Out	26.41	N/A	1530	900	571.82	454.38	2344	1079.1	0.0044	0.0085

Section	De Haller	Diffusion Ratio	Critical Mach
Rotor	0.8573	1.5800	1.0931
Stator	0.8614	1.5780	0.9175

Blade Geometries

Section	Pitch/Chord	Thickness/Chord	Aspect Ratio	Tip/Chord	Number of Blades
Rotor	2.5872	0.06	2	0.02	8
Stator	2.5612	0.06	2.6667	0.02	21

Blade Angles [degree]						
Section	Inlet	Outlet	Camber	Stagger	Incidence	Deviation
Rotor	44.00	2.00	41.99	18.48	-4.51	25.71
Stator	43.73	-0.49	44.22	16.20	-5.42	26.90

		Radius [m]		
section		Tip	RMS	Hub
Rotor In		0.4731	0.4111	0.3380
Rotor Out		0.4725	0.4108	
Stator Out		0.4638	0.4058	

## Stage 5

Flow Properties

Pressure Ratio	1.1307
Temperature Rise	75.16
Enthalpy Increase	81784
Entropy Increase	54.53
Load Distribution (psi)	0.2311
Stage Flow Efficiency (phi)	0.7484
Stage Reaction	0.5603
Isentropic Efficiency	37.71%
Polytrophic Efficiency	39.59%
Mass Flow	0.57

Velocity [m/s]							
Section	$C_m$	$U$	$C$	$C_\theta$	$W$	$W_\theta$	Sound S
R In	434.11	573.67	484.64	215.46	562.82	358.21	528.21
R Out	425.91	575.42	549.21	346.74	483.42	228.67	541.71
S Out	417.87	N/A	472.38	220.30	N/A	N/A	553.73

Section	Flow Angles [degree]		Pressure [Pa]		Enthalpy [kJ/kg]		Entropy [J/K]	Specific Heat	Density	Viscosity
	$\alpha$	$\beta$	Total	Static	Total	Static				
R In	26.40	39.53	1530	900	571.82	454.38	2343	1079.1	0.0044	0.0085
R Out	39.15	28.23	1810	960	647.74	496.92	2383	1088.5	0.0044	0.0087
S Out	27.82	N/A	1730	1090	647.74	536.17	2398	1097.0	0.0048	0.0083

Section	De Haller	Diffusion Ratio	Critical Mach
Rotor	0.8589	1.5792	1.0138
Stator	0.8601	1.5786	0.8531

Blade Geometries

Section	Pitch/Chord	Thickness/Chord	Aspect Ratio	Tip/Chord	Number of Blades
Rotor	2.6950	0.06	1.8333	0.02	7
Stator	2.6377	0.06	2.3889	0.02	19

Blade Angles [degree]						
Section	Inlet	Outlet	Camber	Stagger	Incidence	Deviation
Rotor	46.74	-3.14	49.88	14.59	-7.22	31.37
Stator	46.71	-2.97	49.68	14.31	-7.56	30.78

		Radius [m]		
section		Tip	RMS	Hub
Rotor In		0.4647	0.4063	0.3380
Rotor Out		0.4660	0.4070	
Stator Out		0.4592	0.4032	

## Stage 6

Flow Properties

Pressure Ratio	1.1082
Temperature Rise	70.96
Enthalpy Increase	78427
Entropy Increase	49.57
Load Distribution (psi)	0.2221
Stage Flow Efficiency (phi)	0.7237
Stage Reaction	0.5604
Isentropic Efficiency	36.09%
Polytrophic Efficiency	37.31%
Mass Flow	0.57

Velocity [m/s]							
Section	$C_m$	$U$	$C$	$C_\theta$	$W$	$W_\theta$	Sound S
R In	417.87	569.97	472.38	220.30	544.86	349.67	553.73
R Out	409.04	572.64	535.45	345.53	467.86	227.11	565.74
S Out	400.41	N/A	459.23	224.87	N/A	N/A	576.64

Section	Flow Angles [degree]		Pressure [Pa]		Enthalpy [kJ/kg]		Entropy [J/K]	Specific Heat	Density	Viscosity
	$\alpha$	$\beta$	Total	Static	Total	Static				
R In	27.80	39.92	1730	1090	647.74	536.17	2397	1097.0	0.0048	0.0083
R Out	40.19	29.04	2000	1140	720.04	576.68	2434	1105.5	0.0048	0.0085
S Out	29.34	N/A	1910	1280	720.04	614.59	2447	1113.2	0.0052	0.0081

Section	De Haller	Diffusion Ratio	Critical Mach
Rotor	0.8587	1.5793	0.9465
Stator	0.8577	1.5798	0.7964

Blade Geometries

Section	Pitch/Chord	Thickness/Chord	Aspect Ratio	Tip/Chord	Number of Blades
Rotor	2.7652	0.06	1.6667	0.02	7
Stator	2.6820	0.06	2.1111	0.02	17

Blade Angles [degree]						
Section	Inlet	Outlet	Camber	Stagger	Incidence	Deviation
Rotor	49.48	-7.05	56.53	11.66	-9.56	36.09
Stator	49.65	-4.50	54.15	13.11	-9.46	33.84

		Radius [m]		
section		Tip	RMS	Hub
Rotor In		0.4603	0.4038	0.3380
Rotor Out		0.4625	0.4051	
Stator Out		0.4571	0.4020	

## Stage 7

Flow Properties

Pressure Ratio	1.0932
Temperature Rise	67.21
Enthalpy Increase	75305
Entropy Increase	45.26
Load Distribution (psi)	0.2131
Stage Flow Efficiency (phi)	0.6944
Stage Reaction	0.5604
Isentropic Efficiency	34.91%
Polytrophic Efficiency	36.04%
Mass Flow	0.57

Velocity [m/s]							
Section	$C_m$	$U$	$C$	$C_\theta$	$W$	$W_\theta$	Sound S
R In	400.41	568.27	459.23	224.87	527.50	343.40	576.64
R Out	391.07	571.45	521.19	344.54	452.13	226.91	587.47
S Out	381.94	N/A	445.52	229.36	N/A	N/A	597.45

Section	Flow Angles [degree]		Pressure [Pa]		Enthalpy [kJ/kg]		Entropy [J/K]	Specific Heat	Density	Viscosity
	$\alpha$	$\beta$	Total	Static	Total	Static				
R In	29.32	40.62	1910	1280	720.04	614.569	2446	1113.2	0.0052	0.0081
R Out	41.38	30.12	2180	1330	789.14	653.32	2480	1120.7	0.0052	0.0083
S Out	31.01	N/A	2090	1470	789.14	689.90	2491	1127.6	0.0055	0.0080

Section	De Haller	Diffusion Ratio	Critical Mach
Rotor	0.8571	1.5801	0.8872
Stator	0.8548	1.5812	0.7457

Blade Geometries

Section	Pitch/Chord	Thickness/Chord	Aspect Ratio	Tip/Chord	Number of Blades
Rotor	2.8095	0.06	1.5	0.02	6
Stator	2.7171	0.06	1.8333	0.02	15

Blade Angles [degree]						
Section	Inlet	Outlet	Camber	Stagger	Incidence	Deviation
Rotor	52.26	-9.79	62.05	9.59	-11.64	39.92
Stator	52.68	-5.57	58.25	12.26	-11.30	36.58

Radius [m]			
section	Tip	RMS	Hub
Rotor In	0.4582	0.4026	0.3380
Rotor Out	0.4611	0.4042	
Stator Out	0.4567	0.4018	

## Stage 8

Flow Properties

Pressure Ratio	1.0817
Temperature Rise	63.88
Enthalpy Increase	72450
Entropy Increase	41.30
Load Distribution (psi)	0.2042
Stage Flow Efficiency (phi)	0.6618
Stage Reaction	0.5605
Isentropic Efficiency	34.42%
Polytrophic Efficiency	35.28%
Mass Flow	0.57

Velocity [m/s]							
Section	$C_m$	$U$	$C$	$C_\theta$	$W$	$W_\theta$	Sound S
R In	381.94	567.98	445.52	229.36	510.43	338.62	597.45
R Out	372.18	571.60	506.67	343.82	436.35	227.78	607.34
S Out	362.67	N/A	431.39	233.61	N/A	N/A	616.53

Section	Flow Angles [degree]		Pressure [Pa]		Enthalpy [kJ/kg]		Entropy [J/K]	Specific Heat	Density	Viscosity
	$\alpha$	$\beta$	Total	Static	Total	Static				
R In	30.99	41.56	2090	1470	789.14	689.90	2491	1127.6	0.0055	0.0080
R Out	42.73	31.47	2350	1510	855.40	727.03	2522	1134.3	0.0055	0.0082
S Out	32.81	N/A	2260	1650	855.40	762.35	2532	1140.4	0.0058	0.0079

Section	De Haller	Diffusion Ratio	Critical Mach
Rotor	0.8549	1.5812	0.8343
Stator	0.8514	1.5829	0.6997

Blade Geometries

Section	Pitch/Chord	Thickness/Chord	Aspect Ratio	Tip/Chord	Number of Blades
Rotor	2.8422	0.06	1.3333	0.02	5
Stator	2.7365	0.06	1.5556	0.02	12

Blade Angles [degree]						
Section	Inlet	Outlet	Camber	Stagger	Incidence	Deviation
Rotor	55.17	-11.73	66.90	8.11	-13.61	43.20
Stator	55.74	-5.92	61.66	11.90	-13.01	38.73

		Radius [m]		
section	Tip	RMS	Hub	
Rotor In	0.4579	0.4024	0.3380	
Rotor Out	0.4612	0.4043		
Stator Out	0.4578	0.4024		

## Stage 9

Flow Properties

Pressure Ratio	1.0733
Temperature Rise	60.74
Enthalpy Increase	69613
Entropy Increase	37.90
Load Distribution (psi)	0.1952
Stage Flow Efficiency (phi)	0.6266
Stage Reaction	0.5605
Isentropic Efficiency	34.00%
Polytrophic Efficiency	34.50%
Mass Flow	0.57

Velocity [m/s]							
Section	$C_m$	$U$	$C$	$C_\theta$	$W$	$W_\theta$	Sound S
R In	362.67	568.83	431.39	233.61	493.86	335.22	616.53
R Out	352.59	572.76	491.96	343.07	420.80	229.68	625.63
S Out	342.80	N/A	417.26	237.90	N/A	N/A	634.12

Section	Flow Angles [degree]		Pressure [Pa]		Enthalpy [kJ/kg]		Entropy [J/K]	Specific Heat	Density	Viscosity
	$\alpha$	$\beta$	Total	Static	Total	Static				
R In	32.79	42.75	2260	1660	855.40	762.35	2532	1140.4	0.0058	0.0079
R Out	44.22	33.08	2510	1700	919.01	798.00	2560	1146.3	0.0058	0.0081
S Out	34.76	N/A	2430	1840	919.01	831.96	2570	1151.7	0.0061	0.0078

Section	De Haller	Diffusion Ratio	Critical Mach
Rotor	0.8521	1.5826	0.7863
Stator	0.8482	1.5846	0.6580

Blade Geometries

Section	Pitch/Chord	Thickness/Chord	Aspect Ratio	Tip/Chord	Number of Blades
Rotor	2.8670	0.06	1.1667	0.02	5
Stator	2.7612	0.06	1.2778	0.02	10

Blade Angles [degree]						
Section	Inlet	Outlet	Camber	Stagger	Incidence	Deviation
Rotor	58.28	-12.96	71.24	7.13	-15.53	46.04
Stator	59.07	-6.38	65.46	11.49	-14.86	41.14

Radius [m]			
section	Tip	RMS	Hub
Rotor In	0.4590	0.4030	0.3380
Rotor Out	0.4627	0.4051	
Stator Out	0.4601	0.4037	

## Stage 10

Flow Properties

Pressure Ratio	1.0695
Temperature Rise	61.43
Enthalpy Increase	71074
Entropy Increase	34.63
Load Distribution (psi)	0.1862
Stage Flow Efficiency (phi)	0.5896
Stage Reaction	0.5600
Isentropic Efficiency	34.18%
Polytrophic Efficiency	35.88%
Mass Flow	0.57

Velocity [m/s]							
Section	$C_m$	$U$	$C$	$C_\theta$	$W$	$W_\theta$	Sound S
R In	342.80	570.66	417.26	237.90	477.74	332.76	634.12
R Out	332.52	574.74	477.36	342.50	405.59	232.24	642.52
S Out	322.54	N/A	392.60	223.84	N/A	N/A	651.41

Section	Flow Angles [degree]		Pressure [Pa]		Enthalpy [kJ/kg]		Entropy [J/K]	Specific Heat	Density	Viscosity
	$\alpha$	$\beta$	Total	Static	Total	Static				
R In	34.76	44.15	2430	1850	919.01	831.96	2569	1151.7	0.0061	0.0078
R Out	45.85	34.93	2680	1880	980.10	866.17	2595	1156.9	0.0061	0.0080
S Out	34.76	N/A	2600	2060	980.10	903.03	2604	1162.3	0.0064	0.0077

Section	De Haller	Diffusion Ratio	Critical Mach
Rotor	0.8490	1.5842	0.7429
Stator	0.8224	1.5980	0.6027

Blade Geometries

Section	Pitch/Chord	Thickness/Chord	Aspect Ratio	Tip/Chord	Number of Blades
Rotor	2.8885	0.06	1	0.02	4
Stator	2.1699	0.06	1	0.02	10

Blade Angles						
Section	Inlet	Outlet	Camber	Stagger	Incidence	Deviation
Rotor	61.63	-13.70	75.33	6.48	-17.48	48.63
Stator	56.81	9.67	47.14	22.28	-10.97	25.09

		Radius [m]		
section		Tip	RMS	Hub
Rotor In		0.4611	0.4042	0.3380
Rotor Out		0.4651	0.4065	
Stator Out		0.4621	0.4048	

## OGV

Pressure [Pa]		Temperature [K]		Enthalpy [kJ/kg]		Entropy [J/K]	Specific Heat	Density	Viscosity
Total	Static	Total	Static	Total	Static				
2430	2080	905	860.5	980.1	928.1	2623	1165.8	0.0064	0.0078

De Haller	Diffusion Ratio	Critical Mach	Pitch/Chord	Thickness/Chord	Tip/Chord
0.8215	1.4566	0.4907	0.5978	0.06	0.02

Number of Blades	Angles [degree]					
	Inlet	Outlet	Camber	Stagger	Incidence	Deviation
35	36	-8	44.2912	12.6145	-1.5431	7.9880

Radius [m]			Velocity [m/s]
Tip	RMS	Hub	
0.4621	0.4048	0.3380	322.5405

## Appendix B: Air compressor Matlab code

### Main Calculation

```

clear all;
clc;

%##### Numerical Setting #####
RLX_reaction = 0.8; %set up a damping for the stage reaction loop
RLX_PR = 0.95; % damping for the pressure ratio loop

%##### Figures needed to be import #####
%## Compressor Specification ##
n_stage = 10; %input number of stage
ratio_comp = 21; %input desired compressor ratio
p_inlet = 0.00099; %input inlet pressure
t_inlet = 19; %input inlet temperature
RPM = 13500; %input rotation speed of compressor

for i = 1:n_stage
    mflow(i) = 0.57; %input mass flow rate
end

for i = 1:n_stage
    tipclearance(i) = 0.02; %input tip clearance (epsilon/c)
    ratio_aspect_r = linspace(2.5,1,n_stage); %input aspect ratio (H/c
blade hieght over chord) for rotor
    ratio_aspect_s = linspace(3.5,1,n_stage); %aspect ratio for stator
    ratio_thickchord(i) = 0.06; %input thickness cord ratio (t/c)
    DF(i) = 0.45; %input diffusion factor
    AVR = linspace(0.99,0.97,n_stage); %input axial velocity ratio
    BLK = linspace(0.98,0.88,n_stage); %input blockage
    PSI_input = linspace(1,0.8,n_stage); %input loading(PSI) distribution
end

%## Inlet Specification ##
alpha_inlet = 15; %input alpha - inlet flow angle
phi_inlet = 0.65; %input stage flow coefficient

```

```

hubtip_ratio_inlet = 0.51;      %input hub and tip ratio

typeofcom = 'CID';           %input a compressor type

for i = 1:n_stage
stage_react(i) = 0.56;    %input a constant degree of reaction
end
%module 1
%rotor inlet

[P, T, H, S, Cp, rho, Visc, lambda, kappa, R, a, crit, FARsto, LHV,y_SO2,
y_H2O, y_CO2,y_N2, ...
y_O2, y_Ar, y_He]=state('PT',p_inlet,t_inlet,0,1);

Cp_inlet = Cp;          %specific heat of inlet air flow
rho_inlet = rho;         %air desity of the inlet
Visc_inlet = Visc;       %viscosity of inlet air flow
kappa_inlet = kappa;
a_inlet = a;             %sound velocity of the inlet air flow
s0_inlet = S;

[r_rms, r_m, r_hub, r_tip,H0] = Inletgeom(p_inlet, t_inlet, mflow(1), RPM,
hubtip_ratio_inlet, phi_inlet, alpha_inlet, BLK(1));
r_rms_inlet = r_rms;      %RMS radius of compessor inlet
r_m_inlet = r_m;          %mean radius of compressor inlet
r_hub_inlet = r_hub;      %blade hub radius of compressor inlet
r_tip_inlet = r_tip;       %blade tip radius for the inlet
h0_inlet = H0;            %stagnation enthalpy
U_inlet = r_rms_inlet*pi*RPM/30;   %blade speed of the inlet
U_tip_inlet = r_tip_inlet*pi*RPM/30; %tip blade speed of inlet flow
Cm_inlet = U_inlet*phi_inlet;     %inlet meridional velocity based on the
inlet diameter
C_inlet = Cm_inlet/cosd(alpha_inlet); %absolute velocity of the inlet flow
M_inlet = C_inlet/a_inlet;        %Mach of inlet flow
M_tip_inlet = (Cm_inlet^2+(U_tip_inlet-...
    Cm_inlet*tand(alpha_inlet))^2)^0.5/a_inlet;   %Mach of the inlet blade
tip
area_inlet = mflow(1)/(Cm_inlet*rho_inlet);        %availbabe inlet area for
the air flow

##### Pressure Ratio Iteration #####
for i = 1:n_stage
alpha3(i) = alpha_inlet;    %constant alpha3 from constant reaction stage
end

#####
%##### Start Values for PSI(load distrubution) #####
factor = 1.01;
PSI = 0.4*PSI_input;      %creat a variation of PSI
PSI(2,:) = PSI*factor;    %for calculating the derivative a second is needed

#####
%##### the begining of iterations for compressor calculations#####
n_PR = 0;    %initial step of the pressure ratio iteration
error_PR_rel = 1;  %set up initial error of pressure ratio
correct_PR = 0;

while correct_PR == 0;
if abs(error_PR_rel) < 10^(-4)
    correct_PR = 1;
end

```

```

for j = 1:2

%##### Stage Reaction Loop #####
%##### Beginning of stages loop #####
for i = 1: n_stage %start of the loop for all stages

    if typeofcom == 'CMD' %constant mean diameter compressor
        r_rms(i) = r_rms_inlet;
    elseif typeofcom == 'CID' %constant hub diameter compressor
        r_hub(i) = r_hub_inlet;
    elseif typeofcom == 'COD' %constant outer diameter compressor
        r_tip(i) = r_tip_inlet;
    end

    ##### Rotor Inlet Figures #####
    if i == 1 %first stage/ inlet of the compressor
        r1_rms(i) = r_rms_inlet;
        Cm1(i) = Cm_inlet;
        alpha1(i) = alpha_inlet;
        h01(i) = h0_inlet;
        s01(i) = floor(s0_inlet);
        s1(i) = floor(s0_inlet);
        [P, T, H, S, Cp, rho, Visc, lambda, kappa, R, a, crit, FARsto,
        LHV, y_SO2, y_H2O, y_CO2,y_N2,...,
        y_O2, y_Ar, y_He]=state('HS',h0_inlet,s0_inlet,0,1);
        p01(i) = P;
        t01(i) = T;
    else
        r1_rms(i) = r3_rms(i-1);
        Cm1(i) = Cm3(i-1);
        alpha1(i) = alpha3(i-1);
        p01(i) = p03(i-1);
        t01(i) = floor(t03(i-1));
        h01(i) = h03(i-1);
        s01(i) = floor(s3(i-1));
        s1(i) = floor(s3(i-1));
    end

    U1(i) = r1_rms(i)*pi*RPM/30; %speed of rotor blades
    C1_theta(i) = tand(alpha1(i))*Cm1(i); %absolute tangential velocity at
    the rotor inlet
    W1_theta(i) = U1(i)-C1_theta(i); %relative tangential velocity at the
    rotor inlet
    beta1(i) = atand(W1_theta(i)/Cm1(i)); %blade angle ant the rotor inlet
    C1(i) = Cm1(i)/cosd(alpha1(i)); %absolute air speed
    W1(i) = Cm1(i)/cosd(beta1(i)); %relative velocity at the rotor inlet

    ##### Rotor Inlet Static Properties #####
    h1(i) = h01(i)-(C1(i)^2)/2; % static enthalpy at the rotor inlet
    [P, T, H, S, Cp, rho, Visc, lambda, kappa, R, a, crit, FARsto, LHV, y_SO2,
    y_H2O, y_CO2,y_N2,...,
    y_O2, y_Ar, y_He]=state('HS',h1(i),s1(i),0,1); %calcualtion of static

```

```

air properties of rotor inlet
p1(i) = P;
t1(i) = T;
Cp1(i) = Cp;
rho1(i) = rho;
Visc1(i) = Visc;
kappa1(i) = kappa;
a1(i) = a;

MW1(i) = W1(i)/a1(i); % relative Mach at rotor inlet
MCm1(i) = Cm1(i)/a1(i); % meridional mach at rotor inlet

%##### Rotor inlet relative properties #####
h01rel(i) = h1(i)+0.5*W1(i)^2; %relative enthalpy at the rotor inlet
[P, T, H, S, Cp, rho, Visc, lambda, kappa, R, a, crit, FARsto, LHV, y_SO2,
y_H2O, y_CO2, y_N2, ...]
[y_O2, y_Ar, y_He]=state('HS',h01rel(i),s1(i),0,1); %relative stagnation
air properties
p01rel(i) = P; %relative stagnation pressure at the rotor inlet
t01rel(i) = T; %relative stagnation temperature at the rotor inlet

I1(i) = h01rel(i)-0.5*U1(i)^2; %rothalpy of air flow at the rotor
inlet

%##### Rotor Geometries at Inlet #####
area1(i) = mflow(i)/(rho1(i)*Cm1(i)*BLK(i)); %##### with settleed
blockage factor #####
if typeofcom == 'COD'; % constant tip diameter type compressor
    r1_tip(i) = r_tip(i);
    r1_rms(i) = (r1_tip(i)^2-area1(i)/(2*pi))^0.5;
    r1_hub(i) = (r1_rms(i)^2-area1(i)/(2*pi))^0.5;
elseif typeofcom == 'CMD'; % constant RMS diameter type compressor
    r1_tip(i) = (r1_rms(i)^2+area1(i)/(2*pi))^0.5;
    r1_hub(i) = (r1_rms(i)^2-area1(i)/(2*pi))^0.5;
else %constant blade hub type compressor
    r1_hub(i) = r_hub(i);
    r1_rms(i) = (r1_hub(i)^2+area1(i)/(2*pi))^0.5;
    r1_tip(i) = (r1_rms(i)^2+area1(i)/(2*pi))^0.5;
end

height1(i) = r1_tip(i)-r1_hub(i); %blade height of rotor inlet
chord1(i) = height1(i)/ratio_aspect_r(i); %calculate cord based on
input aspect ratio (aspect ratio = height/chord)

##### Part 2 #####
##### Rotor Output / Stator Input #####
r2_rms(i) = r1_rms(i); % set a initial value for r2_rms

if i == 1
    ds_rotor(i) = 10; % set up a initial number for the entropy
increase through the rotor
else
    ds_rotor(i) = ds_rotor(i-1); %set up increase of rotor entropy from
the rotor before
end

##### Iteration of Entropy Increase through the rotor #####
error_ds_rotor = 1; %set up initial error
n_ds = 0; %set up intial step

while abs(error_ds_rotor) > 10^(-4) %Out loop for solving entropy

```

```

increase

    error_rms = 1;      %set up initial error for the rotor outlet radius
    n_rms = 0;      %set up initial step

while abs(error_rms)>10^(-4)

    Cm2(i) = Cm1(i)*AVR(i);  %axial velocity at rotor outlet
    U2(i) = r2_rms(i)*pi*RPM/30;      %blade velocity at the rotor outlet
    C2_theta(i) = U2(i)*PSI(j,i)+C1_theta(i)*r1_rms(i)/r2_rms(i);
%##### Based on delH/U2^2
    W2_theta(i) = U2(i) - C2_theta(i);
    alpha2(i) = atand(C2_theta(i)/Cm2(i));
    beta2(i) = atand(W2_theta(i)/Cm2(i));
    C2(i) = (Cm2(i)^2+C2_theta(i)^2)^0.5;
    W2(i) = (Cm2(i)^2+W2_theta(i)^2)^0.5;
    deHaller_rotor(i) = W2(i)/W1(i);    %Rotor deHaller

%##### Rotor Outlet static properties #####
    s2(i) = s1(i)+ds_rotor(i);
    I2(i) = I1(i);      %rothalpy is constant through a rotor
    h2(i) = I2(i)-W2(i)^2/2+U2(i)^2/2;

    [P, T, H, S, Cp, rho, Visc, lambda, kappa, R, a, crit, FARsto, LHV, y_SO2,
    y_H2O, y_CO2,y_N2,...]
    y_O2, y_Ar, y_He]=state('HS',h2(i),s2(i),0,1);
    p2(i) = P;
    t2(i) = T;
    Cp2(i) = Cp;
    rho2(i) = rho;
    Visc2(i) = Visc;
    kappa2(i) = kappa;
    a2(i) = a;

    MC2(i) = C2(i)/a2(i);    %absolute Mach at the rotor outlet
    MCM2(i) = Cm2(i)/a2(i);    % meridional Mach at the rotor outlet

%##### Rotor Outlet Relative Properties #####
    h02rel(i) = h2(i)+W2(i)^2/2;    %relative stagnation enthalpy at rotor
outlet

    [P, T, H, S, Cp, rho, Visc, lambda, kappa, R, a, crit, FARsto, LHV, y_SO2,
    y_H2O, y_CO2,y_N2,...]
    y_O2, y_Ar, y_He]=state('HS',h02rel(i),s2(i),0,1);
    p02rel(i) = P;
    t02rel(i) = T;

%##### Rotor Outlet Stagnation Properties #####
    h02(i) = h2(i)+C2(i)^2/2;

    [P, T, H, S, Cp, rho, Visc, lambda, kappa, R, a, crit, FARsto, LHV, y_SO2,
    y_H2O, y_CO2,y_N2,...]
    y_O2, y_Ar, y_He]=state('HS',h02(i),s2(i),0,1);
    p02(i) = P;
    t02(i) = T;

%##### Rotor Outlet Geometry #####
    area2(i) = mflow(i)/(rho2(i)*Cm2(i)*BLK(i));      ##### with settleed
blockage factor #####
    if typeofcom == 'COD';
        r2_tip(i) = r_tip(i);
        r2_rms_new(i) = (r2_tip(i)^2-area2(i)/(2*pi))^0.5;

```

```

r2_hub(i) = (r2_rms_new(i)^2-area2(i)/(2*pi))^0.5;
elseif typeofcom == 'CMD';
    r2_tip(i) = (r2_rms(i)^2+area2(i)/(2*pi))^0.5;
    r2_hub(i) = (r2_rms(i)^2-area2(i)/(2*pi))^0.5;
    r2_rms_new(i) = r2_rms(i);
else
    r2_hub(i) = r_hub(i);
    r2_rms_new(i) = (r2_hub(i)^2+area2(i)/(2*pi))^0.5;
    r2_tip(i) = (r2_rms_new(i)^2+area2(i)/(2*pi))^0.5;
end

height2(i) = r2_tip(i)-r2_hub(i);
chord2(i) = height2(i)/ratio_aspect_r(i);

error_rms = r2_rms_new(i)/r2_rms(i)-1;
r2_rms(i) = r2_rms_new(i);

n_rms = n_rms+1;
if n_rms > 50 %Emergency break
    error_rms = 0;
    warning('RMS radius error in rotor outlet');
end

end %##### End of the inner RMS loop

%##### Geometry of the Whole Rotor #####
r_rms_r(i) = (r1_rms(i)+r2_rms(i))/2;
r_hub_r(i) = (r1_hub(i)+r2_hub(i));
r_tip_r(i) = (r1_tip(i)+r2_tip(i));
hubtip_ratio_r(i) = r_hub_r(i)/r_tip_r(i);
height_r(i) = r_tip_r(i)-r_hub_r(i);
chord_r(i) = height_r(i)/ratio_aspect_r(i);
Re_r(i) = W1(i)*chord_r(i)/Viscl(i); %Reynolds number

%### Rotor Pitch-chord ratio and diffusion factor #####
beta_in_r(i) = betal(i); %relative inlet angle of rotor
beta_out_r(i) = beta2(i); %relative outlet angle of rotor

AVDR_r(i) = rho2(i)*Cm2(i)/(rho1(i)*Cm1(i)); % ##### Axial Velocity
Density Ratio for the rotor

ratio_pitchchord_r(i) = (DF(i)-
1+W2(i)/W1(i))*W1(i)*(r1_rms(i)+r2_rms(i))...
/abs((r2_rms(i)*W2_theta(i)-r1_rms(i)*W1_theta(i))); % DF method to
calculate pitch chord ratio

%##### Diffusion ratios ??????????????????????????????????
[DF_lbl,Deq_star_lbl,Deq,Deq_star_ks] = Deq_star1(beta_in_r(i),
beta_out_r(i),Cm1(i),...);

Cm2(i),r1_rms(i),r2_rms(i),ratio_pitchchord_r(i),ratio_thickchord(i),AVDR_r
(i),MCm1(i));
DF_lbl_r(i) = DF_lbl;
Deq_star_lbl_r(i) = Deq_star_lbl;
Deq_r(i) = Deq;
Deq_star_ks_r(i) = Deq_star_ks;

%##### Rotor Entropy Increase ##### =
[omega_p,omega_ew,K_Re]
WRTMLR(DF_lbl_r(i),Deq_r(i),deHaller_rotor(i),...
beta_out_r(i),MW1(i),ratio_aspect_r(i),tipclearance(i),Re_r(i));
K_Re_r(i) = K_Re; %Correction factor for Reynolds number

```

```

omega_p_r(i) = omega_p;
omega_ew_r(i) = omega_ew;
omega_r(i) = omega_p+omega_ew;
omega_r(i) = omega_r(i)*K_Re;

dp_rotor(i) = omega_r(i)*(p01rel(i)-p1(i)); %total pressure drop through
the rotor
ds_rotor_new(i) = -R*log(1-dp_rotor(i)/p01(i)); %update the entropy
change

error_ds_rotor = ds_rotor_new(i)/ds_rotor(i)-1; % error for the entropy
rise
ds_rotor(i) = ds_rotor_new(i); % set the entropy rise for the next
iteration

n_ds = n_ds+1;
if n_ds > 20 %emergency break
    error_ds_rotor = 0;
    warning('entropy rise error on rotor');
end
end
##### End of the outer entropy loop #####
##### Stator Outlet #####
r3_rms(i) = r2_rms(i); %set intial value of RMS radius at stator outlet

ds_stator(i) = ds_rotor(i); %initial guess value
error_ds_stator = 1;
n_ds = 0;
while abs(error_ds_stator) > 10^(-4) %criteria for the entropy rise error
    n_rms = 0;
    error_rms = 1;
    while abs(error_rms) > 10^(-4); %criteria for the RMS radius error
        Cm3(i) = Cm2(i)*AVR(i); %axial velocity of the stator outlet

        if i == n_stage;
            alpha3(i) = alpha3(i-1); %absolute flow outlet angle in the
final stage
        end

        C3_theta(i) = Cm3(i)*tand(alpha3(i));
        C3(i) = Cm3(i)/cosd(alpha3(i));

        deHaller_stator(i) = C3(i)/C2(i); %deHaller of the stator;

        ##### Stator Outlet static properties #####
        h03(i) = h02(i); %total enthalpy does not change through stator
        h3(i) = h03(i)-C3(i)^2/2;
        s3(i) = s2(i)+ds_stator(i);

        [P, T, H, S, Cp, rho, Visc, lambda, kappa, R, a, crit, FARsto,
LHV,y_SO2, y_H2O, y_CO2,y_N2,...,
y_O2, y_Ar, y_He]=state('HS',h3(i),s3(i),0,1);
        p3(i) = P;
        t3(i) = T;
        Cp3(i) = Cp;
        rho3(i) = rho;
        Visc3(i) = Visc;
        kappa3(i) = kappa;
        a3(i) = a;

```

```

MC3(i) = C3(i)/a3(i); %absolute flow mach at stator outlet
MCm3(i) = Cm3(i)/a3(i); %meridional Mach at stator outlet

%##### Stator Outlet Stagnation Properties #####
#####
[P, T, H, S, Cp, rho, Visc, lambda, kappa, R, a, crit, FARsto,
LHV, y_SO2, y_H2O, y_CO2,y_N2, ...
y_O2, y_Ar, y_He]=state('HS',h03(i),s3(i),0,1);
p03(i) = P;
t03(i) = T;

%##### Stator Outlet Geometry #####
area3(i) = mflow(i)/(Cm3(i)*rho3(i)*BLK(i));

if typeofcom == 'COD';
r3_tip(i) = r_tip(i);
r3_rms_new(i) = (r3_tip(i)^2-area3(i)/(2*pi))^0.5;
r3_hub(i) = (r3_rms_new(i)^2-area3(i)/(2*pi))^0.5;
elseif typeofcom == 'CMD';
r3_tip(i) = (r3_rms(i)^2+area3(i)/(2*pi))^0.5;
r3_hub(i) = (r3_rms(i)^2-area3(i)/(2*pi))^0.5;
r3_rms_new(i) = r3_rms(i);
else
r3_hub(i) = r_hub(i);
r3_rms_new(i) = (r3_hub(i)^2+area3(i)/(2*pi))^0.5;
r3_tip(i) = (r3_rms_new(i)^2+area3(i)/(2*pi))^0.5;
end

height3(i) = r3_tip(i)-r3_hub(i);
chord3(i) = height3(i)/ratio_aspect_s(i);

error_rms = r3_rms_new(i)/r3_rms(i)-1;
r3_rms(i) = r3_rms_new(i);

n_rms = n_rms+1;
if n_rms > 50 %emergency break
    error_rms = 0;
    warning('RMS radius error at stator outlet');
end
end %##### End of inner RMS loop #####
%##### Stator geometry #####
area_s(i) = (area2(i)+area3(i))/2;
r_rms_s(i) = (r2_rms(i)+r3_rms(i))/2;
r_hub_s(i) = (r_rms_s(i)^2-area_s(i)/(2*pi))^0.5;
r_tip_s(i) = (r_rms_s(i)^2+area_s(i)/(2*pi))^0.5;

hubtip_ratio_s(i) = r_hub_s(i)/r_tip_s(i);
height_s(i) = r_tip_s(i)-r_hub_s(i);
chord_s(i) = height_s(i)/ratio_aspect_s(i);

Re_s(i) = C2(i)*chord_s(i)/Visc2(i); %Reynolds number

%##### Pitch-chord Ratio of Stator and diffusion factor #####
alpha_in_s(i) = alpha2(i); %relative inlet angle of stator
alpha_out_s(i) = alpha3(i); %relative outlet angle of stator

AVDR_s(i) = rho3(i)*Cm3(i)/(rho2(i)*Cm2(i)); %Axial Velocity Density
Ratio for the stator

ratio_pitchchord_s(i) = (DF(i)-1+(Cm3(i)/cosd(alpha_out_s(i)))/...

```

```

((Cm2(i)/cosd(alpha_in_s(i))))*((Cm2(i)/cosd(alpha_in_s(i))))*...
(r2_rms(i)+r3_rms(i))/abs((r3_rms(i)*Cm3(i)*tand(alpha_out_s(i))...
-r2_rms(i)*Cm2(i)*tand(alpha_in_s(i)))); % DF method to calculate
pitch chord ratio

[DF_lbl,Deq_star_lbl,Deq,Deq_star_ks] = Deq_star1(alpha_in_s(i),
alpha_out_s(i),Cm2(i),...

Cm3(i),r2_rms(i),r3_rms(i),ratio_pitchchord_s(i),ratio_thickchord(i),AVDR_s
(i),MCm2(i));
DF_lbl_s(i) = DF_lbl;
Deq_star_lbl_s(i) = Deq_star_lbl;
Deq_s(i) = Deq;
Deq_star_ks_s(i) = Deq_star_ks;

%##### Stator Entropy Increase #####
[omega_p,omega_ew,K_Re] = WRMLR(DF_lbl_s(i),Deq_s(i),deHaller_stator(i),...
alpha_out_s(i),MC2(i),ratio_aspect_s(i),0,Re_s(i));
K_Re_s(i) = K_Re; %Correction factor for Reynolds number
omega_p_s(i) = omega_p;
omega_ew_s(i) = omega_ew;
omega_s(i) = omega_p+omega_ew;
omega_s(i) = omega_s(i)*K_Re;

dp_stator(i) = omega_s(i)*(p02(i)-p01(i));
ds_stator_new(i) = -R*log(1-dp_stator(i)/p02(i));

error_ds_stator = ds_stator_new(i)/ds_stator(i)-1;
ds_stator(i) = ds_stator_new(i);

n_ds = n_ds+1;
if n_ds > 200 %emergency break
    error_ds_stator = 0;
    warning('entropy rise error on stator')
end
end %End of outer entropy loop

end %end of the loop for all stages (start from around 104 lines)

%#####
%##### OGV Calculation #####
ds_OGV = ds_stator(n_stage); %initial guess value of entropy loss
error_ds_OGV = 1;
n_ds = 0;

while abs(error_ds_OGV) > 10^(-4)
    AVR_OGV = 1;
    Cm_OGV = Cm3(n_stage)*AVR_OGV;
    C_OGV = Cm_OGV;

    %##### OGV static properties #####
    h0_OGV = h03(n_stage); %No enthalpy loss through OGV
    h_OGV = h0_OGV-C_OGV^2/2;
    s_OGV = s3(n_stage)+ds_OGV;

    [P, T, H, S, Cp, rho, Visc, lambda, kappa, R, a, crit, FARsto, LHV,y_SO2,
y_H2O, y_CO2,y_N2,...,
y_O2, y_Ar, y_He]=state('HS',h_OGV,s_OGV,0,1);
    p_OGV = P;
    t_OGV = T;

```

```

Cp_OGV = Cp;
rho_OGV = rho;
Visc_OGV = Visc;
kappa_OGV = kappa;
a_OGV = a;

MCm_OGV = Cm_OGV/a_OGV;
MC_OGV = C_OGV/a_OGV;

deHaller_OGV = C_OGV/C3(n_stage);    %deHaller number of ogv

%##### OGV Stagnation Properties #####
[P, T, H, S, Cp, rho, Visc, lambda, kappa, R, a, crit, FARsto, LHV, y_SO2,
y_H2O, y_CO2, y_N2, ...]
y_O2, y_Ar, y_He]=state('HS',h0_OGV,s_OGV,0,1);
p0_OGV = P;
t0_OGV = T;

%##### OGV Geometry #####
r_rms_OGV = r3_rms(n_stage);
r_tip_OGV = r3_tip(n_stage);
r_hub_OGV = r3_hub(n_stage);
hubtip_ratio_OGV = r_hub_OGV/r_tip_OGV;
height_OGV = r_tip_OGV-r_hub_OGV;
chord_OGV = height_OGV/ratio_aspect_s(n_stage);

Re_OGV = C_OGV*chord_OGV/Visc_OGV;

angle_inOGV = alpha3(n_stage);
angle_outOGV = 0;

AVDR_OGV = rho_OGV*Cm_OGV/(rho3(n_stage)*Cm3(n_stage));  %axial velocity
density ratio of the OGV

W_inOGV = Cm3(n_stage)/tand(angle_inOGV);
W_outOGV = C_OGV;
C_theta_in = Cm3(n_stage)*tand(angle_inOGV);
C_theta_out = 0;

ratio_pitchchord_OGV = (DF(n_stage)-1+W_outOGV/W_inOGV)*...
W_inOGV*(r_rms_OGV+r3_rms(n_stage))...
/abs((r_rms_OGV*C_theta_out-r3_rms(n_stage)*C_theta_in));      % DF
method to calculate pitch chord ratio

[DF_lbl,Deq_star_lbl,Deq,Deq_star_ks] = Deq_star1(angle_inOGV, ...
angle_outOGV,Cm3(n_stage),Cm_OGV,r3_rms(n_stage),r_rms_OGV, ...
ratio_pitchchord_OGV,ratio_thickchord(n_stage),AVDR_OGV,MCm_OGV);
DF_lbl_OGV = DF_lbl;
Deq_star_lbl_OGV = Deq_star_lbl;
Deq_OGV = Deq;
Deq_star_ks_OGV = Deq_star_ks;

%##### OGV Entropy Increase #####
[omega_p,omega_ew,K_Re] = WRTMLR(DF_lbl_OGV,Deq_OGV,deHaller_OGV, ...
angle_outOGV,MC3(n_stage),ratio_aspect_s(n_stage),0,Re_OGV);
K_Re_OGV = K_Re;    %Correction factor for Reynolds number
omega_p_OGV = omega_p;
omega_ew_OGV = omega_ew;
omega_OGV = omega_p+omega_ew;
omega_OGV = omega_OGV*K_Re;

```

```

dp_OGV = omega_OGV*(p03(n_stage)-p3(n_stage));
ds_OGV_new = -R*log(1-dp_OGV/p03(n_stage));

error_ds_OGV = ds_OGV_new/ds_OGV-1;
ds_OGV = ds_OGV_new;

n_ds = n_ds+1;
if n_ds > 20
    error_ds_OGV = 0;
    warning('entropy rise error on OGV');
end

end % End of OGV loop

##### stage reaction and slope calculation #####
for i = 1 : n_stage
    reaction(i) = (h2(i)-h1(i))/(h03(i)-h01(i));
    reaction_slope(i) = Cm1(i)/U1(i)*AVR(i)*pi/(180*cosd(alpha3(i))^2);
end

##### set up a new value for alpha3 #####
for i = 2 : n_stage
    error_reaction(i) = reaction(i)-stage_react(i);
    error_reaction_rel(i) = stage_react(i)/reaction(i)-1;
    alpha3(i-1) = alpha3(i-1)+error_reaction(i)/reaction_slope(i)*RLX_reaction;
end

##### Calculate RMS error of stage reaction #####
error_reaction_rms = 0;

for i = 1 : n_stage
    error_reaction_rms = error_reaction_rms + error_reaction_rel(i)^2;
end

if abs(error_reaction_rms) < 10^(-4)
    correct_reaction = 1;
end

n = n_reaction+1;
if n_reaction > 50
    error_reaction_rms = 0;
    warning ('stage reaction error');
end

end ##### end of reaction loop

##### End of Stage Reaction Loop #####
##### PR(j) = p_OGV/p_inlet; %achieve the new pressure ratio from the pressure loop

if correct_PR == 1
    break
end

##### calculation of PR slope #####
if correct_PR == 0
    PR_slope = (PR(1)-PR(2))/(mean(PSI(1,:))-mean(PSI(2,:))); %the

```

```

numerical derivative dPR/dPSI
error_PR_rel = ratio_comp/PR(1)-1;
error_PR = ratio_comp-PR(1);

%##### New PSI Values Calculation #####
for i = 1:n_stage
    PSI(1,i) = PSI(1,i)+error_PR/PR_slope*RLX_PR;

    PSI(2,i) = PSI(1,i)*factor;
end

n_PR = n_PR+1;
if n_PR > 20 %emergency break
    error_PR_rel = 0;
    warning('Pressure Ratio Error');
end
end

%##### End of Pressure Ratio Loop #####
%##### End of the whole loop #####
%##### Calculations for Rotor and Stator Angles #####
ratio_pressure = p_OGV/p01(1); %the calcuated pressure ratio through the
compressor

%##### Rotor Blades #####
pitch_r(i) = chord_r(i)*ratio_pitchchord_r(i);
diameter_r(i) = 2*pi*r_rms_r(i);
n_blade_r(i) = ceil(diameter_r(i)/pitch_r(i));

[incidence, deviation, camber, attack, stagger...
    blade_angle_in,     blade_angle_out] = Bladeangles(beta1(i),
beta2(i),...
    ratio_pitchchord_r(i), ratio_thickchord(i), MW1(i));
incidence_angle_r(i) = incidence;
deviation_angle_r(i) = deviation;
camber_angle_r(i) = camber;
attack_angle_r(i) = attack;
stagger_angle_r(i) = stagger;
blade_angle_in_r(i) = blade_angle_in;
blade_angle_out_r(i) = blade_angle_out;

%##### Stator Blade #####
pitch_s(i) = chord_s(i)*ratio_pitchchord_s(i);
diameter_s(i) = 2*pi*r_rms_s(i);
n_blade_s(i) = ceil(diameter_s(i)/pitch_s(i));

[incidence, deviation, camber, attack, stagger...
    blade_angle_in,     blade_angle_out] = Bladeangles(alpha2(i),
alpha3(i),...
    ratio_pitchchord_s(i), ratio_thickchord(i), MC2(i));
incidence_angle_s(i) = incidence;
deviation_angle_s(i) = deviation;
camber_angle_s(i) = camber;
attack_angle_s(i) = attack;

```

```

stagger_angle_s(i) = stagger;
blade_angle_in_s(i) = blade_angle_in;
blade_angle_out_s(i) = blade_angle_out;

%##### Compressor Housing angle #####
housing_angle_r(i) = atand((r1_tip(i)-r2_tip(i))/(chord_r(i)...
    *cosd(stagger_angle_r(i)))); 
housing_angle_s(i) = atand((r2_tip(i)-r3_tip(i))/(chord_s(i)*cosd(stagger_angle_s(i))));

end

%##### OGV Blade Angle #####
pitch_OGV = chord_OGV*ratio_pitchchord_OGV;
diameter_OGV = 2*pi*r_rms_OGV;
n_blade_OGV = ceil (diameter_OGV/pitch_OGV);

[incidence, deviation, camber, attack, stagger...]
blade_angle_in, blade_angle_out] = Bladeangles(alpha3(n_stage), 0, ...
    ratio_pitchchord_OGV, ratio_thickchord(n_stage), MC3(n_stage));
incidence_angle_OGV = incidence;
deviation_angle_OGV = deviation;
camber_angle_OGV = camber;
attack_angle_OGV = attack;
stagger_angle_OGV = stagger;
blade_angle_in_OGV = floor(blade_angle_in);
blade_angle_out_OGV = floor(blade_angle_out);

%##### Power Calculation #####
power = 0;

for i = 1:n_stage
    %##### Static Pressure Rise Coefficient #####
    Cp_r(i) = (p2(i)-p1(i))/(p01rel(i)-p1(i));
    Cp_s(i) = (p3(i)-p2(i))/(p02(i)-p2(i));
    %##### Stage Pressure Ratio #####
    PR_stage(i) = p03(i)/p01(i);
    %##### Accumulated Pressure Ratio #####
    PR_accumulated(i) = p03(i)/p01(i);
    %##### Stage Temperature Rise #####
    dt0_stage(i) = t03(i)-t01(i);
    %##### Polytropic efficiency of each stage #####
    [P, T, H, S, Cp, rho, Visc, lambda, kappa, R, a, crit, FARsto, LHV, y_SO2,
    y_H2O, y_CO2, y_N2, ...]
    y_O2, y_Ar, y_He]=state('PT',1,t03(i),0,1);
    as1 = S;
    [P, T, H, S, Cp, rho, Visc, lambda, kappa, R, a, crit, FARsto,
    LHV, y_SO2, y_H2O, y_CO2, y_N2, ...]
    y_O2, y_Ar, y_He]=state('PT',1,t01(i),0,1);
    as2 = S;
    e_poly(i) = R*log(p03(i)/p01(i))/(as1-as2);

    %##### Isentropic Stage Efficiency #####
    [P, T, H, S, Cp, rho, Visc, lambda, kappa, R, a, crit, FARsto, LHV, y_SO2,
    y_H2O, y_CO2, y_N2, ...]
    y_O2, y_Ar, y_He]=state('PS',p03(i),s01(i),0,1);
    h_isen = H;
    e_isen(i) = (h_isen-h01(i))/(h03(i)-h01(i));

    %##### Overall Isentropic Efficiency #####
    [P, T, H, S, Cp, rho, Visc, lambda, kappa, R, a, crit, FARsto, LHV, y_SO2,
    y_H2O, y_CO2, y_N2, ...]

```

```

y_O2, y_Ar, y_He]=state('PS',p3(n_stage),s3(1),0,1);
h2s = H;
e_isen_total = (h2s-h1(1))/(h3(n_stage)-h1(1));

%##### Overall Polytropic Efficiency #####
[P, T, H, S, Cp, rho, Visc, lambda, kappa, R, a, crit, FARsto, LHV,y_SO2,
y_H2O, y_CO2,y_N2,...]
y_O2, y_Ar, y_He]=state('PT',1,t03(n_stage),0,1);
as1 = S;
[P, T, H, S, Cp, rho, Visc, lambda, kappa, R, a, crit, FARsto,
LHV,y_SO2, y_H2O, y_CO2,y_N2,...]
y_O2, y_Ar, y_He]=state('PT',1,t01(1),0,1);
as2 = S;
e_poly_total = R*log(p03(n_stage)/p01(1))/(as1-as2);

%##### Stage flow coefficient #####
phi_stage(i) = (Cm1(i)+Cm2(i))/(U1(i)+U2(i));
%##### Compressor Power #####
power = power+mflow(i)*(h03(i)-h01(i))/1000;
end

%##### Compressor Length #####
length = 0;
for i = 1:n_stage;
    length = length + chord_r(i)*(0.2+cosd(stagger_angle_r(i)));
    length = length + chord_s(i)*(0.2+cosd(stagger_angle_r(i)));
end
length = length - 0.2*chord_s(n_stage);

%##### Rises #####
for i = 1:n_stage;
    t_rise(i) = t3(i)-t1(i);
    s_rise(i) = s3(i)-s1(i);
    h_rise(i) = h3(i)-h1(i);
end

```

## Compressor Inlet Geometry Calculation

```

function [r_rms, r_m, r_hub,r_tip,H0] ...
    = Inletgeom(p0,t0,mflow,RPM,hubtip_ratio,phi,alpha,BLK)

[P, T, H, S, Cp, rho, Visc, lambda, kappa, R, a, crit, FARsto, LHV,y_SO2,
y_H2O, y_CO2,y_N2,...]
y_O2, y_Ar, y_He]=state('PT',p0,t0,0,1);

s0 = S; %static and stagnation entropy
h = H; %static enthalpy
Cm = 0.6*a; %initial velocity guess
RLX = 0.15; %damping range
error_Cm = 1; %set up the first error

n = 0; %initial step
while abs(error_Cm) > 10^(-3) %searching for relative correct velocity

Cm_old = Cm; % set up new value for the next iteration
C = Cm/cos(alpha); %absolute inlet velocity

```

```

[P, T, H, S, Cp, rho, Visc, lambda, kappa, R, a, crit, FARsto, LHV, y_SO2,
y_H2O, y_CO2, y_N2, ...
y_O2, y_Ar, y_He]=state('HS',h,s0,0,1);

area = mflow/(Cm*rho*BLK); %area of the compressor inlet cross section
r_tip = (area/(pi*(1-hubtip_ratio^2)))^0.5; %tip radius
r_hub = hubtip_ratio*r_tip; %blade hub radius
r_m = (r_tip+r_hub)/2; %mean radius
r_rms = ((r_tip^2+r_hub^2)/2)^0.5; %RMS radius
U_m = r_m*pi*RPM/30; %blade speed based on mean radius
U_rms = r_rms*pi*RPM/30; %blade speed based on RMS radius

Cm = U_rms*phi; %updated meridional velocity
error_Cm = Cm/Cm_old -1;
Cm = Cm+(Cm_old-Cm)*RLX; %damping
H0 = h+C^2/2; %stagnation enthalpy of the motor inlet

n = n+1;
if n > 20 %emergency break
    error_Cm = 0;
    warning('Velocity Cm Convergence Error')
end
end
end

```

## Blade Angles

```

function[incidence,deviation,camber,attack,stagger,blade_angle_in,blade_angle_out] = ...

Bladeangles(beta_inlet,beta_outlet,ratio_pitchchord,ratip_pitchchord,MW_inlet)

K_it = -0.0214+19.17*ratip_pitchchord-122.3*ratip_pitchchord^2+...
312.5*ratip_pitchchord^3;

i_010 = (0.0325-0.0674/ratio_pitchchord)+(-0.002364+0.0913/ratio_pitchchord)...
*beta_inlet+(1.64e-5-2.38e-4/ratio_pitchchord)*beta_inlet^2;
K_sh = 0.7;

n = (-0.063+0.02274/ratio_pitchchord)+(-0.0035+0.0029/ratio_pitchchord)*...
beta_inlet-(3.79e-5+1.11e-5/ratio_pitchchord)*beta_inlet^2;

%##### Mach # correction #####
n = (-0.063+0.02274/ratio_pitchchord)+(-0.0035+0.0029/ratio_pitchchord)*...
beta_inlet-(3.79e-5+1.11e-5/ratio_pitchchord)*beta_inlet^2;

delta_010 = (-0.0443+0.1057/ratio_pitchchord)+(0.0209-0.0186/ratio_pitchchord)*beta_inlet+(-0.0004+0.00076/ratio_pitchchord)*beta_inlet^2;

K_deltat = 0.0142+6.172*ratip_pitchchord+36.61*ratip_pitchchord^2;

```

```

m_dot = 0.249+7.4e-4*beta_inlet-1.32e-5*beta_inlet^2+3.16e-7*beta_inlet^3;
b = 0.9655-2.538e-3*beta_inlet+4.221e-5*beta_inlet^2-1.3e-6*beta_inlet^3;
m = m_dot*ratio_pitchchord^b;

%##### Loop to achieve suitable camber angle #####
camber_angle = 1.2*(beta_inlet-beta_outlet); %set a initial for the
camber

i = 0;
error_camber = 1;

while error_camber > 0.0001;
    camber_old=camber_angle;

    angle_incidence = K_sh*K_it*i_010-1+10*(MW_inlet-0.7)+n*camber_old;
    %incidence angle based on camber
    angle_deviation = K_sh*K_deltat*delta_010+m*camber_old; %deviation
angle

    inlet_blade = beta_inlet-angle_incidence;
    outlet_blade = beta_outlet-angle_deviation;

    camber_angle = inlet_blade-outlet_blade; % new camber angle

    error_camber = abs(camber_angle/camber_old-1);

    i=i+1;
    if i > 10
        error_camber = 0;
    end
    error(i) = error_camber;
end

camber = camber_angle;
incidence = angle_incidence;
deviation = angle_deviation;
blade_angle_in = inlet_blade;
blade_angle_out = outlet_blade;
stagger = beta_inlet - camber/2;
attack = beta_inlet - stagger;

```

## Appendix C: Air suspension bearings code

```

% mass_flow_rate.m

% Script to find the variation of mass flow rate with respect to inlet
pressure

% Yuzhe Zhou, 28/11/2015

% Variable dictionary

% M

% Ps

```

```

clear M Ps; % Clear all variables from workspace
clc; % Clear command windowx = 740:10:11000; %Inlet pressure

D = 0.06; % diameter of the orifice
g = 0.002; % depth of the air conduction grooves
h = 0.001; % bearing gap
Pz = 3993; % air cushion pressure
k = 1.4; % specific heat ratio
R = 8.314; % gas constant
T = 400; % air outlet temperature
m = 0.02897; % molar mass of the gas

Ps = 7600:10:11000; % intlet pressure
Alpha = (2*k/(k-1))^(1/2).*((Pz./Ps).^(2/k)-(Pz./Ps).^( (k+1)/k)).^1/2;
Beta = pi.*D*(g+h);

M = Beta.*Ps.*Alpha/(R*T)^(1/2); % calculation of mass flow for single
orifice

Total_mass_flow_rate = M*28; % total mass flow required

density = m.*Ps/(T*R); % density of air outlet
V = M./density; % volume flow rate
v = V/(pi.* (D/2).^2); % outlet velocity

subplot (3,1,1)
plot(Ps,Total_mass_flow_rate,'k-'), grid minor, xlabel('Inlet pressure/Pa'), ylabel('Mass flow rate/kg/s'), ...
title('Total mass flow rate - Inlet pressure')

subplot (3,1,2)
plot(Ps,V,'k-'), grid minor, xlabel('Inlet pressure/Pa'), ylabel('Volume flow rate/m^3/s'), ...
title('Volume flow rate - Inlet pressure')

```

```

subplot (3,1,3)

plot(Ps,v,'k-'), grid minor, xlabel('Inlet pressure/Pa'),
ylabel('Velocity/m/s'), ...
title('Injection velocity - Inlet pressure')

% Flow_bank_angle.m

% Script to find the variation of flow pattern with respect to ski bank
% angle

% Yuzhe Zhou, 28/11/2015

% Variable dictionary

% Bank_angle

% Ps

clear M Bank_angle; % Clear all variables from workspace
clc; % Clear command windowx = 740:10:11000; %Inlet pressure

D = 0.06; % diameter of the orifice
g = 0.002; % depth of the air conduction grooves
h = 0.001; % bearing gap
Bank_angle = pi/4:pi/180:pi/2; % bank angle range
Pz = 3993./sin (Bank_angle); % air cushion pressure
k = 1.4; % specific heat ratio
R = 8.314; % gas constant
T = 400; % air outlet temperature
m = 0.02897; % molar mass of the gas
Ps = 11000; % intlet pressure

Alpha = (2*k/(k-1))^(1/2).*((Pz/Ps).^(2/k)-(Pz/Ps).^((k+1)/k)).^1/2;
Beta = pi.*D*(g+h);

M = Beta*Ps.*Alpha/(R*T)^(1/2); % calculation of mass flow rate for single
orifice

Total_mass_flow_rate = M*28; % total mass flow requiried

```

```

density = m.*Ps/(T*R); % density of air outlet
V = M./density; % volume flow rate
v = V/(pi.* (D/2).^2); % outlet velocity

subplot (3,1,1)
plot(Bank_angle*180/pi,Total_mass_flow_rate,'k-'), grid minor, xlabel('bank angle/Degree'), ylabel('Mass flow rate/kg/s'), ...
title('Total mass flow rate - bank angle')

subplot (3,1,2)
plot(Bank_angle*180/pi,V,'k-'), grid minor, xlabel('bank angle/Degree'), ylabel('Volume flow rate/m^3/s'), ...
title('Volume flow rate - bank angle')

subplot (3,1,3)
plot(Bank_angle*180/pi,v,'k-'), grid minor, xlabel('bank angle/Degree'), ylabel('Velocity/m/s'), ...
title('Injection velocity - bank angle')

```

## Appendix D: Clark Y Aerofoil Section

Wing Chord 1500 mm

Adjustment Factor 0%

X %	Ordinate %	X mm	Ordinate mm	X %	Ordinate %	X mm	Ordinate mm
0	0	0	0	100	0.00	1500.00	0.00
0.5	4.90	7.50	73.50	90	0.00	1350.00	0.00
1	5.55	15.00	83.25	80	0.00	1200.00	0.00
1.75	6.15	26.25	92.25	70	0.00	1050.00	0.00
2.5	6.60	37.50	99.00	60	0.00	900.00	0.00
3.75	7.12	56.25	106.80	50	0.00	750.00	0.00
5	7.90	75.00	118.50	40	0.00	600.00	0.00
7.5	8.85	112.50	132.75	30	0.00	450.00	0.00
10	9.60	150.00	144.00	25	0.00	375.00	0.00
15	10.68	225.00	160.20	20	0.00	300.00	0.00
20	11.36	300.00	170.40	15	0.03	225.00	0.45
25	11.60	375.00	174.00	10	0.15	150.00	2.25
30	11.70	450.00	175.50	7.5	0.42	112.50	6.30
40	11.40	600.00	171.00	5	0.88	75.00	13.20
50	10.52	750.00	157.80	3.75	1.20	56.25	18.00
60	9.15	900.00	137.25	2.5	1.47	37.50	22.05
70	7.35	1050.00	110.25	1.75	1.85	26.25	27.75
80	5.22	1200.00	78.30	1	2.30	15.00	34.50
90	2.80	1350.00	42.00	0.5	2.80	7.50	42.00
100	0.12	1500.00	1.80	0	3.50	0.00	52.50

## Appendix E: Volume calculations

time pod in tube (minutes)	fraction of total volume	total volume of one pod journey (m <sup>3</sup> )	total Volume at each stage
36	1	568.2647	568.2647
34	0.944444444	568.2647	536.6944389
32	0.888888889	568.2647	505.1241778
30	0.833333333	568.2647	473.5539167
28	0.777777778	568.2647	441.9836556
26	0.722222222	568.2647	410.4133944
24	0.666666667	568.2647	378.8431333
22	0.611111111	568.2647	347.2728722
20	0.555555556	568.2647	315.7026111
18	0.5	568.2647	284.13235
16	0.444444444	568.2647	252.5620889
14	0.388888889	568.2647	220.9918278
12	0.333333333	568.2647	189.4215667
10	0.277777778	568.2647	157.8513056
8	0.222222222	568.2647	126.2810444
6	0.166666667	568.2647	94.71078333
4	0.111111111	568.2647	63.14052222
2	0.055555556	568.2647	31.57026111
0	0	568.2647	0
		true total volume=	5398.51465

```

Patm=1013.25; % atmospheric pressure
Pneed=1;      % desired pressure in tube

% V is range of possible volumes that one pump will need to evacuate. the
% time taken at each volume will help determine the number of pumps needed
% for system.
% q is the mass flow rate of the chosen vacuum pump

V=22:100:22022;
for i=1:length(V);

q=0.0183333
t(i)=V(i)/(q*(log(Patm/Pneed)));
end

%air from pod

% density of air at 25 degrees celsius, temperature of the air, is shown as
% "dens" below

dens=0.887;

```

```

% mfr= is the mass flow rate of the air exiting the pod
mfr=0.2362

% qmod= the volume flow rate of the air exiting the pod

qpod=mfr/dens;

% Vpod is total volume of air released by one pod in complete journey

Vpod=qpod*2134

% Vmax is total volume of air released by all pods in worst case scenario
Vmax=5400; |
```

%Ppod= pressure of air exiting the pod  
Ppod=110;  
Vpods=5:1:250;

```

for j=1:length(Vpods);

tn(j)=Vpods(j) / (q*(log(Ppod/Pneed))) ;

end
```

Name	Value
dens	0.8870
i	221
j	246
mfr	0.2362
Patm	1.0133e+03
Pneed	1
Ppod	110
q	0.0183
qpod	0.2663
t	1x221 double
tn	1x246 double
V	1x221 double
Vmax	5400
Vpod	568.2647
Vpods	1x246 double